IONIZED CLUSTER BEAM TECHNIQUE FOR DEPOSITION AND EPITAXY(Dissertation_全文)

AUTHOR(S):

Takaoka, Hiroshi

IONIZED CLUSTER BEAM TECHNIQUE FOR DEPOSITION AND EPITAXY

by

Hiroshi TAKAOKA

FEBRUARY 1981

DEPARTMENT OF ELECTRONICS
KYOTO UNIVERSITY
KYOTO, JAPAN

IONIZED CLUSTER BEAM TECHNIQUE FOR DEPOSITION AND EPITAXY

by

Hiroshi TAKAOKA

FEBRUARY 1981

DEPARTMENT OF ELECTRONICS
KYOTO UNIVERSITY
KYOTO, JAPAN

PREFACE

Recently, much interest and attention is concentrated on the "Ion-based technique" extending over the wide and significant applications, where fusion control, nuclei physics (heavy ion science), ion rocket, ion implantation, sputtering (sputter deposition), ion plating, crystal growth (ion beam epitaxy), synthesis of compound materials (plasma polymerization, activated reactive evaporation, reactive sputtering, reactive ion plating, etc.), ion milling (ion etching, ion beam milling), surface analysis (ion microanalyzer, secondary ion mass spectrometry, etc.), medical application (radiotherapy, biophia by ion irradiation) are included. In the ion-based technique, the purpose of ionizing evaporant materials is to give some kinetic energy and/or chemical activity to the materials. In the above mentioned applications, the comparably lower kinetic energy from a few eV to not more than 500 keV is used, although the ion current is higher in comparison with that used in a conventional accelerator (e.g. a few tens to a few hundred mA). Considering the relation between thermal and electrical energies, i.e. $kT/e = T/1.16 \times 10^4$ eV, even by the acceleration of a few eV high equivalent temperature of particles can be achieved. By using these accelerated particles, new types of deposition of films or synthesis of the compound materials which could not be expected by the conventional thermal or chemical methods is achieved.

Much progress in the ion-based technique for film formation is reported in the proceedings of international conferences, e.g.

(1) International Conference on Ion Plating and Allied Techniques — IPAT'77, Edinburgh, England (1977), (2) IPAT'79, London, England (1979) and (3) International Conference on Metallurgical Coatings, San Diego, U.S.A. (1979). Further, in Japan, the Symposium on Ion Sources and Application Technology — ISAT was held in Tokyo (1977), and since then it has been held every year under the name of ISAT. Such a great interest in the ion-based technique for film formation is considered to be due to the necessity and importance of thin film devices with many functionable properties, which can not be produced by the conventional method under the thermal equilibrium conditions. Applying the ion-based technique to film formation, the film properties such as mechanical, optical, electrical and crystallographic properties can be easily controlled by adjusting the growth and deposition conditions, which is one of the important factors to prepare the above mentioned thin film devices.

In this thesis, the role of the ionized particles for film formation by using the Ionized Cluster Beam (ICB) technique and the cluster formation phenomena are investigated theoretically and experimentally. The ICB technique was originally developed by Professor T. Takagi, Department of Electronics in Kyoto University. The first data concerning the technique were published by T. Takagi et al. at the Second International Conference on Ion Sources at Vienna (1972). Since then, the data related to the ion source and the characteristics of the films prepared by the ICB technique have been published by the author and his coworkers. This thesis is mainly composed

of these reported publications and is intended to summarize the many significant findings obtained during the research about the film formation using the ICB technique and its applications to the electron devices. In particular, the emphasis is placed on the ion actions for film formation and the several advantages of the ICB technique. The author hopes that the studies in this thesis will stimulate the further development in the ion-based techniques and will provide the usefulness for the study on the film formation.

February 1981

Hiroshi TAKAOKA

ACKNOWLEDGMENTS

The author wishes to express his deep appreciation to Professor Toshinori Takagi, this thesis advisor, for his continuous encouragement and guidance, invaluable advice given by this present research. The author also wishes to express his grateful thanks to Professor Akio Sasaki for his stimulating discussions and criticism on this manuscript. The author is grateful to Associate Professor Isao Yamada for his valuable suggestions and discussions on the manuscript. The author is also grateful to Associate Professor Kakuei Matsubara for his stimulating discussions during this research.

Grateful appreciation is due to Dr. Junzo Ishikawa, Dr. Yoshikazu Takeda and Dr. Fumimichi Sano for their useful discussions. Appreciation is also due to Associate Professor Hiroyuki Matsunami, Dr. Junji Saraie, Dr. Akira Suzuki and Mr. Shigeru Nishino for their discussions and experimental facilities.

The author is indebted to Associate Professor Mitsuzo Osamura in the department of Metallurgy and the members of Heavy Ion Groups in the department of Nucleus for their interest and experimental facilities.

The author is indebted to Dr. Peter H. Rose and Mr. Allen Kirkpatrick in Eaton Corporation for their useful comments and proofreading on the manuscript. Thanks are also due to Mr. Ali Motamed Ektessabi for his comments on the manuscript.

The author thanks the members of Professor Takagi's Research Groups for their useful discussions.

The author acknowledges the construction of the ICB system used for the Si deposition and epitaxy by Osaka Koon Co., Ltd., and the construction of the ICB system used for the cluster beam analysis by World Engineering Co., Ltd.

The author wishes to thank Miss K. Chikazawa who typed various sections of this manuscript.

Finally, the author would like to thank his past father for his support and encouragement, who was looking forward to the success of this research.

CONTENTS

LIST OF FIGURES

LIST OF TABLES

I INTRODUCTION

Recently many scientists have shown much interest in the research and development of surface processes by "Ion-based techniques", in which the kinetic energy and the ion content of the deposited materials are easily controlled by changing experimental conditions. The object of ionization is to utilize the inherent properties of materials by giving some kinetic energy through the ionization process. Chemical activity includes the film formation activity and the enhancement of the chemical reaction by ionization. The presence of the ionized particles in the evaporated materials, even without acceleration of the ionized particles, greatly influences the critical parameters of the condensation process for the film formation. Moreover, adhesion strength, packing density, surface morphology, crystalline state and structure of the deposited films, or efficiency of synthesis of deposited compound materials, etc. are improved remarkably by the acceleration of the ionized particles [1)-13)].

From the standpoint that the ionization of the material is only a step to provide them with some kinetic energy or to enhance their chemical activity, it is not always necessary to ionize each atom and/or all of the atoms if ionized vapor aggregates, i.e. clusters can be produced. Based on this idea, the Ionized Cluster Beam (ICB) technique was proposed by T.Takagi in 1972 [14)]. Clusters which consist of about 500 - 2000 individual atoms loosely coupled together are generated by an adiabatic expansion of the vaporized material through a

nozzle. Several tens per cent of these clusters are ionized by electron bombardment and are accelerated to a substrate surface. Both ionized and neutral clusters are broken up into atoms and are scattered over the surface (migration effects), resulting in a great improvement in the crystalline state of the deposited film. In addition to the general effects of accelerated ions in the ion-based technique, the enhanced migration effect of adatoms after bombardment of the clusters on the substrate surface is one of the most important characteristics of the technique [15),16)]. As an ionized cluster is always singly charged, i.e. only one atom in a cluster is ionized, ionized clusters possess a small charge-to-mass ratio, which reduces the charging up of the insulator substrate due to an accumulation of positive charge and also eliminates problems caused by space charge repulsion in high current ion beam transport [17)].

The objects of the research by the author are as follows:

(1) to develop and extend the Ionized Cluster Beam (ICB) technique as one of the ion-based techniques, which is promising for film formation used for active and passive thin film devices, and

(2) to investigate the cluster formation mechanism and the film formation mechanism by using the ICB technique.

Although it is difficult to make clear the film formation mechanism because of complicated interdependences among the experimental conditions, the results obtained in this thesis are considered to be useful basis for a discussion of the mechanism of film growth.

In this thesis, the cluster formation and film formation mechanisms are discussed and also the structures and characteristics of the ICB technique and the physical and crystallographic properties of films prepared by the ICB technique as practical applications are described.

Chapter II describes the various kinds of film formation methods and the ICB technique from a standpoint of the ion-based technique. In chapter III, the cluster formation and growth is studied theoretically and experimentally together with the characteristics of the ionized cluster beam. The vaporized-metal clusters are formed by using an adiabatic expansion of various flow, but according to the classical theory of the droplet model, it was considered that a cluster of metal atoms could not be formed, when the value of the surface tension of the bulk liquid is applied. A recent theory predicts that the concept of the surface tension conventionally used can not be applied to the cluster, although the classical theory such as the Kelvin equation is considered to be able to be used for a qualitative discussion on the cluster formation [18)-20)]. In this chapter, the theoretical considerations on cluster formation are provided. Chapter IV deals with the film formation mechanism by the ICB deposition and epitaxy, taking account of the effects of the kinetic energy and the presence of ions for film formation. In addition, this chapter is concerned with the characteristic properties of thin films prepared by the ICB technique, and the applications to electron devices of the films. Chapter V provides the concluding remarks of this thesis.

II ION-BASED TECHNIQUE FOR FILM FORMATION

§2.1 INTRODUCTION

Ions transfer energy, momentum and charge with all the inherent properties of the neutral materials to a substrate or to a depositing film surface. The kinetic energy due to an accelerating voltage and/or the enhanced chemical activity by the exsistence of charge can be utilized effectively for deposition and epitaxy in the "Ion-based technique". Using the relation between thermal and electrical energies, i.e. $kT/e = T/1.16 \times 10^4$ eV, equivalent temperature of the accelerated particles can be estimated. For example, T = 2300 K corresponds to 0.2 eV from the direct calculation by the above relationship. Therefore, a high equivalent temperature of the particles can be achieved by acceleration. By using these accelerated particles, a new type of film deposition or synthesis of the compound material which would not be expected by conventional thermal and chemical methods may be obtained. Figure 2.1 shows the typical preparation methods for film formation from a view point of the kinetic energy of the source materials.

The kinetic energy of ions produces the fundamental effects on the film formation, that is, sputtering, implantation, nucleation, heating, etc. The principal objectives are; (1) to sputter and clean the substrate surface (improvement of the degree of cleanliness and of the adhesion strength), (2) to etch the surface deeply (mechanical improvement of the adhesion), (3) to blend the sputtered substrate material with the evaporated particles (forming an interfacial layer), (4) to produce many

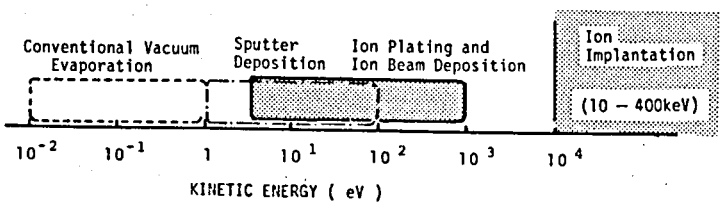

Fig.2.1 Typical preparation methods for film formation from a view point of the kinetic energy of the source materials

defects on the substrate surface which can act as nucleation centers during the initial stages of film formation and to produce additional nucleation sites through the displacement of atoms in the substrate lattice (enhancement of interfacial formation and strengthening of the interfacial bonding), (5) to bombard and sputter the depositing film surface during film formation (change in the growth morphology), (6) to introduce an ion implantation effect (enhancement of interfacial layer formation), and (7) to provide the thermal energy, converted from kinetic energy of bombarded ions to the surface of a substrate and depositing layer, and to heat the surface resulting in a self annealing effect (change in the growth morphology and increase in chemical reaction rates). Although the effectiveness of these factors alters by a combination of deposited film and substrate materials, it can be controlled by changing acceleration voltages and the number of ions, or moderating the annealing temperature of substrate during deposition.

For the case of the process of film formation by the Ionized Cluster Beam (ICB) deposition as shown in Fig.2.2, kinetic energy of accelerated cluster ions is converted to thermal energy, sputtering energy, implantation energy and migration energy upon impinging the substrate surface. In particular, the migration energy affects substantially to the crystalline state of the deposited film. In order to grow a single crystal layer, the diffusion speed is required to be greater than the growing speed of the film. The migration effect of this technique enhances the surface diffusion energy, and thus yields a good crystalline state of the deposited film with a high

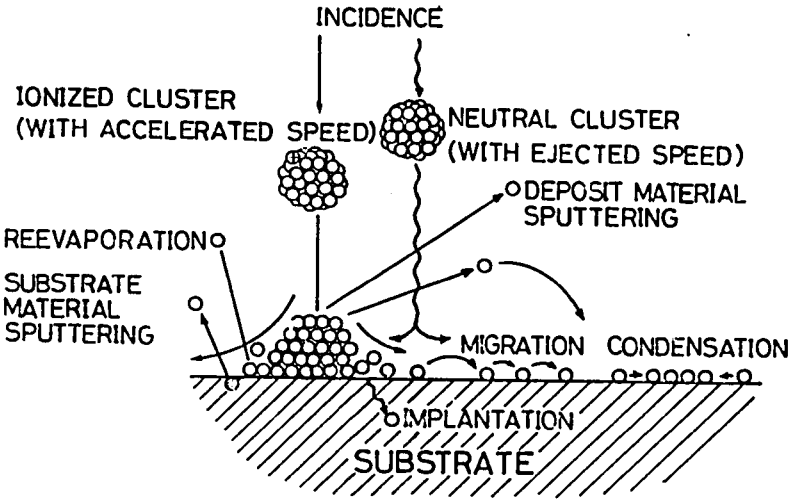

Fig.2.2 Film formation process by the ICB deposition technique

growing rate.

On the other hand, the presence of ions produces a remarkable change in the chemical activity, which includes the chemical film formation activity and the enhancement of chemical reaction. In particular, it greatly influences the critical parameters of the condensation process for film formation, even without the acceleration of the ionized particles and even when only a few per cent of ionized particles are included in the source materials. Therefore, the physical and crystallographical characteristics of the deposited films can be remarkably improved by adjusting the ion content.

In this chapter, the role of ions for film formation will be discussed. Further, several kinds of ion-based techniques including the Ionized Cluster Beam (ICB) technique will be investigated and summarized, based on the processes of the ionization and the acceleration of the source materials.

§2.2 ROLE OF IONS FOR FILM FORMATION

2.2.1 Effect of Inert Gas Ion Bombardment during Film Formation

The attention of a large number of scientists has recently been directed to the idea of film growth control by means of ion bombardment. For example, the effects of ion bombardment (10 keV Ar ions with an ion current of 8 μA) on the crystallographic orientation in vacuum condensed Ag and Au films were investigated by D.D.Dobrev and M.V.Marinov in 1972 [11]. It was also shown by the same group that vacuum condensed Cd and Co thin films on the glass substrates change their crystallographic

structure after bombardment with 10 keV energy ions (2 - 3 μA/mm^2) [9]. The films of Cd showed a $<11\bar{2}0>$ orientation of the crystal after bombardment. This orientation does not depend on the initial orientation and corresponds to the direction of minimum loss of energy per unit distance of the incident Ar ions. M.V.Marinov also discussed the effect of ion bombardment on the initial stages of thin film growth by using Ag deposition onto amorphous substrate with accelerated Ar ions of 1 to 10 keV energy [10]. Thus, the ion bombardment enhanced the surface mobilities of both adatoms and crystallite, thereby accelerating the nucleation, growth and coalescence of the nuclei. The change in structure of the substrate surface that takes place under ion bombardment leads to the creation of active sites that stimulate the nucleation process. Moreover, the appearance of a preferential crystal orientation from the very beginning of the process reveals some possibilities for the formation of epitaxial films of good quality.

A study of the effects of ion bombardment (Ar^+, Ne^+, 100 eV - 3 keV, 0 - 10 μA/cm^2) on the process of metallic (Zn, Sb) film formation on semiconductor (Cu_2O) and ionic crystal (NaCl, KCl) substrates has been made by V.O.Babaev et al. in 1975 [5]. In the experiment, effects of the inert gas ion bombardment on critical pressures of the condensation process were investigated. Figure 2.3 shows the observed dependences of the critical pressure P on the substrate temperature with ion bombardment and without ion bombardment. The figure shows that ion bombardment decreases the critical pressure, which results in the increase of the number of nuclei, but does not change the film-

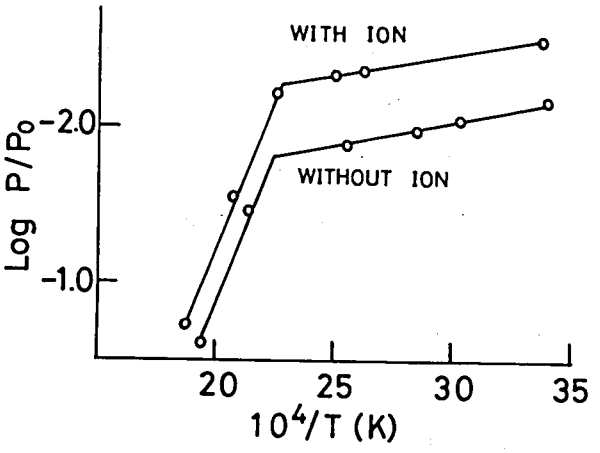

Fig.2.3 Effect of the ion bombardmnet on the critical pressure: with ion bombardment and without ion bombardment

substrate binding energy, which is indicated from the parallel shift of the curves. As a result of the experiment, it was concluded that increased adatom mobility, increased nucleation rate and effective supersaturation are considered to be due to the effects of ion bombardment. The increase in concentration of smaller condensation centers observed under ion bombardment caused the development of nucleus orientation. Also, ion bombardment stimulates the coalescence on non-oriented substrates.

Studies on Ge films deposited under simultaneous Ar ion bombardment were made by E.H.Hirsch et al. [6] in 1978 to investigate the effect of ion bombardment on the adherence of Ge films. In the experiments, the Ar ion beam was adjusted to only 2 μA with 1.65 keV. The ions constituted only 4 % of the total particle flux reaching the substrate, but nevertheless ion bombardment had a profound effect on the properties of the Ge films as shown in Fig.2.4. In the absence of ion bombardment, the intrinsic stress within the film had increased to such an extent that the material was lifted from the substrate in long flakes, but when the surface was bombarded with Ar ions during the evaporation, the deposit was then strongly adherent and showed no sign of flaking or fracture anywhere on the bombarded area. It follows that ion bombardment causes stronger bonding between the film and the substrate, or that it leads to a decrease in the intrinsic film stress, or that possibly it produces a combination of these two effects.

Recently, a dual ion beam deposition technique has been proposed by Chr. Weissmantel and his group [3),4)]. As shown

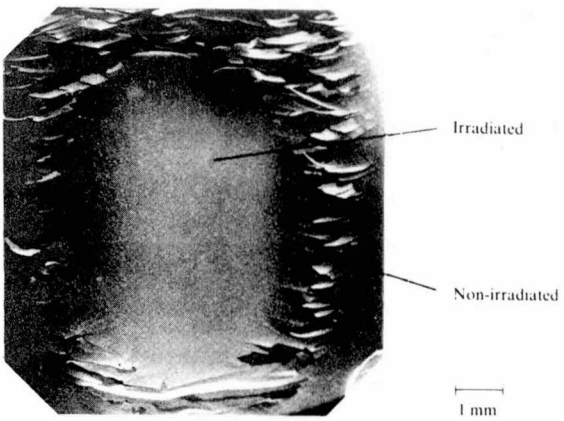

An irradiated germanium film.

Fig.2.4 Effect of the Ar ion bombardment on the Ge film

in Fig.2.5, two ion beam sources are attached to a chamber in such a way that one source is used to produce a flux of sputtered particles from a solid target, while the other source allows the growing film to be bombarded with inert or reactive ions at the low energy of 1 keV and the ion current of a few hundred mA/cm^2. In the experiments, normal ion beam sputtering of a graphite target yielded only blackish amorphous layers. However, when the growing film was bombarded with Ar ions of about 1 keV at a current density of the order of some 100 mA/cm^2, the layers become transparent and very hard. Diamond-like carbon films were obtained. It should be noted that the bombardment of ion beam sputtered metal films during their growth by inert gas ions also causes distinct changes of the film properties. Table 2.1 listed the irradiation effects of inert gas ions during film formation reported so far [3),5),6),9)-11)].

2.2.2 Kinetic Energy of Source Material Ions

The kinetic energies of the source particles with the inherent properties of the neutral materials greatly influence the film formation. Figure 2.6 shows the predominant ion actions at different energy ranges [21)]. The predominant ion energy for film deposition can be expected in the energy range of 10^{-2} - 10^4 eV. For example, the energy which mainly contributes to initial conditions of film formation is in the range of 10^{-2} - 10 eV, and the energy corresponding to the desorption of adsorbed atoms, that is, the release of chemical and physical adsorbed atoms on a surface, is in the range of 10^{-1} - 100 eV. In the

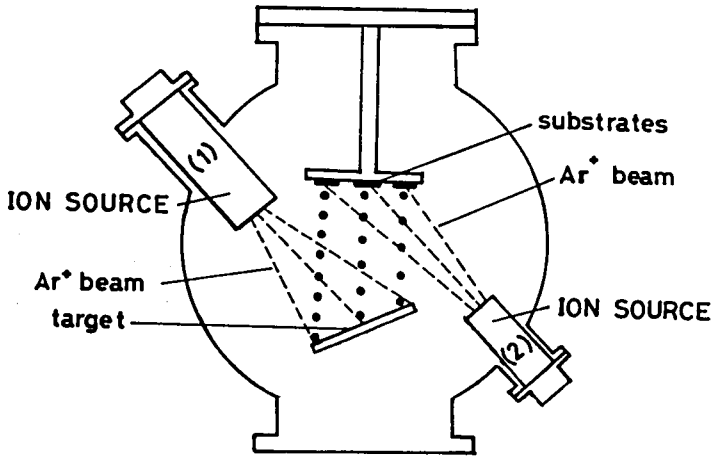

Fig.2.5 Schematic diagram of dual ion beam deposition

Table 2.1 Irradiation effect of inert gas ion bombardment during the film formation

Bombarding Ion		Deposited Materials by Vacuum Evaporation (by Sputter Deposition*) / Substrate Materials	Results
Ar^+ Ne^+	100eV-3keV (0 - 10uA)	Zn , Sb / semiconductor(Cu_2O), ionic crystal substrate (NaCl , KCl)	◦ Change of critical pressures of the condensation process ◦ Change of the capture cross section of an atom ◦ Increasing of adatom mobility and nucleation rate ◦ Stimulation of coalescence
Ar^+	10keV,8μA	Ag , Au / glass substrate	Crystallographic orientation
	10keV ($2-3\mu A/mm^2$)	Cd , Co / glass substrate	$(11\bar{2}0)$ orientation
	1 - 10 keV	Ag / amorphous substrate	◦ Enhancement of the depositing surface mobility ◦ Acceleration of the nucleation,growth and coalescence of the nuclei ◦ Preferential crystal orientation
	1.65keV (2 μA) (Only 4% of the total particle flux reaching the substrate)	Ge / glass substrate	Improvement of adhesion (Stronger bonding, decrease in the film stress)
	0.5 - 1 keV (Some $10^2\mu A$ - $10^2 mA/cm^2$)	Carbon* / glass substrate	Formation of diamond-like carbon film

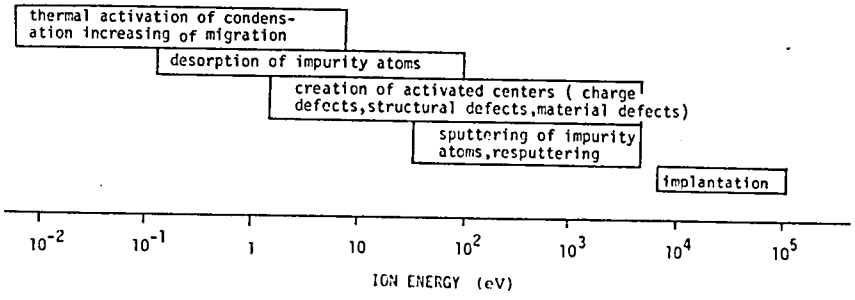

Fig.2.6 Predominant ion actions within different energy range

energy range between 1 and 10^4 eV, a part of the kinetic energy is converted to thermal energy and the substrate surface will be heated, and lattice defects may also occur due to impingement of such energetic particles. In the range of several tens to 10^4 eV, sputtering effects become predominant, although the effectiveness depends upon the combination of the incident particles and the substrate materials. Further, as the energy increases over 10^4 eV, implantation effects become of growing importance. In addition to the irradiation effects by accelerated particles, nucleation and growth effects as mentioned in the previous section, should be considered and are important for film formation.

The efficiency of material collection is controlled by the sticking probability and the self-sputtering ratio. Film formation can not be obtained in the case of the sputtering rate $S(E) \simeq 1$, which is given at energies lower than 1 keV by [22]

$$S(E) = \frac{3\alpha_0 M_1 M_2}{\pi^2 (M_1+M_2)^2} \cdot \frac{E}{V_0} , \qquad (2.1)$$

where M_1, M_2 are the mass of the incident ion and the mass of the element in the substrate, E is the energy of the incident ions, V_0 is the potential barrier height of the substrate surface, and α_0 is the factor depending on M_2/M_1. In a case of Ge^+/Ge system, which represents the deposition of Ge ions onto the Ge substrate, $S(E) \simeq 1$ at E = 400 eV, and in the Ge^+/Si system $S(E) \simeq 1$ at E = 700 eV [23),24)]. Therefore, the incident ion energies should be adjusted below these values.

The direct collection of Co, Ni, Cu, Zn and Sn ions onto a graphite substrate was investigated by A.Fontell et al. in 1969 [25]. For these ions, the highest energies at which the building-up of a layer was observed are shown in Table 2.2. Further, if the sticking probability is too low, the film can not be formed even though $S(E) < 1$. For the results obtained by A.Fontel et al., the sticking probabilities reach unity at the energies as low as 100 - 200 eV except for Zn. However, at the energy of about 10 eV the sticking probabilities decrease to very low values. The collection efficiencies measured around this low energy depend only on the sticking probability, because sputtering losses in the building-up process of film can be neglected. Following these considerations, the optimum energy should be less than that for which $S(E) = 1$ and also larger than that at which the sticking probability is small. An optimum value of kinetic energy of ionized and accelerated particles is estimated to be in the range of a few eV to a few hundred eV for film formation. Of course the optimum energy range depends on the type of film desired which varies according to purpose and the combination of deposit and substrate materials.

2.2.3 Influence of Presence of Ions on Film Quality

It is significant to summarize the influence of the ionized particles on the film quality from the view point of enhanced chemical activity through the presence of ionized atoms as distinct from kinetic energy effects. A profound effect caused by the presence of the ions is the production of a marked change

Table 2.2 Energy regions where the building-up of a layer starts

ION SPECIES	CRITICAL ENERGY (keV)
Fe^+	2.0 - 1.5
Co^+	1.5 - 1.0
Ni^+	1.0 - 0.8
Cu^+	0.4 - 0.3
Zn^+	0.4 - 0.3
Sn^+	0.5 - 0.45

in the critical condensation pressure of the deposited materials, which is closely related to the growing mechanism of the nuclei. The presence of charged particles increases the free energy which is the sum of the surface energy and the electrostatic energy. The increase in the free energy would be accommodated by an increase in the surface area, i.e. the island becomes flattened and the coalescence of the islands is stimulated effectively [26),27)]. Although several possible origins for the force of stimulating coalescence have been proposed, D.B.Dove evaluated the electrostatic force F between the two electrically charged islands using the following expression [28)],

$$F = \frac{q_1 q_2}{4\pi\varepsilon_0 d^2} - \frac{q_1^2 r_2 d}{4\pi\varepsilon_0 (r_1^2 - d^2)^2} - \frac{q_2^2 r_1 d}{4\pi\varepsilon_0 (r_2^2 - d^2)^2} , \quad (2.2)$$

where r_1 and r_2 are the radi of the two islands, q_1 and q_2 are the charges, d is the separation distance and ε_0 is the permittivity constant. Thus, if either charge is much larger than the other, or the radi are nearly equal to the separation distance, the attractive image forces as expressed in the second and third terms of Eq. (2.2) dominate irrespective of the sign of charges, which would enhance the probability of the coalescence of the islands. Therefore, the physical and crystallographical characteristics of the deposited films can be expected to be remarkably improved, when ionized particles are included. The films deposited and grown in the presence of ions have not only good crystallinity or a high lusterous

surface compared to the case where no-ions are involved, but also have high adhesion to a substrate surface. Moreover, with only a few per cent ionization, the substrate temperature for epitaxial growth decreases, and so the amount of strain in the growing film can be reduced. The experimental results of simultaneous Ar ion bombardment during the evaporation of Ge, and of the dual ion beam deposition, which were mentioned in the previous section, arouse interest in this connection. It was demonstrated by Y.Namba et al. [7),8)] that heteroepitaxial growth of Ag or ZnTe on NaCl substrates was notably favoured by the presence of ions in the deposit particle flux, and no distinct dependence on ion energy could be found.

The presence of ions is also important to enhance the chemical reaction activity of the evaporated materials, and it is useful to obtain good quality thin films of oxide, nitride, carbide, e.g. ZnO, BeO, GaN, TiC, SiC and other materials with a high melting point. In the case of ZnO films prepared by a reactive Ionized Cluster Beam (R-ICB) technique to be described later, a good quality film having a preferential orientation to the c-axis could be obtained by only increasing the electron current for ionization without acceleration of the ionized particles. Figure 2.7 shows the RHEED patterns of the ZnO films deposited onto a glass substrate with varying electron current for ionization. The crystallinity of the film is improved as the current becomes larger. It should be added that the respective amount of the clusters which were ionized was approximately 15 % at I_e = 150 mA and 30 - 35 % at I_e = 300 mA in the experiment and moreover, each ionized cluster

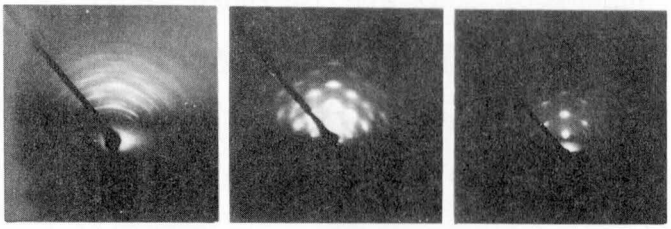

(A) I_E=0 mA (B) I_E=150 mA (C) I_E=300 mA

Fig.2.7 Influence of electron current for ionization on the crystallinity of the ZnO films

had only a single charge in spite of consisting of 500 - 2000 atoms per cluster.

§2.3 VARIOUS KINDS OF FILM FORMATION METHODS FROM A STANDPOINT OF ION-BASED TECHNIQUES

2.3.1 Vacuum Evaporation Method [29)]

A source material is evaporated from a heated metal wire or boat with the thermal energy corresponding to about 0 eV in the apparatus of the type shown in Fig.2.8. When the source material is thermally evaporated and drifts to a substrate, only a very small number of ions are included in it. Therefore, the physical and crystallographic properties of the film deposited on the substrate can be expected to be altered by applying an acceleration voltage parallel or perpendicular to the substrate [26),27)].

As another improved and modified method, the activated reactive evaporation process as shown in Fig.2.9 was made to prepare compound films such as carbides, oxides and nitrides [30)-33)]. The metal or alloy vapors are produced in the presence of a partial pressure of reactive gas to form a compound either in the gas phase or on the substrate. In this process, the low energy secondary electrons from the plasma sheath are pulled upwards into the reaction zone by the positive potential of 20 - 100 eV applied at the electrode. These low energy electrons ionize or activate the metal and gas atoms, which results in increasing the reaction probability on collision of these atoms.

In the vacuum evaporation method, most of the source materials are neutral and their kinetic energies are in a range of

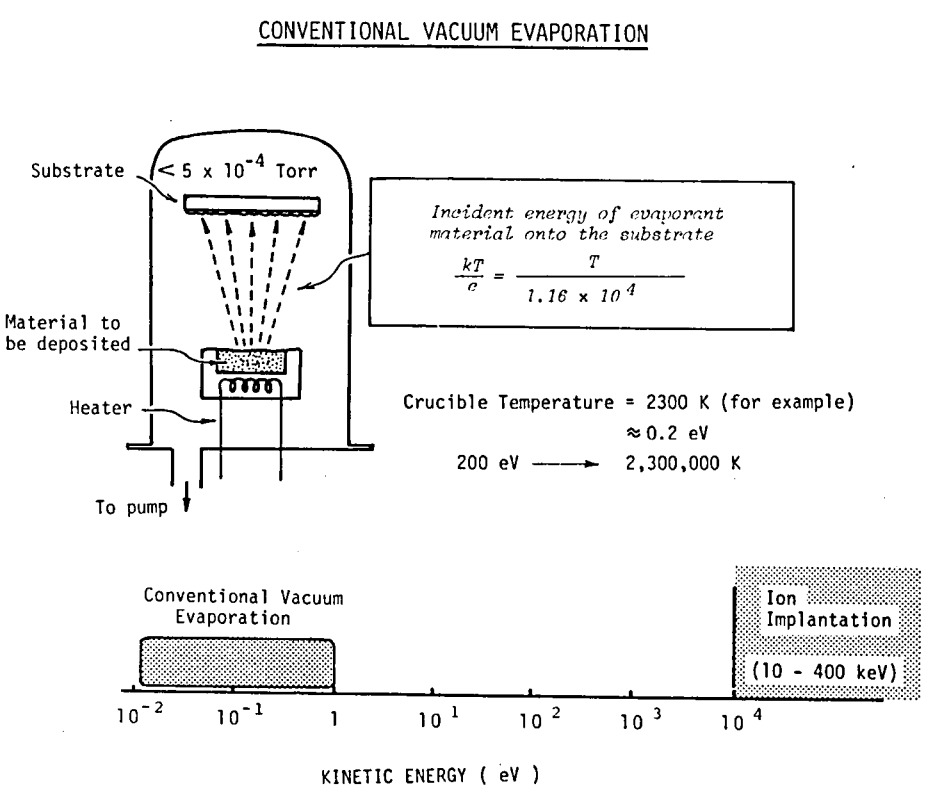

Fig.2.8 Schematic diagram of conventional vacuum evaporation method together with the used energy range

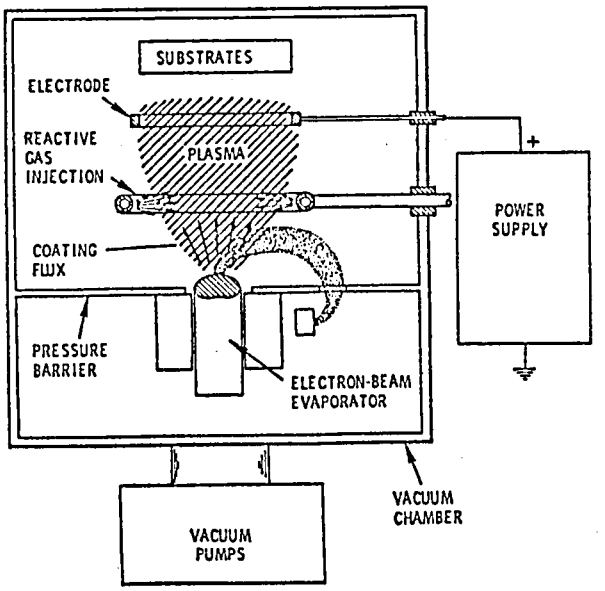

Fig.2.9 Schematic diagram of the activated reactive evaporation process

0.01 - 1 eV. However, by accelerating only a small amount of ions contained in the source material, the physical and crystallographical properties of films can be altered and in addition by ionizing or activating the metal and gas atoms, the chemical reaction can be enhanced and the compound films can be easily prepared.

2.3.2 Sputter Deposition Method [34)-36)]

Sputtering is the process by which surface atoms of a target are ejected by bombardment by energetic atoms, which can be created by ions from a plasma (10^{-3} - 10^{-1} Torr) or by accelerated ions moving in a high vacuum region (10^{-7} - 10^{-4} Torr). The surface atoms ejected by bombarding positive ions such as a heavy inert gas like argon can be deposited on a substrate to form a thin film. As shown in Fig.2.10, the energy range of the depositing material, most of which are neutral atoms and molecules, lies between a few eV and a hundred eV, although the incident ions on the sputter target may have an energy from a few hundred eV to a few tens keV.

When deposition is done by sputtering from a plasma, the sputtered atoms undergo many collisions with gas atoms before reaching the substrate, and indeed a high proportion may be backsputtered onto the target surface. These collisions attenuate the initially high ejection energy and as a result the energy range of the sputtered paticles arriving on the substrate is between a few eV and a hundred eV as already mentioned above. In this sputter deposition method, both DC sputtering and RF sputtering must be considered. DC sputtering, as shown in

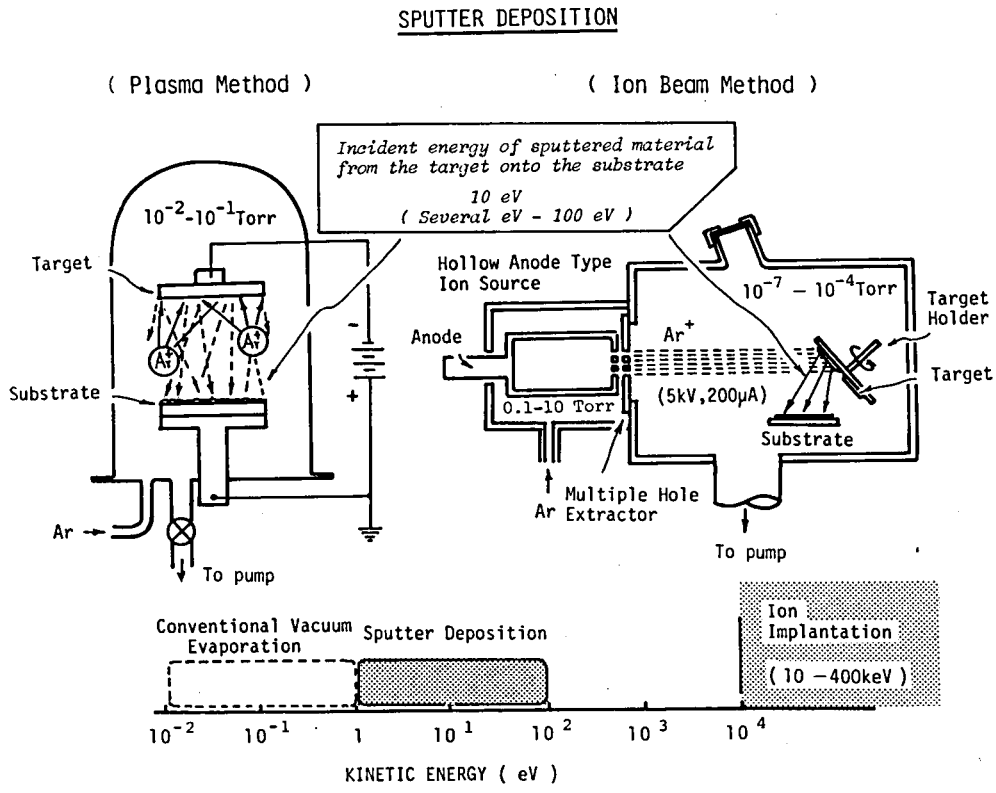

Fig.2.10 Schematic diagram of sputter deposition process including the plasma method and the ion beam method, together with the used energy range

Fig.2.10, is the method by which material is sputtered mostly in the neutral state from the metal cathode bombarded by Ar ions into the space between the cathode and the anode, where the DC acceleration voltage, e.g. a few kV, is applied. In this method, sputtered particles possess much higher energies than particles generated by thermal evaporation, and the mean energy is as high as 10 eV, which depends on the energy of the bombarding ions. On the other hand, the RF sputtering [37),38)] is the sputtering process directly from a target by applying a RF potential with a typical frquency of the range of 50 kHz and 50 MHz between the cathode, on which even the insulating target is possible to be supported, and the anode. The more efficient ionization in the glow discharge region caused by the RF excitation of electrons enables the discharge to be maintained at low pressure (e.g. 5×10^{-3} - 10^{-2} Torr). The growing film is subjected to bombardment by energetic neutral atoms and ionized particles, which have an important influence upon structural quality and possibly upon physical properties.

As a modified type of sputter deposition in the plasma, a magnetron type of sputtering system shown in Fig.2.11 was developed in order to increase the sputter rate [39),40)]. The use of a magnetic field to trap electrons near the cathode surface increasing ionization efficiency, is the basis of high rate magnetron sputtering. The ionized particles included in the plasma promote chemical reactions and are used to produce compound films of high quality. In addition, if a reactive gas such as oxygen or nitrogen mixed with an argon gas is introduced in a glow discharge region, it reacts with the depositing mate-

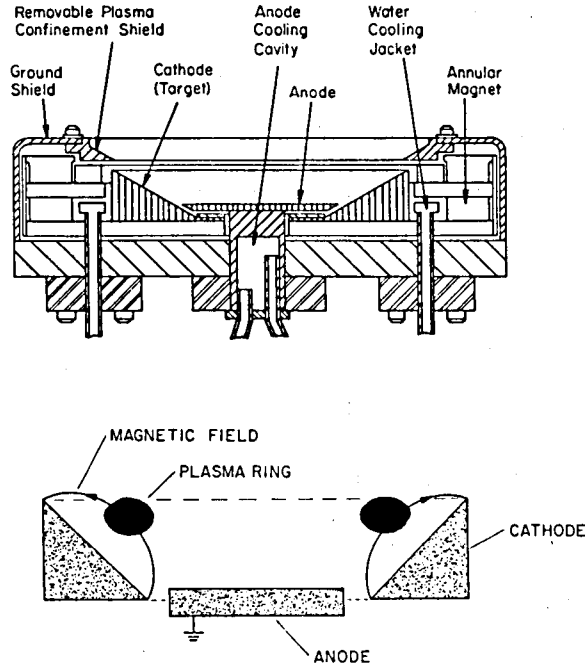

Fig.2.11 Schematic diagram of magnetron type sputter deposition source

rial, and the films of completely reacted materials, i.e. oxide or nitride films can be obtained. This method is known as reactive sputtering, and occurs not only with magnetron sputtering but also with any of the sputtering methods referred to above [41)-44)]. The ionization of the sputtered material and the reactive gas enhances the chemical reaction and the good compound films can be obtained.

In the ion beam method of sputtering [45)], the ion beam of inert gas such as argon gas is extracted at a few tens kV from an ion source into a high vacuum region, where a target material is sputtered by the energetic ion beam, and then the material sputtered mostly in a neutral state deposits on a substrate to form a thin film. This process is also shown in Fig.2.10. Most of the work on ion beam sputtering has been done so far with the Duoplasmatron type of ion source, which is capable of producing 5 - 25 mA of ion current with energies of 1 to 25 keV. In this method, the sputtered particles have the mean energy as high as up to 100 eV, depending on the energy of the bombarding ions and on the crystallographic direction of ejection. Studies on energies of ejection from Au target bombarded by Ar ions by M.W.Thomson et al. [46)] indicate that for two different crystal directions, energies along the more close-packed <110> directions are significantly higher, giving mean value of 93.5 eV compared with 22.7 eV for the <100> directions.

Among the experimental parameters used to distinguish between the plasma and ion beam methods is the vacuum pressure in a chamber. In plasma sputtering the operating pressure is between 10^{-4} - 10^{-3} Torr, and the mean free path of the gas

atoms is comparable to the working distances in the chamber. For the ion beam method, films are deposited in a high vacuum region using neutral atoms sputtered by the bombarding ions. A difference of the plasma method is that ions produced by the glow discharge have an influence on film formation. The kinetic energies of the sputtered particles by either method are higher than that of the conventional vacuum evaporation method and lie between a few eV and a hundred eV.

2.3.3 Ion Plating and Ion Beam Deposition Methods [45),47),48)]

Ion plating has been developed by D.M.Mattox as shown in Fig.2.12 [49),50)]. This method is essentially a combination of the evaporation from a heated wire and the use of a glow discharge. The ions in an abnormal glow discharge are produced in the negative glow region and are accelerated across the cathode dark space to the cathode. The mean free path at 10^{-2} Torr is about 0.5 cm and the cathode dark space is close to 10 cm at a bias voltage of 3 kV. Each ion will experience about 20 collisions on average before arriving at the cathode and will lose enery in the process. The number dN of ions arriving on the cathode in a unit time with energy V_c-V is given by [51)]

$$dN = \frac{N_0 \, Z_c}{2 \lambda \, V_c \cdot V} \exp\{ - \frac{Z_c (1 - V/V_c)}{\lambda} \} dV, \quad (2.3)$$

and the energy E is given by

$$E = \int_{V=0}^{V=V_c} (V_c - V) \, dN \simeq N_0 V_c \frac{2 \lambda}{Z_c} , \quad (2.4)$$

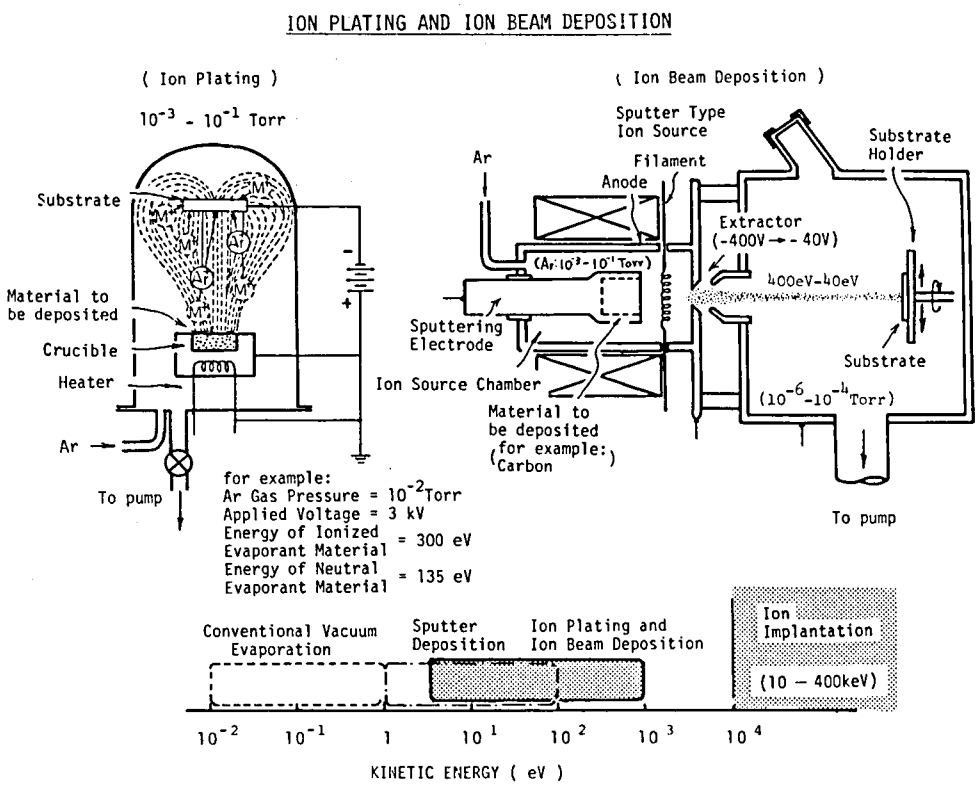

Fig.2.12 Schematic diagram of ion plating and ion beam deposition methods, together with the used energy range

where N_0 is the number of ions leaving the negative glow in unit time, Z_c is the length of the cathode dark space, λ is the mean free path, and V_c is the voltage across the cathode dark space (nearly equal to the applied voltage) [52]. It is apparent that if λ/Z_c is small, then the ion energy loss is large. The ions lose their energy in symmetric charge transfer collision, i.e. they transfer their energy to neutral atoms. If λ = 0.5 cm and Z_c = 10 cm, which are typical conditions for the plasma method, then on the average the ions lose almost 90 % of the energy dissipated in the glow discharge by transferring this energy to neutral atoms in traversing the cathode dark space. Therefore, the total number of energetic neutrals, i.e. $(Z_c/\lambda)\cdot N_0$ are produced. The average energy of the arriving ions is approximately $(V_c/Z_c)\cdot 2\lambda$ = 300 eV for a 3 kV discharge at 10^{-2} Torr gas pressure. The average energy of the neutral particles is $V_c(Z_c - 2\lambda)\cdot(\lambda/Z_c)/Z_c$ = 135 eV for the same conditions, assuming they suffer no further collisions after gaining their energy. From these considerations, it can be said that energetic neutral atoms (less than 135 eV) are in the majority and ions with not-so-high energy (about 300 eV) are in the minority for film formation, even where the substrate is set in the plasma region and the applied voltage is 3 kV.

Ion beam deposition is the generic term for the film deposition method in a high vacuum region (10^{-7} - 10^{-4} Torr) using ions with or without a neutral atom component. Inert gas ions or reactive gas ions are used separately or together.

The concept of the ion beam deposition without mass analysis was proposed by W.E.Flynt [53] in 1961 to fabricate micromini-

aturized electronic circuits. Since then, there are many reported experimental results as listed in Table 2.3 [54)-59)]. As shown in Fig.2.12, ions of the film material are generated in the ion source and extracted into a high vacuum region by suitable acceleration voltage [60)]. In the experiments, the substrate was cleaned by sputtering due to carbon and Ar ions extracted at -400 V before deposition and most of the film deposition occurred at about -40 eV.

As another approach employing the modified ion beam deposition technique, an attempt to combine conventional vacuum evaporation and low energy ion implantation was carried out by T. Takagi et al [58)] in 1972 with an apparatus as shown in Fig.2.13. Using Mn ions at the acceleration voltage of 5 kV and the deposition of ZnS by a conventional vacuum evaporation, low impedance DC electroluminescent ZnS:Mn cells without any coactivator have been developed. The similar study was investigated by J.Dudonis et al [59)] in 1975, where O_2 ion implantation (energy of 1 - 10 keV, Maximum ion current of 3 mA) was used during film growth of evaporated Al and SiO materials. In this technique, the ion acceleration voltage is about a few kV which is not enough to cause penetration into the substrate. Even for these low energy ions, the effect of the ions is enough to change the electrical characteristics of the film, if irradiation of the ions is continued during the film formation.

On the other hand, facilities for film deposition using mass- and energy-selected ion beam in the high vacuum region have been developed since the beginning of the 1970's. In this method, a pure ion beam without neutral particles is used after

Table 2.3 Study on ion beam deposition using atomic or molecular ions without the mass analyzer

Deposited Materials / Substrate Materials	Operation Conditions	Results
Cr^+/glass substrate	230 eV, 2 μA(8.7 μA/mm^2)	Cr film formation (deposition rate 100 Å/min.)
Si^+,C^+/ single-crystal substrate, stainless-steel and glass substrate	40 eV for Carbon	Diamond-like carbon film formation (deposition rate 300 Å/min.)
Ga^++As^+; Ga^++P^+; / GaAs (100) In^++P^+ Si (111)	no additional accelerating voltage (two beam flux from different source)	Synthesis of III-V compounds
Mn^+ during ZnS evaporation	5 keV	Low impedance d.c. EL ZnS:Mn cells without coactivator (simultaneous method of implantation and deposition)
O_2^+ during film growth of evaporated Al and SiO	1 – 10 keV (3 mA max)	Investigation of thin SiO and Al films doped by O^+ ion implantation during film growth

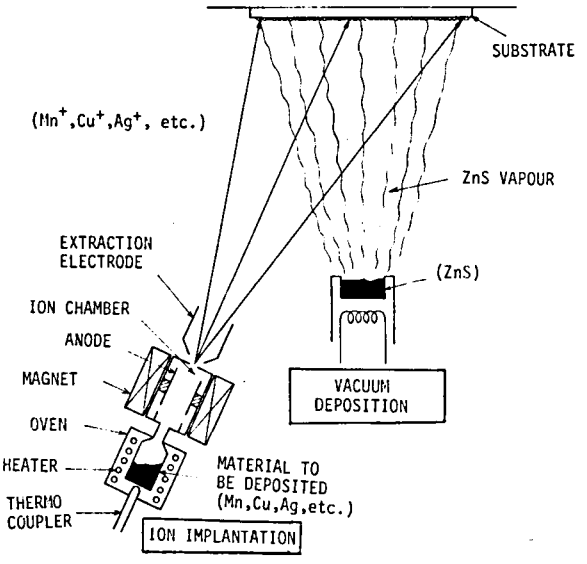

Fig. 2.13 Simultaneous method of ion implantation and deposition

deceleration to a suitable incident energy (a few tens to a few hundred eV) for the film formation. Table 2.4 listed some of the results reported so far [23),24),61)-72)].

Studies on the thin film deposition using low energy ion beam have been carried out by J.Amano et al. [62)-65)] in 1975. Figure 2.14 shows a schematic diagram of the ion beam deposition system. The deposition of Pb ions which are accelerated up to 5 kV and then decelerated to 24 - 256 V, was carried out on carbon and NaCl substrates with 9 - 12 μA ion beam under 10^{-8} Torr vacuum pressure. Ion energy of 50 eV is an optimum energy of deposition when parameters such as space charge expansion, self-sputtering, film thickness and surface coverage are taken into account. As the deposition energy is increased to above 50 eV, the crystalline structure of deposits grown on single crystal NaCl substrates becomes more ordered with a strongly preferred <111> orientation. The deposition of Mg ions on carbon substrates was studied in a range of energies between 24 and 500 eV. An incident Mg ion beam energy of about 100 eV produced the optimum film. The adhesion of the film was improved at high energies.

A similar system with an E x B mass analyzer was used for the deposition of Ag ions on a polycrystalline Pd and single crystal Si substrates by G.E.Thomas et al. [66)] in 1979. They named this type of deposition "Ion beam epiplantation". Ions extracted from the source at 10 keV were formed into a beam by an Einzel lens and were decelerated from 10 keV to roughly 20 eV after mass selection. Ag ion currents in the range 5 - 25 μA were deposited onto the substrate under 2 x 10^{-9} Torr vacuum

Table 2.4 Study on ion beam deposition using atomic or molecular ions with the mass analyzer

Deposited Materials / Substrate Materials	Operation Conditions	Results
Pb^+,Cu^+/ Si single-crystal substrate	(ion extraction voltage 20 kV) 60 eV, 15 μA for Pb^+	Pb film formation (deposition rate 100 Å/hr.) Si-Cu-Pb multiple layer film formation
Pb^+/ carbon and NaCl substrate	(ion extraction voltage 5 kV) 24 – 256 eV (9 – 12 μA)	strongly preferred (111) orientation
Mg^+/ carbon substrate	24 – 500 eV (100 eV optimum)	
Ag^+/ poly-crystalline Pd substrate, single crystal Si substrate	(ion extraction voltage 10 kV) 25 – 100 eV 5 – 25 μA	epitaxial growth of Ag (111)/ Si (111) at room temp.
Zn^+,Ag^+/ single crystal Al and Cu substrate, stainless substrate	30 – 300 eV	fundermental research on deposition mechanics
Ge^+/ single crystal Si and Ge substrates	(ion extraction voltage 30 kV) several 10 eV – several 100 eV	epitaxial growth of Ge film on Si (111) or Ge (111) substrate at a substrate temp. of 300°c
O_2^+ sputtering of Pb atoms	50 eV	Oxcide formation
Cu^+ in O_2, H_2S gas	20 eV – 500 eV for O_2, H_2S ambients	Formation of CuO or CuS films

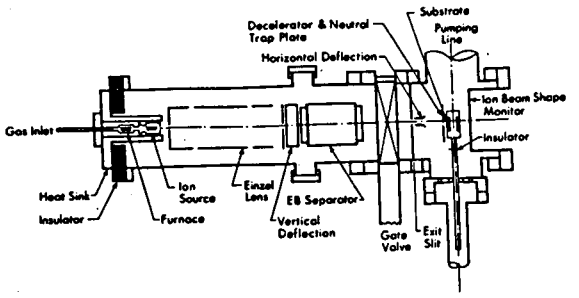

Fig.2.14 Ion gun and ion beam transportation sysyem

pressure. In the energy range 25 - 100 eV, Ag layers deposited onto Si (111) substrate at room temperature grew epitaxially with Ag(111)//Si(111).

From the considerations mentioned above, for the conventional ion plating in the plasma, the kinetic energy of the depositing particles is about 100 - 300 eV and the neutral particles also play an important role for film formation. For ion beam deposition with decelerating field, high energetic ions extracted into a high vacuum region are utilized for film formation after deceleration in the order of several tens to several hundred eV.

2.3.4 Ionized Cluster Beam Technique [14)-17),73)-90)]

The Ionized Cluster Beam (ICB) technique, which has been developed by T.Takagi et al., are classified as (1) standard and (2) reactive types. A schematic diagram of these sources is shown in Fig.2.15. Figure 2.15 (a) shows the standard type of ICB system and Fig.2.15 (b) shows one of the types for the R-ICB system.

For the ICB epitaxy, metal or semiconductor vapor to be deposited is ejected into a high vacuum chamber through the small nozzle of a special crucible in which material is vaporized at high temperature. The temperature of the crucible is controlled to maintain the optimum vapor pressure, usually 10^{-2} to several Torr. The clusters are formed from supercondensation phenomena following adiabatic expansion through the nozzle. The clusters contain 500 - 2000 atoms loosely coupled together, which is different from the droplet (liquid par-

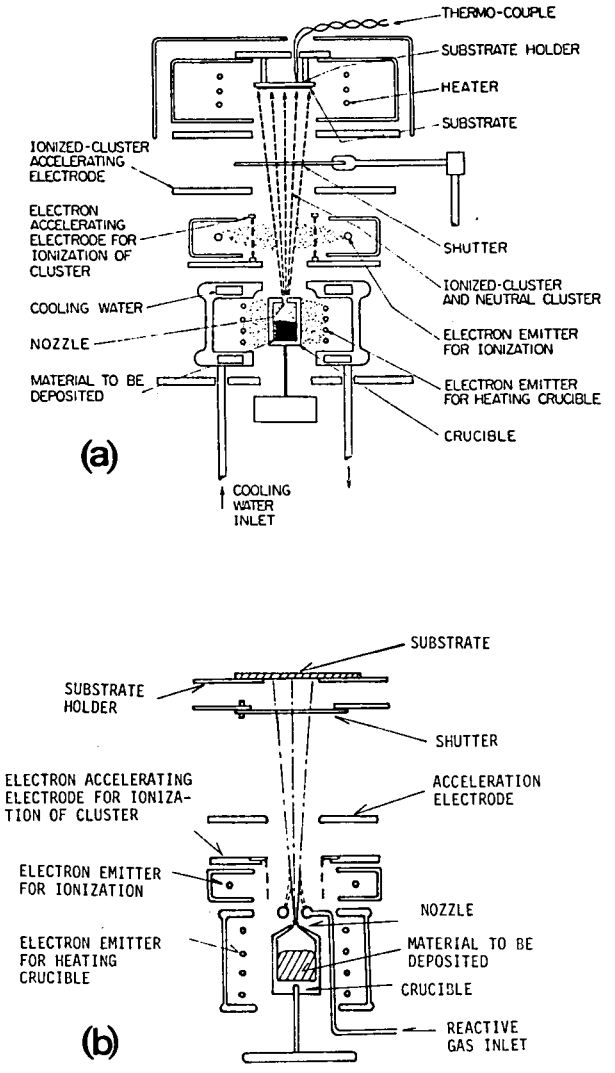

Fig.2.15 Schematic diagram of the ICB source for epitaxy: (a) standard type and (b) reactive type

ticle) in that the droplet contains 5 x 10^8 - 5 x 10^9 atoms per droplet closely coupled to each other [91)-95)]. The clusters are ionized to be singly charged by electron bombardment in the ionization electrode assembly located above the crucible. The cluster ions are accelerated toward the substrate by a negative high potential applied to the accelerating electrode. Besides the ionized clusters, there are neutral clusters which remain unionized during flow in the ionization region. Although the neutral clusters are not accelerated by the voltage, they move toward the substrate at ejection velocity. Compared with other atomic- or molecular-ion-based techniques such as sputter deposition, ion plating, etc. which were described previously, one of the attractive features of the ICB technique was as follows: when the cluster is broken at its arrival on the substrate, each atom of the cluster has an average energy per atom of $\bar{E} = QV_a/N$, where Q is the electric charge, V_a is the acceleration voltage, N is the cluster size (number of atoms per cluster). By controlling V_a, it is possible to provide each atom with an energy high enough for surface diffusion ($\bar{E} \simeq 1$ eV) but not sufficient for inducing defects in the layer ($\bar{E} < 5$ eV). By monitoring the electric charge, it can be shown that although the charge on the cluster is sufficient to influence film formation, the actual electric charge content in the total cluster is very low. These features open the energy range of 1 to 20 eV per atom to investigation, whereas space-charge spreading effects require the accessible energy range to be as high as possible for deposition using charged atomic or molecular ions to ensure proper beam focusing and the maximum intensity [88)].

For the R-ICB technique, a reactive gas, e.g. oxygen gas is supplied from a gas nozzle near the metal vapor ejection area through a controlled leak valve to maintain a desired pressure in the chamber during the deposition. Some oxygen atoms or molecules are ionized together with the vaporized-metal clusters and accelerated toward the substrate, though the ionization efficiency of the oxygen atom or molecule is generally smaller than that of the cluster. The vaporized-metal cluster and the oxygen atoms react to form the metal oxide with the aid of the electric charge and/or the converted energy from the accelerated cluster ions. Therefore, film formation of an oxide is carried out by the impingement of ionized and neutral particles of vaporized-metal clusters and of ionized and neutral gas molecules.

For each type, a single and a multiple crucible system can be considered. The single crucible system is available for the deposition of a single element and some compound materials, where the vapor pressure of the composite element is almost equal. The multiple crucible system as shown in Fig.2.16, is used in the case that the vapor pressure of the composite elements is different. Some other ICB deposition systems have also been developed for special purposes, e.g. a single crucible system with multiple nozzles to form a ribbon beam for producing a wide sheet with high uniformity, which is shown in Fig.2.17.

The films deposited by the ICB and R-ICB technique and their features are listed in Table 2.5. As shown in this Table the ICB and R-ICB deposition are quite useful to grow thin films with good quality of not only metals, but also compounds and semi-

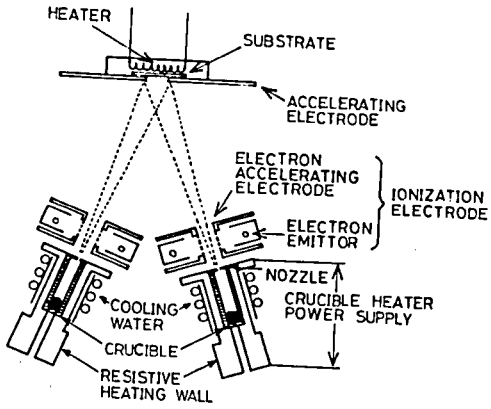

Fig.2.16 Schematic diagram of the ICB source with the multiple crucibles

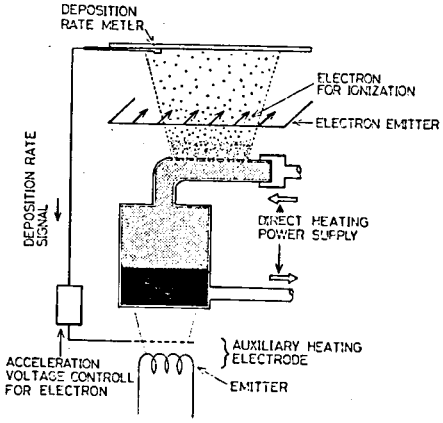

Fig.2.17 Schematic diagram of the ICB deposition system using the crucible with the multiple nozzles

Table 2.5 Optimum condition for film growth and advantages

(*Annealing temperature)

Film/substrate	Acceleration voltage (kV)	Substrate temperature (°C)	Crucible system	Advantages
Au, Cu/Glass, Capton	1 - 10	RT	Single	Strong adhesion, high packing density, good electric conduction in a very thin film
Ag/Si	5	RT(n-type) 400*(p-type)	Single	Ohmic contact without alloying process
Au-Sb/GaP	2	400	Single	Ohmic contact, strong adhesion
Pb/Glass	5	RT	Single	Controllable crystal structure, strong adhesion, smooth surface, improved stability on thermal cyclings
Si/(111)Si, (100)Si Si/(1$\bar{1}$02)Sapphire	6	620	Single	Low temperature epitaxy in a high vacuum (10^{-7}-10^{-5} Torr), shallow and sharp p-n junction
Amorphous Si/Glass	2	200	Single	Thermal stability
GaAs/Cr-doped GaAs	6	550	Multiple	Epitaxy in a high vacuum (10^{-7}-10^{-5} Torr)
GaP/GaP GaP/Si	4	550 450	Multiple	Low cost, low temperature in a high vacuum (10^{-7}-10^{-5} Torr)
ZnS/NaCl	1	200	Single	Single crystal formation
ZnS:Mn/Glass	1	200	Single	AC/DC low impedance type EL cell
CdTe/Glass	2	250	Single	Improved monocrystalline domains
C-axis preferentially oriented MnBi/Glass	0 (ejection velocity 300* only)		Multiple	Spatially uniform magnetic domain high density optical memory
Li-doped ZnO/(1$\bar{1}$02)Sapphire	0.5-1	230	Single (R-ICB)	Single crystal formation
C-axis preferentially oriented ZnO/Glass	0	150	Single (R-ICB)	Controllable crystal structure Controllable optical transmission
BeO/(0001)Sapphire	0	400	Single (R-ICB)	Single crystal formation, transparent film
C-axis preferentially oriented BeO/Glass	0	400	Single (R-ICB)	High electrical insulating and good thermal conducting coating, low temperature growth
PbO/Glass	3	RT	Single (R-ICB)	Low temperature growth, smooth surface, accurately controllable thickness, good adhesion
GaN/Glass	0	450	Single (R-ICB)	Low cost light emitting diode

conductors by adjusting the deposition conditions. In addition, it is thought that these techniques will become important for the fabrication of various kinds of solid state devices, e.g. electrooptic devices, etc.

§2.4 SUMMARY

In this work the main roles of ions in film formation were investigated. The summary is as follows: The effective incident energy required for film formation is found to be in the order of a few eV to several hundred eV. Chemical activity, which includes chemical film formation activity and chemical reaction enhanced through ionization, has strong influence on the film formation processes at a given kinetic energy. Therefore, the physical and crystallographic characteristics are affected by the presence of even a few per cent of ions.

Further, various kinds of preparation techniques for film formation and the Ionized Cluster Beam (ICB) technique were studied from a standpoint of the ion-based techniques. These techniques utilize the vapor of source materials in a state of thermal non-equilibrium, that is, the source materials are deposited on a substrate with the high energies corresponding to ejection velocity or accelerated velocity. For the vacuum evaporation and sputter deposition methods, most of the particles which contribute to film formation are neutral, and their kinetic energies are 0.01 to a few eV in the former method and a few to a few hundred eV in the latter method, respectively. In the conventional ion plating in a plasma, most part of the kinetic energy of ions is transferred to the neutral particles,

and both the ions and the neutral particles with the kinetic energy of the order of a few hundred eV contribute to film formation. In the technique which uses ion beam deposition directly for thin film formation, the high energetic ions extracted from an ion source are decelerated to be several tens or several hundred eV in energy, and form a film by themselves with or without the presence of neutral particles.

In the Ionized Cluster Beam (ICB) technique, clusters which consist of about 500 - 2000 individual atoms loosely coupled are used. These clusters are partially ionized (practically, ionized cluster comprises 10 - 50 % of the total and each ionized cluster has only one charge), and accelerated to the substrate by the applied voltage of 0 - a few kV. By this means, the number of charged atoms included in the total mass flux is very small and the energy of each atom is in the order of a few eV, an important energy range not easily realized by other deposition methods.

III IONIZED CLUSTER BEAM TECHNIQUE

The idea and the first data related to the generation and the ionization of the vaporized-metal cluster were reported by T.Takagi et al. at the Second International Conference on Ion Sources at Vienna in 1972 [14]. The cluster which consists of 500 - 2000 atoms loosely coupled is obtained by ejecting the vapor of many kinds of solid materials (metal, semiconductor and insulator) into a high vacuum region through a nozzle of a heated crucible. Some of the clusters are ionized to singly charged state by electron bombardment and accelerated toward the substrate.

In this chapter, the cluster formation and growth are investigated theoretically and the conditions of the vaporized-metal cluster formation are studied by measuring the energy and velocity of the cluster, because the kinetic energy of a cluster should be higher than that of an atomic state of the same element.

§3.1 CLUSTER FORMATION MECHANISM

With regard to vaporized-metal cluster formation in a supersonic nozzle beam by gaseous material, the theory of homogeneous nucleation and condensation in the supersaturated state [96)-105)] can be used and demonstrated. Figure 3.1 shows the conceptional picture of cluster formation and growth. The metal atoms in a crucible (region 1) collide and transfer their energies to each other and then they are in a supersaturated state by an adiabatic expansion, when they are ejected

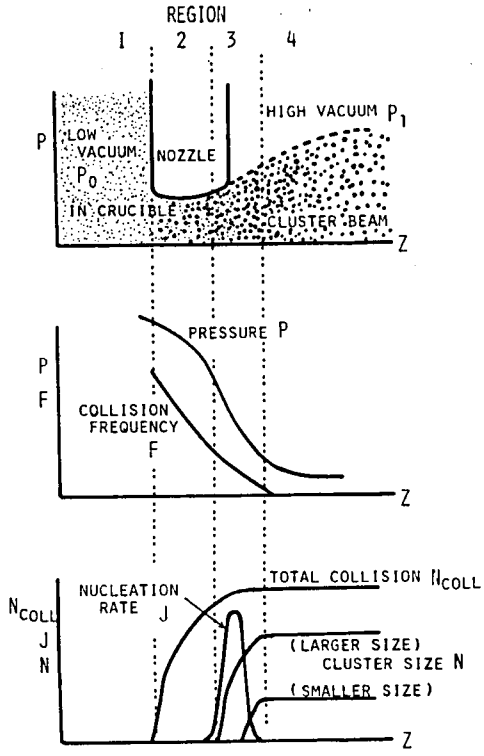

Fig.3.1 Conceptional picture of cluster formation and growth

through a nozzle into a high vacuum region (region 4). The atoms, which lose their energies by collision, start to aggregate to form nuclei. Nuclei smaller than the critical nuclear size are not stable and they break up into small pieces (region 2). However, the larger nuclei formed in the supersaturated state than the critical size grow to form clusters. The growth of the clusters slows down after the maximum rate of the cluster formation, and ceases finally in the region where the pressure decreases and collision frequency becomes lower (region 3). In a high vacuum region (region 4), the most of the clusters are keeping their sizes constant because there is little collision between clusters and atoms. The mechanism of the vaporized-metal cluster formation in a nozzle beam source can be discussed by using the adiabatic expansion process, during which the vapor cools to the very low temperature and becomes supersaturated, resulting in homogeneous nucleation and condensation process.

3.1.1 Adiabatic Expansion Process

In a case of a nozzle beam source, the vapor stream issuing from the nozzle source is accelerated considerably upon leaving the crucible by an adiabatic expansion [106)-108)]. Assuming frictionless, non-viscous flow through the nozzle without heat transfer, an expression for the flow velocity is derived from the thermodynamics of flow processes. The governing equations for the nozzle flow are:

Bernoulli equation,

$$VdP + \frac{1}{2} \underline{m}\, d(U^2) + \underline{m}gdh = 0 \qquad (3.1)$$

Energy conservation,

$$dE = dQ - PdV \qquad (3.2)$$

Continuity equation,

$$\frac{d\rho}{\rho} + \frac{dA}{A} + \frac{dU}{U} = 0 \qquad (3.3)$$

and the Equation of state,

$$P = nkT \qquad (3.4)$$

where $\underline{m}$ is the mass of the vapor at a height h, n is the number of particles, g is the gravitation constant, k is the Boltzmann's constant, dE is the gain of the total energy of a system and dQ is the heat transferred to the system. In addition, P, V, T, ρ, A and U are the local pressure, the local volume, the local temperature, the density, the nozzle area and the nozzle flow velocity concerned with the vapor, respectively. From these equations, P, V, T, ρ, A and U are expressed as

$$P/P_0 = (\rho/\rho_0)^{\gamma} = \left(1 + \frac{\gamma - 1}{2} M^2\right)^{-\gamma/(\gamma-1)} \qquad (3.5)$$

$$T/T_0 = \left(1 + \frac{\gamma - 1}{2} M^2\right)^{-1} \qquad (3.6)$$

$$(U/U^*)^2 = M^2 \left[\frac{2}{\gamma + 1}\left(1 + \frac{\gamma - 1}{2} M^2\right)\right]^{-1} \qquad (3.7)$$

$$(A/A^*)^2 = \frac{1}{M^2}\left[\frac{2}{\gamma+1}\left(1+\frac{\gamma-1}{2}M^2\right)\right]^{(\gamma+1)/(\gamma-1)}, \quad (3.8)$$

where M is the Mach number, γ is the ratio of the specific heats, and the variables with the suffixes 0 and * stand for those in the crucible and at the throat of the nozzle, respectively. The changes of T/T_0, U/U^*, A/A^* and M plotted as a function of the distance from the nozzle are shown in Fig.3.2, providing $P = P_0 \cdot \exp(-bZ)$. As M increases through the adiabatic expansion, the velocity of the clusters approaches to the $U_{max} = \sqrt{5kT_0/Nm}$ for the case of $\gamma = 5/3$. Therefore, the flow velocity of the nozzle beam is higher than that streaming from a conventional source, i.e. $\sqrt{3kT_0/m}$.

3.1.2 Nucleation and Condensation Process

The random thermal energy of a gas can be converted into directed kinetic energy, when the gas expands out of a nozzle into a vacuum region. Under the proper stagnation condition, the expanding gas becomes supersaturated by the adiabatic expansion, resulting in the nucleation and condensation of the gas [109)-119)]. The clustering process is essentially related to the interaction between the supersaturated vapor atoms. The collision frequency per atom f is

$$f = \sqrt{2}\, S \cdot n \cdot \bar{V}, \quad (3.9)$$

where the average thermal velocity $\bar{V}$ is $(8kT/\pi m)^{1/2}$, and S is the cross section for collision. The total number of colli-

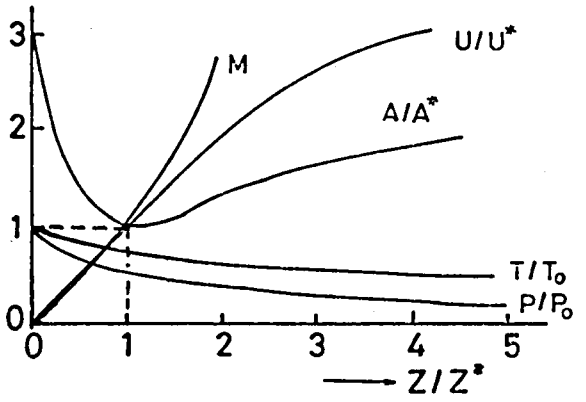

Fig.3.2 Change of T/T_0, U/U^*, A/A^* and M plotted as a function of the distance from the nozzle, providing $P=P_0 \cdot \exp(-bZ)$

sions F from the point Z_1 where the vapor flow becomes saturated to the point Z_2 where it becomes collisionless, can be given by [119]

$$F = \int f \, dt = \int_{Z_1}^{Z_2} \frac{4 S P}{(\pi m k T)^{1/2}} \frac{dZ}{U} . \qquad (3.10)$$

An increase of the inner pressure P_0 or a decrease of the temperature T_0 of the vapor in the crucible increases the total number of collision F and results in saturating the vapor sooner, that is, the point Z_1 is smaller. Also, increasing P_0 increases the length Z_2 to the collisionless region, which increases the total number of collisions. Through these collisions, the supersaturated vapor atoms stick together and form a critical nuclei with a critical radius $r^{\#}$, which is given by

$$r^{\#} = 2 \sigma V_c / kT \cdot \ln(P/P_\infty) \quad , \qquad (3.11)$$

where σ is the surface tension of a cluster, V_c is the averaged volume for an atom in a cluster, and P_∞ is the saturated vapor pressure expressed by $P_\infty = \exp(B/T + C)$. Here, B and C are the constants. In addition, the nucleation rate J with the critical radius $r^{\#}$ is given by [120]

$$J = K \cdot \exp(- \Delta G^{\#}/kT) \quad , \qquad (3.12)$$

where $\Delta G^{\#}$ is the energy change involved in the formation of a critical nucleus having the radius $r^{\#}$. With the addition of

the slight amount of growth to a cluster of critical size, the cluster will irreversibly grow to a larger size at the expense of the supersaturated vapor until there are relatively few collisions between clusters and atoms in the expanding flow. In addition, it should be noted that the formation of appreciable quantities of condensation necessarily causes the release of latent heat, which tends to prevent the expanding flow from cooling under the adiabatic expansion. Therefore, in order to obtain the appreciable condensation, very high supersaturation is required. However, the number density $\tilde{N}(Z)$ of the cluster at a position Z in the expanding flow is expressed by

$$\tilde{N}(Z) = \rho(Z) \int_{-\infty}^{Z} J(Z')/\rho(Z') \cdot U(Z') \, dZ' \ , \qquad (3.13)$$

where J is given by Eq.(3.12), and U is the local flow velocity. These phenomena occur by mutual interaction of vapor atoms during their passage through the nozzle and just after ejection. The nuclei having a radius larger than $r^{\#}$ are stable and grow with the rate

$$dr/dZ = \alpha \, (\rho/\rho_c) \cdot M^{-1} \cdot (2\pi\gamma)^{-1/2} \ , \qquad (3.14)$$

where α is the condensation coefficient ($0 < \alpha < 1$), ρ_c is the density of a cluster. Then, the cluster size N is calculated from

$$N = (4/3) \cdot \pi \cdot (r^3/V_c) \ . \qquad (3.15)$$

§3.2 DESCRIPTION OF THE CLUSTER ION SOURCE

3.2.1 Generation Part of Cluster Beam

A cluster source used is a cylindrical nozzle source. The dimensions and factors for design of the cluster source are different from those of molecular beam source as shown in Fig.3.3. The clusters grow by collisions with the surrounding vaporized atoms in the nozzle region, where the nozzle diameter D has to be larger than the mean free path λ of the atoms in the crucible. In order to make the adiabatic expansion more effective, the nozzle diameter is reduced to satisfy the condition that the ratio of the inner pressure P_0 of the crucible to the vapor pressure P outside the crucible is larger than 10^4, and it is also desirable for D to be larger than the nozzle thickness L, that is, $L/D < 1$. A simple nozzle shape, e.g. a cylindrical type with a diameter D = 0.5 - 2.0 mm is found to be enough to form a cluster beam with a high drift velocity [121].

In Table 3.1, the range of the source temperatures necessary to obtain the required pressure P_0 for several materials is listed. These are determined from the inner pressure P_0 in the crucible corresponding to 10^{-2} and 10 Torr, respectively. Since the source temperature in the ICB deposition is required to be higher than that used in the conventional methods, the techniques of the direct resistive heating of the source or of heating by electron bombardment are used.

3.2.2 Ionization Part

The cluster beam is ionized mostly to be singly charged by electron bombardment. In Table 3.2, the estimated ionization

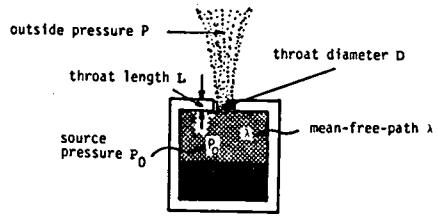

Molecular beam	Cluster beam
Nonsupersaturated vapour	Supersaturated vapour in an adiabatic expansion
$D < \lambda$	$D >> \lambda$ (for example; D: 0.1 - 2 mm)
$\frac{P_0}{P} < 10^4 - 10^5$	$\frac{P_0}{P}$ > about $10^4 - 10^5$ (for example; P : 10^{-7}-10^{-5}Torr, P_0 : 10^{-2}-several Torr)
$\frac{L}{D}$: not strong districted, tunnel type nozzle also available (L >> D)	$\frac{L}{D} \leq 1$ (in a case of cylindrical nozzle, experimentary $\frac{L}{D} \approx 1$)

Fig.3.3 Dimensions and factors for designing in the cluster beam source compared with those in the molecular beam source

Table.3.1 Source temperatures for cluster source: T_r and T_h are temperatures corresponding to 0.01 and 10 Torr of the inner pressures in the crucible, respectively

Material	T_r(k)	T_h(k)
Ag	1300	1815
Au	1670	2320
Pb	988	1435
Cu	1530	2140
Si	1905	2620
Al	1490	2050

Table.3.2 Ionization voltage of cluster

Material	Minimum (eV)	Maximum (eV)
Ag	4.28	7.58
Au	4.58	9.23
Pb	4.02	7.42
Cu	4.47	7.72
Si	4.10	8.15
Al	3.74	5.97

voltages of a cluster for several materials are listed. The ionization energy of a cluster is estimated to be somewhat lower than that of the single atom but higher than the work function of the bulk material of the same element, since the binding energy of an electron is considered to be reduced by the interaction between the condensed atoms. Further, a cluster has a much larger ionization cross section, and it increases as about $N^{2/3}$ for larger clusters ($N > 50$) [122]. Therefore, a cluster is effectively ionized by electron bombardment.

In order to measure the ionization ratio of the clusters, the ionized clusters are filtered out by a retarding field as shown in Fig.3.4. Then, the thickness of the films formed by the filtered clusters and by not filtered clusters is compared. Figure 3.5 shows the relation between the electron current for ionization and the ionization ratio. The electron current for ionization of 0 - 500 mA is found to give the ionization ratio of 0 - 50 %.

Figure 3.6 shows the ionization part of the ICB apparatus. The height h' of the electron accelerating electrode is designed to be so large ($h' > a$) that the high electric field to accelerate the clusters does not influence the electron current for ionization. In addition, the filaments which emit electrons for ionization are designed to be in a square shape in order to avoid radial concentration of the electrons which would occur with a circular filament. The square geometry results in spatially uniform ionization of the cluster beam, which is desirable to obtain a uniform film. An example of the spatial distribution of electron current density as measured by a current

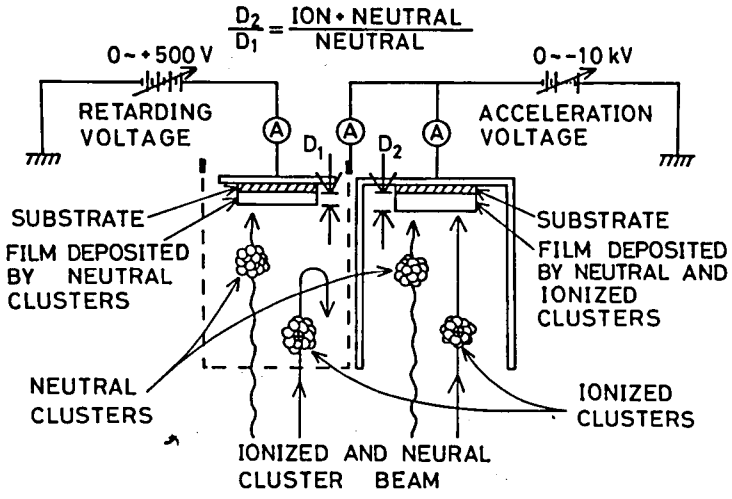

Fig.3.4 Apparatus for the ionization ratio measurement

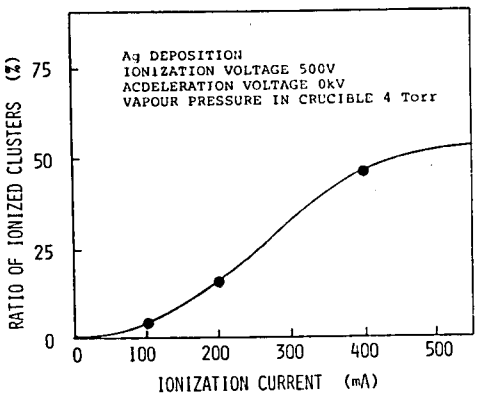

Fig.3.5 Relation between electron current for ionization and the ionization ratio

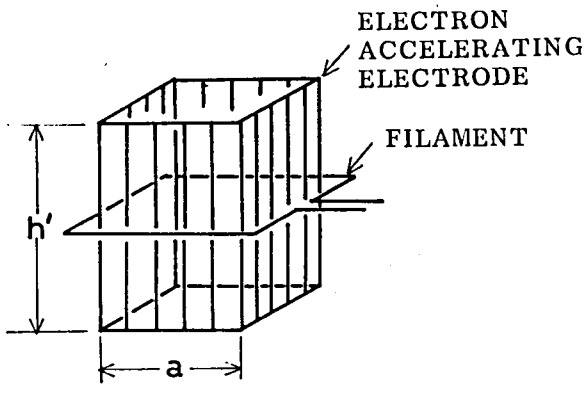

Fig.3.6 Schematic diagram of the ionization part

probe is shown in Fig.3.7. As shown in this figure, a uniform distribution of the electron currents is produced.

Figure 3.8 shows the dependence of the cluster ion current I_i on the electron current for ionization I_e. The density N_i of cluster ions proportional to I_i is defined by

$$N_i = N_0 \cdot \Omega(E_b) \cdot V_b \cdot n_b \cdot \tau_c \ , \qquad (3.16)$$

where N_0 is the density of neutral clusters ejected through the nozzle, $\Omega(E_b)$ is the cross section for ionization, n_b is the density of electrons for ionization, E_b and V_b are the mean energy and the mean velocity of the electrons for ionization, and τ_c is the lifetime of cluster ions. The cluster ion current I_i increases with increasing the crucible temperature T_c and the electron current for ionization I_e, which are predicted from Eq.(3.16). In addition, the ratio of I_i to I_e increases with the crucible temperature, which is considered to be the increase of N_0 and $\Omega(E_b)$ and the improvement of focusing of the cluster ion beam.

3.2.3 Acceleration Part

The ionized clusters are accelerated by the high electric field toward a substrate and deposited on it. The optimum acceleration voltage depends on other deposition parameters such as the substrate temperature and especially with the crystal structure which determines the epitaxial growth [1),2)]. For example, the epitaxial growth of Si on Si substrates was achieved at acceleration voltage V_a of 6 kV (at the substrate temperature

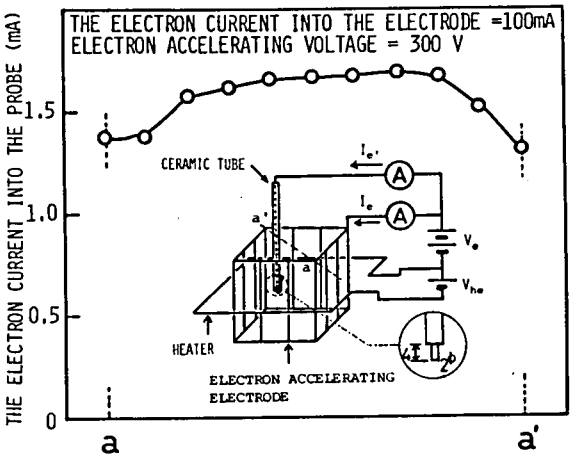

Fig.3.7 Spatial distribution of electron current for ionization

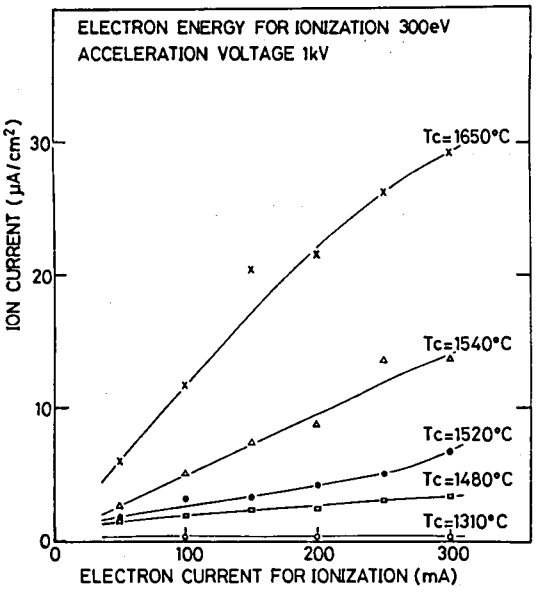

Fig.3.8 Dependence of the cluster ion current on the ionizing electron current

T_s = 620°C), likewise epitaxial films of Si on sapphire, InSb on sapphire, and GaAs on GaAs substrates were obtained at V_a = 4 kV (T_s = 760°C), V_a = 4 kV (T_s = 400°C), and V_a = 4 kV (T_s = 550°C), respectively. The epitaxial growth of ZnO on sapphire was obtained at V_a = 1 kV (T_s = 230°C) using the R-ICB technique, where a reactive gas is combined with the standard ICB.

On the other hand, for the c-axis oriented film growth of MnBi, ZnO and BeO onto an amorphous substrate, additional acceleration voltage was not necessary [84)-86)]. Good quality films showing a hexagonal structure could be obtained using the energy corresponding to the ejection velocity of the clusters alone. In addition, because a cluster has about a thousand times larger than that of an atom, it should be noted that even for the acceleration potential of a few kV, the energy of each atom is still only in the order of a few eV. No space charge forces have been observed which affect the transport process of the clusters. This can be explained by the small charge-mass ratio and the short distance (∿10 cm) from the cluster ion gun to the substrate.

§ 3.3 CHARACTERISTICS OF IONIZED CLUSTER BEAM [121)]

3.3.1 Cluster Size

The procedure of measuring the cluster size, i.e. the number of constituent atoms of a cluster, is based upon energy measurement combined with velocity measurement.

For the energy measurement, a retarding method and an electrostatic 127° energy analyzer are used. The retarding

method is employed to measure the energy distribution of incident cluster. Figure 3.9 shows the energy distribution of the Ag cluster ions. The energy distribution was obtained by differentiation of the ion current with respect to the retarding potential. Assuming that (i) the expansion through the nozzle gives a kinetic energy e_{kin} of the order of kT_0 to every atom in the vapor; (ii) the kinetic energy of the clusters E_{kin} does not change with ionization and (iii) the probability of forming a multiply charged state is small enough to be neglected, the clusters consisting of N atoms will have a kinetic energy

$$E_{kin} = N \cdot e_{kin}. \tag{3.17}$$

Since e_{kin} is of the order of 0.1 eV, we can roughly estimate the cluster size by Eq.(3.17). From these considerations, a cluster size of 500 - 2000 can be obtained.

On the other hand, the method of Fig.3.10 measures the energy distribution of ionized incident clusters only without neutral clusters and electrons. The kinetic energy of the cluster is much greater than the thermal energy of an atom because the velocity and mass of one cluster are greater than those of one atom. The kinetic energy E_{kin} of a cluster consisting of N atoms can be written as

$$E_{kin} = \frac{1}{2} NmU^2, \tag{3.18}$$

where m is the mass of the atom and U is the flow velocity. E_{kin} is measured by means of an electrostatic 127° energy ana-

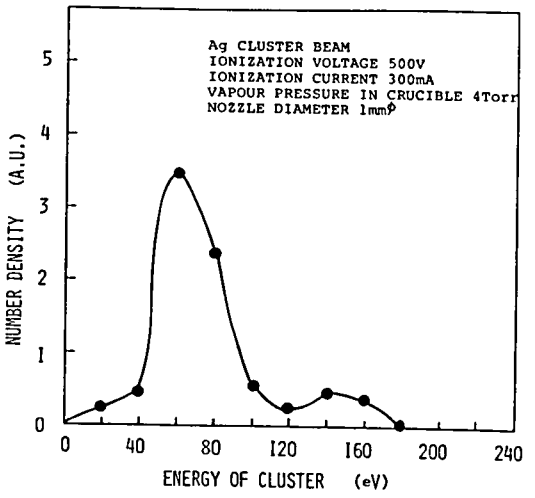

Fig.3.9 Energy distribution of the Ag cluster ion measured by the retarding field method

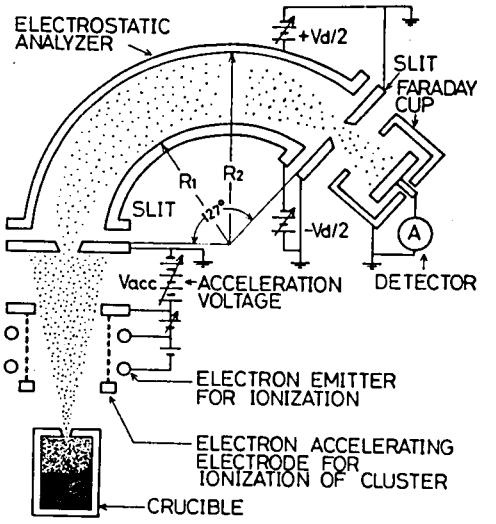

Fig.3.10 Schematic diagram of the electrostatic energy analyzer

lyzer using the equation,

$$E_{kin} = \frac{e\,V_d}{2 \cdot \ln(R_2/R_1)} , \qquad (3.19)$$

where V_d is the deflection voltage between electrodes, R_2 is the radius of curvature of the outer cylinder, and R_1 is the radius of curvature of the inner cylinder. If the ionized cluster is accelerated by the acceleration voltage V_a, the cluster energy E is now the sum of the ejection energy and the acceleration energy, that is,

$$E = e \cdot V_a + E_{kin} . \qquad (3.20)$$

The results obtained by this method will be discussed hereafter in the following section. In both methods, the effect of thermal energy affects the energy measurement, but generally the electrostatic energy analyzer is more precise than the retarding method, and so it is mostly used in the energy measurements.

For the measurement of velocity U expressed in Eq.(3.18), the time-of-flight method is simple and widely used [123)-127)]. The time of flight in the drift space is different from the mass of ions. Therefore, it is possible to measure the velocity distribution by measurement of the used time. The measurement of the time of flight can be made with the rotating disk method as shown in Fig.3.11 [76),78)]. In this method, the ejection speed and/or accelerated speed can be monitored with or without applying the acceleration voltage. The velocity measurement discussed hereafter is made by this method. The cluster size

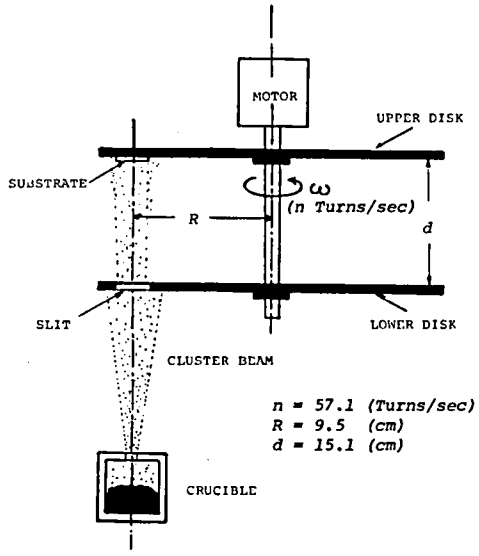

Fig.3.11 Schematic diagram of velocity measurement for the cluster beam by the rotating disk method

can be calculated using Eq.(3.18), where E_{kin} and U are obtained experimentally, and it is estimated to be 500 - 1000 from the obtained results.

Further, in order to analyze the existence and the expected size of the clusters, the beam is sent on a copper grid covered with a carbon film (~200 Å in thickness), which is cooled down to 77 K by liquid nitrogen. The deposition is done about a few seconds in order to prevent the coalescence of deposited particles from occuring. In this way, less than one monolayer coverage of clusters is obtained on an amorphous substrate, i.e. the interactions of the deposited clusters with each other and with a substrate are minimized. A typical transmission electron microscopy micrograph of such a deposit is shown in Fig. 3.12. Figure 3.13 is the histogram of the cluster size distribution obtained from the micrograph. The average diameter of the cluster is around 50 Å. From this result and Eq.(3.15), the cluster size is found to be about 2000, taking account that the Ag film has the f.c.c. structure with the lattice constant of 4.07 Å [88),128)].

3.3.2 Energy Measurement

Figure 3.14 shows the schematic diagram of the experimental apparatus for the energy measurement. In this experiment, heating by electron bombardment is used to vaporize metal in a crucible. The clusters are formed by an adiabatic expansion of the vaporized-metal through the crucible nozzle into a high vacuum. The clusters are ionized by electron bombardment and are accelerated toward an electrostatic energy analyzer. A

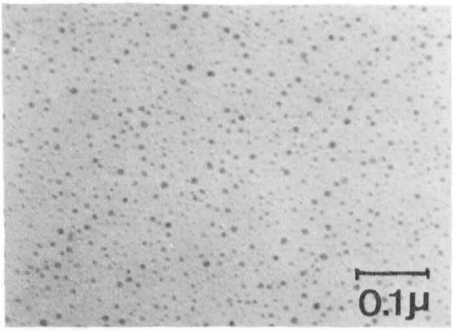

Fig.3.12 TEM photograph of the Ag cluster impinged on the carbon substrate cooled at 77 K by liquid nitrogen

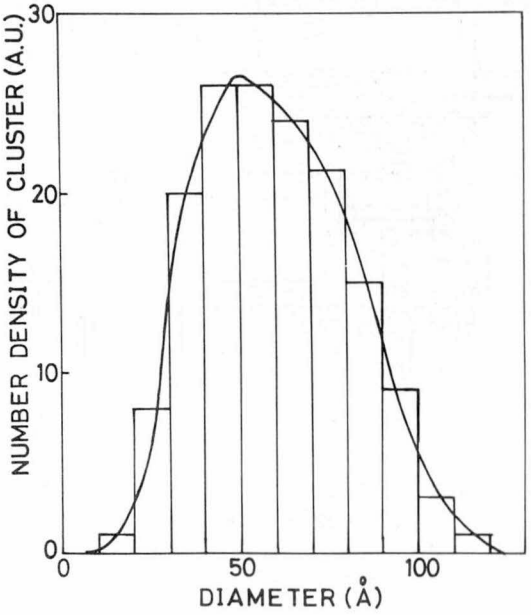

Fig.3.13 Cluster size distribution measured from the TEM photograph

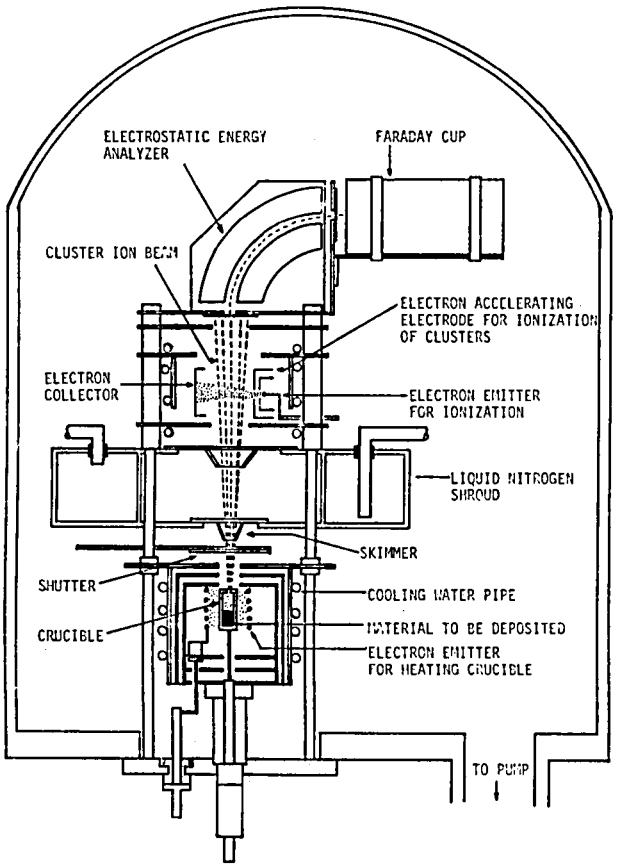

Fig.3.14 Schematic diagram of the experimental apparatus for the energy measurement

liquid nitrogen trap is equipped to prevent scattered clusters from entering into the energy analyzer and ionization electrodes. Background pressure in the chamber is lower than 2×10^{-7} Torr during the operation. Figure 3.15 shows the results of the measurement of the energy distribution of the ionized clusters with the parameter of metal vapor pressure in the crucible. Two kinds of peaks are observed in the spectra; one of them has an energy close to zero and the other has an energy of approximately 80 - 170 eV. The energy distribution of the high energy peaks has been obserbed in many experiments and ranges between 80 - 180 eV. The intensity of this peak increased above the threshold pressure which satisfies the condition of cluster formation then decreases with further increase of the vapor pressure of the metal in the crucible. In this experiment, the nozzle diameter D is 1 mm and L/D = 1. The clusters begin to be observed at a vapor pressure of about 0.5 Torr and the intensity of the cluster beam increases to a maximum at P_0=4.7 Torr. At a higher pressures, more than 5 Torr, the intensity of the cluster beam begins to decrease. This is considered to be due to the fact that the pressure difference across the nozzle decreases because of the large vapor flow from the crucible. Figure 3.16 shows the effect of the nozzle dimension on the energy and intensity of the clusters. The mean free path of the atoms in the vapor at 1.25 Torr of the experimental conditions is in the order of 0.01 mm, and therefore the diameters of all nozzles tested are large enough to make possible many collisions necessary for the cluster growth during the expansion. In

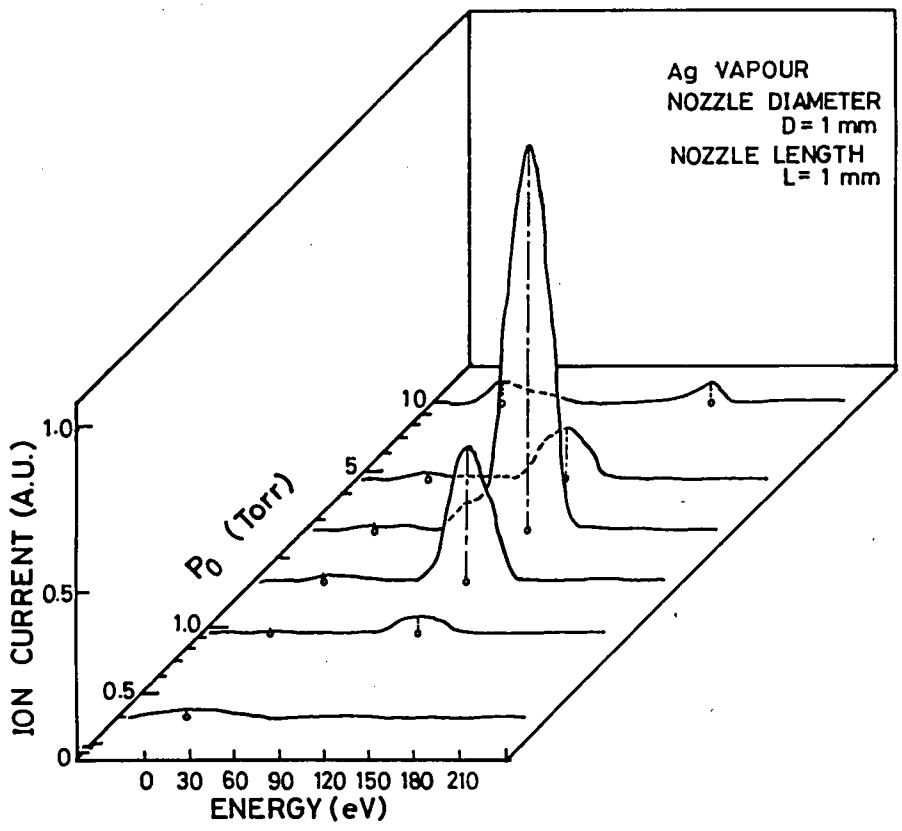

Fig.3.15 Energy distribution of the ionized cluster with the parameter of the metal vapour pressure

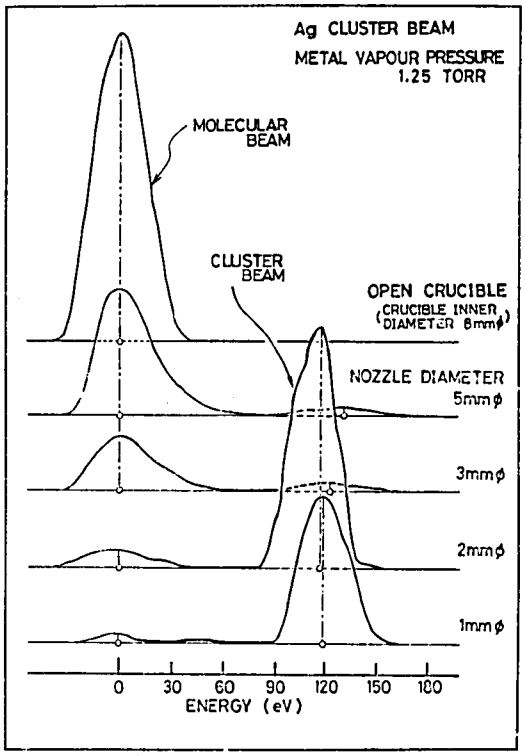

Fig.3.16 Dependence of the energy and the intensity of the clusters on the nozzle diameter

the case of the 2 mm nozzle, clusters were formed most effectively. But no peak at high energy can be seen for a crucible with larger diameter over 5 mm including open crucible or Knudsen cell, because the pressure difference between entrance and exit of crucible is not high enough for cluster growth. Under these conditions the vapor consists of atoms, molecules and/or clusters having several atoms instead of fully formed clusters.

Changing the nozzle dimension leads to a change in the vapor flow and consequently to a change in the number of collisions. The shape of the nozzle has a large effect on the cluster formation characteristics.

The analogous results to the cluster formation from gaseous material are obtained experimentally in this vaporized-metal clusters by comparing the value of $P_{max} \cdot D$ as shown in Fig.3.17 where P_{max} is the maximum pressure which gives the cluster beam with the maximum intensity at the condition of these experimental dimensions. These results show that the vaporized-metal clusters are formed in the similar process to that of gases by homogeneous condensation in an adiabatic expansion[108),129)].

3.3.3 Velocity Measurement

The vapor ejected from a nozzle source is accelerated considerably by expansion in the nozzle. The ejected vapor cools down rapidly by adiabatic expansion and becomes supersaturated which initiates clusters growth. In order to form a cluster beam, a nozzle source is indispensable. Au effusive source used in the conventional vacuum evaporation technique

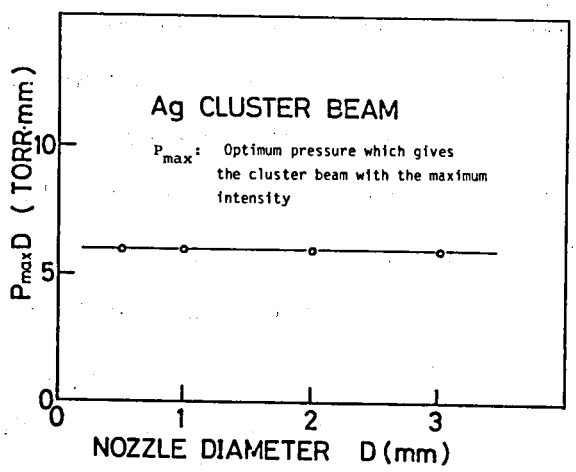

Fig.3.17 Relationship between the nozzle diameter and the maximum pressure which gives the cluster beam with the maximum intensity

is ineffective for this purpose. Figure 3.18 shows the calculated velocity distributions at the collimator for both nozzle and effusive sources (c.f. Appendix)[130]. The velocity distribution for the nozzle source is narrower and the maximum velocity is higher than that of the effusive source. In the case of the nozzle source, the maximum velocity of the vapor is attained when all thermal energy is converted into kinetic energy. Assuming nonviscous flow through the nozzle and the ratio of specific heats γ equal to 5/3 as for a monoatomic gas, the velocity of the vaporized-metal cluster should approach $U_{max} = \sqrt{5kT_0/m}$. Figure 3.19 shows the experimental relation between the inner vapor pressure p_0, which corresponds to the crucible temperature of the cluster source, and the most probable velocity of the clusters as measured by the rotating disk method. As shown in the figure, as P_0 increases, the velocity approaches the value U_{max}. The size of the cluster N is estimated roughly by putting the measured velocity and energy into the equation of $E_{kin} = NmU^2/2$, where Nm is the mass of the cluster ion, m is the mass of the metal atom and U is the flow velocity of the cluster beam. The size distribution calculated was between 500 - 1000 atoms per cluster for the various conditions of crucible temperature and nozzle diameter in this experiment (metal vapor pressure in the crucible; 0.1 - several tens Torr, nozzle diameter; 0.5 - 5 mm, nozzle thickness; 0.5 - 2 mm)..

§3.4 SUMMARY

Cluster formation has been confirmed theoretically and

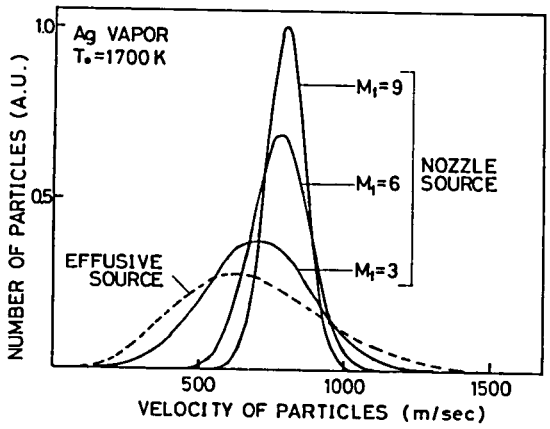

Fig.3.18 Velocity distribution at the collimator for the nozzle source and the effusive source

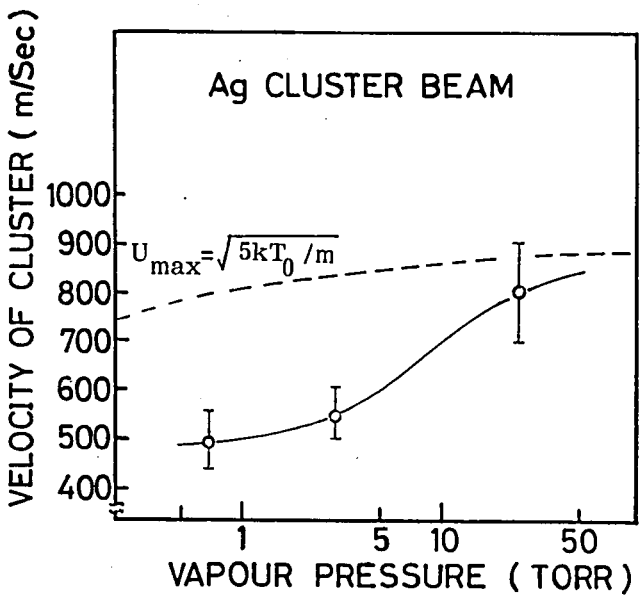

Fig.3.19 Relation between the inner pressure of the source and the most probable velocity of the clusters

experimentally. In the formation process of the cluster, in particular that of the vaporized-metal cluster, the adiabatic expansion occurs which results in a rapid decrease of the vapor temperarure. The vapor becomes supersaturated and condenses, and each atom in the vapor flow becomes loosely coupled in cluster containing about 1000 atoms. It was confirmed experimentally by the energy analysis that metal clusters are formed. The peak energy observed was much higher than the energy of the vapor atoms and had a value between 80 and 180 eV.

The ejection velocity can be measured by a rotating disk method. The high velocity of the clusters is considered to be caused by an adiabatic expansion, since the velocity measured approaches the theoretical asymptotic value. From the experimental results of Ag vapor, the ejection velocity obtained is 500 - 800 m/sec. The theoretical ejection velocity calculated from the Eqs.(3.5) and (3.7), where the flow viscosity is not considered, is about 500 m/sec under the conditions of P_0 = 0.1 Torr and $P_1 = 10^{-6}$ Torr.

APPENDIX

Figure A.1 shows the schematic diagram of the effusive source and nozzle source. In the effusive source, under the condition that the orifice diameter D is much smaller than the mean free path of the atoms, the velocity distribution in the Z direction is given by

$$n_{u,c}\ (\text{effusive}) = \frac{1}{2}\left(\frac{m}{kT_0}\right)^2 u^3 \cdot \exp\left(-\frac{mu^2}{2kT_0}\Delta u\right) \quad (A.1)$$

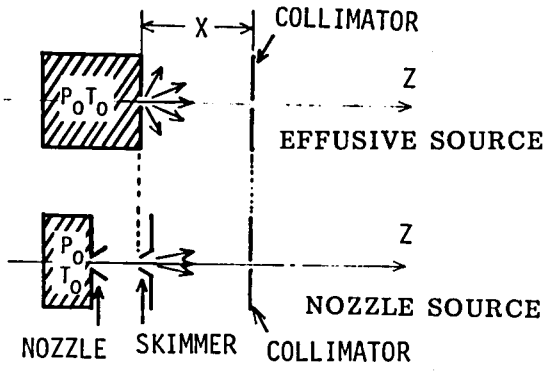

Fig. A.1 Schematic diagrams of the effusive source and the nozzle source

u: velocity of atoms

T_0: source temperature

The total intensity is given by

$$n_c(\text{effusive}) = \frac{S}{\pi X^2} \qquad (A.2)$$

X: the distance between the orifice and the collimator

S: the area of the small hole on the collimator

Assuming that the gas ejected from the nozzle source flows continuously to the skimmer, the velocity distribution is given by

$$n_{u,c}(\text{nozzle}) = \left(\frac{m}{2\pi k T_1}\right)^{1/2} \cdot \exp\left(-\frac{m(u-U)^2}{2kT_1}\right) \Delta u \qquad (A.3)$$

U: the mass flow velocity

T_1: the temperature of the particles at the skimmer

The total intensity is given by

$$n_c(\text{nozzle}) = \frac{mU^2 S}{2\pi k T_1 X^2} \qquad (A.4)$$

Providing that the gas is ideal with the constant specific heat ratio γ, without friction and viscosity, T_1, U and n_c(nozzle) are given by

$$T_1 = T_0 \left(1 + \frac{\gamma - 1}{2} M_1^2\right)^{-1} \qquad (A.5)$$

$$U^2 = M_1^2 \gamma \frac{k T_0}{m} \left(1 + \frac{\gamma - 1}{2} M_1^2\right)^{-1} \qquad (A.6)$$

$$n_c(\text{nozzle}) = \frac{1}{2}\gamma M_1^2 \frac{S}{\pi X^2} \qquad (A.7)$$

M_1: the Mach number of the gas flow at the skimmer

IV CHARACTERISTICS OF FILMS PREPARED BY THE ICB TECHNIQUE AND THEIR APPLICATIONS TO ELECTRON DEVICES

§4.1 MECHANISM OF FILM FORMATION WITH THE ICB TECHNIQUE

In the ICB technique, the kinetics of film growth and the film properties can be varied by adjusting the acceleration voltage, the charged particle content and the substrate temperature. In order to identify film formation mechanisms, some observed growth effects and ICB deposition and epitaxial material results will be discussed.

4.1.1 Migration Effect

In order to observe the migration of deposited particles, an initial deposition state was investigated. Gold was deposited onto a silicon oxide (SiO) film which was deposited on a NaCl substrate. The substrate surface was partially covered with a cleaved NaCl plate to study shadowing at the cleaved edge. The average spacing between the SiO and the NaCl mask was about 80 μm. The gold was deposited both by the Ionized Cluster Beam technique and by the conventional vacuum deposition. Figure 4.1 shows the electron micrographs of the deposited Au film near the edge of the mask. In the case of the ICB deposition, the deposited Au particles were observed to have migrated under the cleaved NaCl cover. Even when the acceleration voltage was zero, the migration distance of the deposited particles was greater in the ICB deposition than in conventional vacuum deposition. The increased migration distance could be the result of the breaking up of deposited macroparticles into

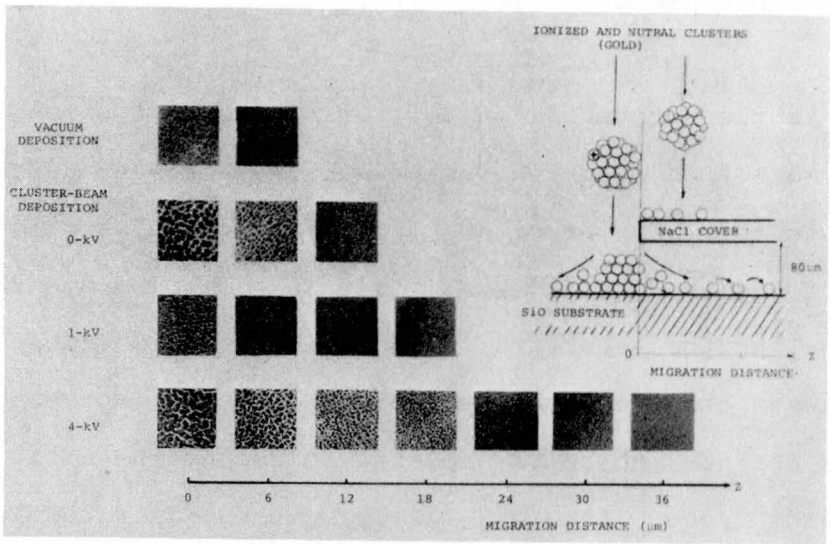

Fig.4.1 Electron micrographs of the films formed by migrated deposits

atoms upon impact with the film surface.

The average distance $\bar{X}$ transversed over the substrate surface for the time of t is given by [131),132)]

$$\bar{X} = (4 D t)^{1/2} . \qquad (4.1)$$

Here D is the diffusion coefficient, which is expressed as

$$D = A \cdot \exp(- \frac{\Phi_d}{k T}) , \qquad (4.2)$$

where Φ_d is the activation energy for surface diffusion, k is the Boltzmann's constant, T is the substrate temperature and A is a constant. The direction of motion of the atom in the macroparticles changes from the direction of bombardment to directions along the substrate surface because of multiple collisions between the atoms when the macroparticles impact the substrate surface, which is expected to reduce the activation energy for surface diffusion. This change in direction of motion can be considered to cause the increase in migration distances.

4.1.2 Effect of the Kinetic Energy

In order to show how the crystallinity of the deposited film is affected by the acceleration voltage, silicon epitaxial film growth was achieved. As shown in Fig.4.2, the crystallinity of Si films grown on a Si substrate could be improved by increasing the acceleration voltage. In this figure, it was found that the Si films grew epitaxially on the single crystal

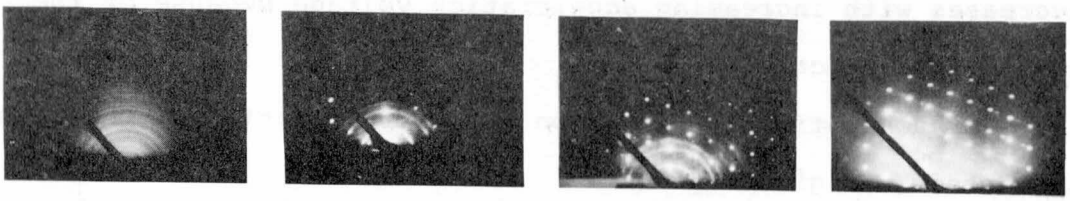

0 kV 4 kV 6 kV 8 kV

Fig.4.2 Effect of the acceleration voltage on the crystallinity of the silicon films grown on the silicon substrate

Si substrate at acceleration voltage of 8 kV. This fact is due to the increase of surface diffusion energy by increasing the acceleration voltage.

The solid lines in Fig.4.3 show the relation between the mass M deposited on the substrate and the reciprocal substrate temperature. For unionized clusters the mass deposited increases with decreasing substrate temperature, whereas for ionized clusters that are accelerated the mass deposited increases with increasing substrate temperature. Moreover, the slope of the mass deposited line changes with increasing acceleration voltage. The mass deposited at a given substrate temperature decreases with increasing acceleration voltage because of the sputtering effect.

For conventional deposition by neutral particles, the mass deposited M is given by [133]

$$M = \dot{M} t - \frac{\dot{M} N_0}{I^*} \exp\left(- \frac{U}{k T} \right) , \qquad (4.3)$$

where the energy U associated with deposition = $\Phi_{ad} - \Phi_d$, $\dot{M}$ is the mass impinging rate on the substrate, I* is the density of critical nuclei, N_0 is the density of adsorption sites on the substrate surface, Φ_{ad} is the activation energy for desorption, Φ_d is the activation energy for surface diffusion and t is the deposition time. For the ICB technique, the change of slope of the solid line in Fig.4.3 with increasing acceleration voltage is considered to be due to the change of values such as N_0, I* and U. This is one of the important features of the ICB deposition process. In the conventional ion beam deposition

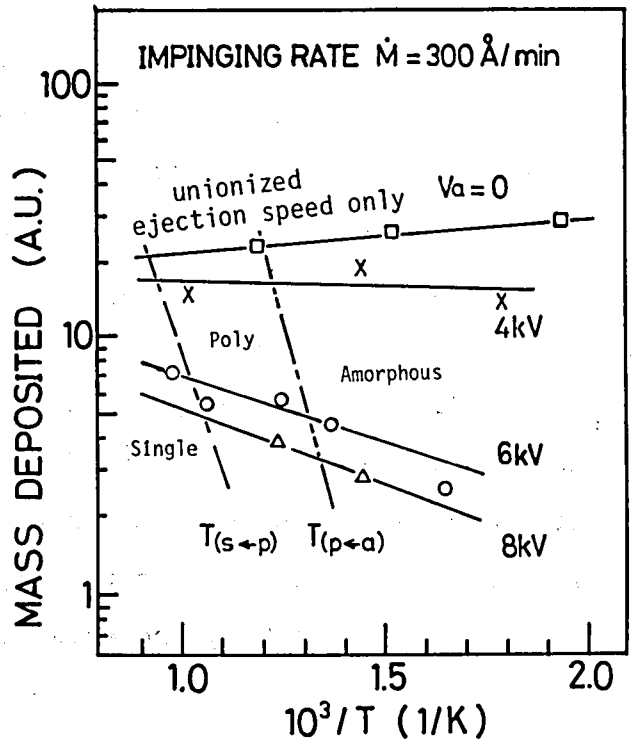

Fig.4.3 Mass deposited vs. reciprocal substrate temperature, and the change of transition temperature for different acceleration voltages

systems which use atomic neutral and ionized particles, the energy U does not change [5].

$T_{(s \leftarrow p)}$ and $T_{(p \leftarrow a)}$ shown in Fig.4.3 by broken lines indicate the polycrystalline to single crystal transition temperature and the amorphous to polycrystalline transition temperature, respectively, for different acceleration voltages. The transition temperatures $T_{(p \leftarrow a)}$ and $T_{(s \leftarrow p)}$ decrease with increasing acceleration voltage as shown in the figure. The decrease in the transition temperatures is expected to be due to the enhancement of a surface diffusion energy on the substrate with increase of the acceleration voltage.

Figure 4.4 illustrates the mass impingement rate as a function of the substrate temperature and shows the transition temperature $T_{(s \leftarrow p)}$ for silicon films prepared at V_a = 0 kV (no acceleration and no ionization) and V_a = 8 kV (in the case where about 10 % of the clusters in the total flux are ionized), respectively. The slope of both lines in the figure yields Φ_d because $T_{(s \leftarrow p)}$ is related to $\dot{M}$ by the equation [132),134)]

$$\dot{M} \leq A' \cdot \exp(- \Phi_d / kT_{(s \leftarrow p)}) , \qquad (4.4)$$

where A' is a constant. Φ_d decreases with increasing acceleration voltage, which results in an enhancement of the surface diffusion energy (migration energy). One of the important characteristics of the ICB technique is that the surface diffusion energy is easily controlled by the acceleration voltage and therefore single crystal film growth can be performed at higher deposition rates when the acceleration voltage is higher.

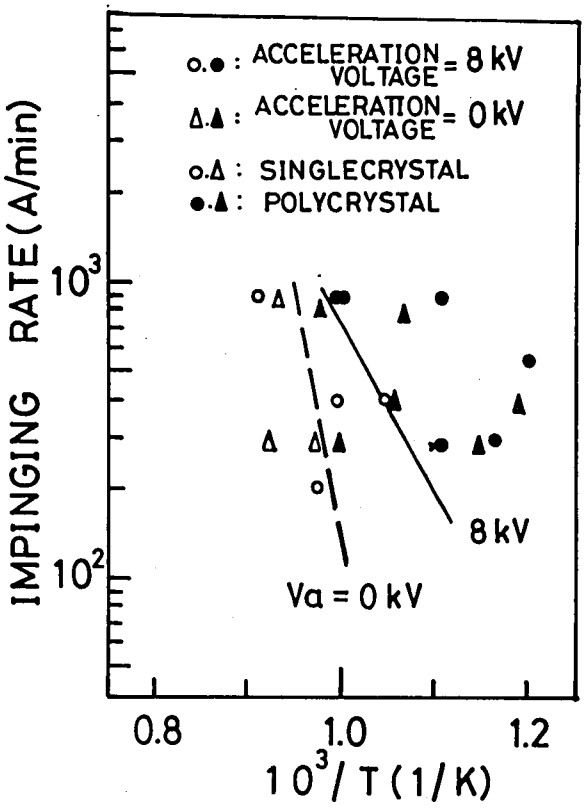

Fig.4.4 Impinging rate vs. reciprocal substrate temperature showing the transition from the poly-crystalline to single crystalline structures

4.1.3 Effect of the Ionization

The physical and crystallographic properties of the deposited films are remarkably improved by the presence of ionized particles, even when only a few per cent of them are included. The influence of ions on the crystal state of the ZnO films has been shown previously in Fig.2.7.

For the case of materials with several crystal structures, which depend on the composition ratio, the ions also have the effect on the crystal structure of the films. Figure 4.5 shows the X-ray diffraction patterns of the tin oxide films deposited by using the R-ICB technique at different values of the electron current for ionization together with RHEED patterns. Tin oxide films have different crystal configurations such as triclinic, orthorhombic and tetragonal structures, depending on the composition ratio of tin and oxygen atoms. When $I_e = 0$, the film consists of mainly tin mono-oxide (SnO) containing a small amount of Sn_2O_3. In the case of I_e = 150 mA and 300 mA, the crystal structures of the obtained films are found to change to a tetragonal structure of SnO_2. The relative intensities of the x-ray diffraction patterns differ remarkably from those tabulated in the ASTM card for powdered SnO_2. The maximum appears at the (101) plane, which indicates that the films grew predominantly along the <101> axis. With increasing electron current I_e, the orientation along the axis tends to increase. This can be considered to be due to the enhancement of the chemical reaction between the Sn-clusters and the reactive oxygen gas [134),135)]. The composition ratio of oxygen to tin (i.e. O/Sn) in the deposited films was measured

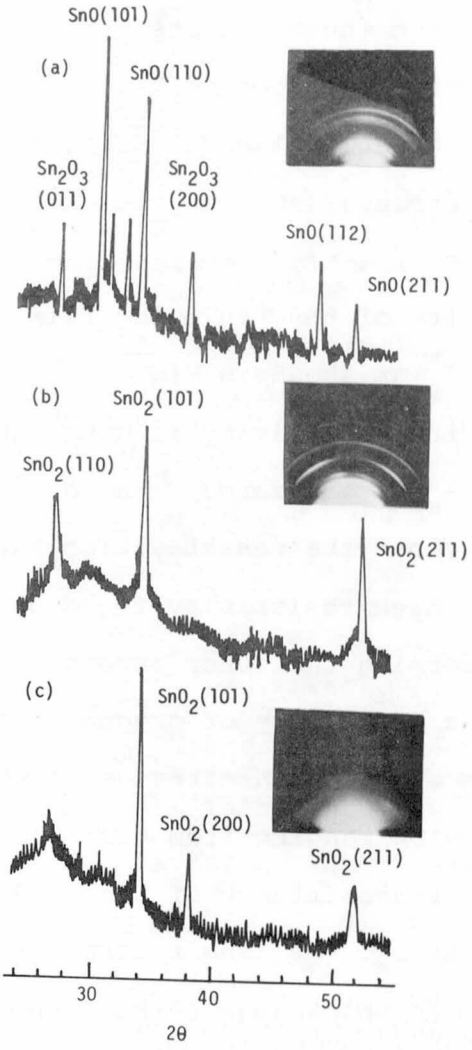

Fig.4.5 x-ray diffraction patterns of the tin oxide films deposited at different values of I_e together with RHEED patterns: (a) I_e=0, (b) I_e=150 mA and (c) I_e=300 mA

by means of an Auger electron spectroscopy. The result is shown in Fig.4.6, from which it was found that the intensity ratios for I_e = 0, 150 and 300 mA were 0.383, 0.575 and 0.637, respectively. From these results, the crystal structures as well as crystal state are seen to be dependent upon the ion content, which has a great influence on the critical parameters in the condensation process (such as coalescence and nucleation) and on the chemical reaction between clusters and reactive gases.

The resistivity of the tin oxide film was found to depend on the values of I_e as shown in Fig.4.7. In the case of I_e = 0 (without ion), the resistivity is extremely high in comparison with those where I_e is not zero. With increasing I_e, the ion content increases, but the resistivities rapidly decrease. Consequently, the high resistivity found at I_e = 0 is considered to be caused by forming the other several oxides such as SnO and Sn_2O_3 because of a deficiency of oxygen atoms.

Measurements of the transmittance of these films were made in the visible region ranging from 0.35 to 0.74 μm. Figure 4.8 shows the optical transmittance of the oxide films deposited at different values of I_e. The transmittance of the film deposited at I_e = 0 is below 10 % in the whole visible region, whereas it increases with increasing the ion content and it rises to 80 - 90 % for the film deposited at I_e = 300 mA. For the film deposited at I_e = 150 mA, a fundamental absorption can be observed at 0.35 μm, from which the optical band gap is estimated to be about 3.54 eV, and this value is in good agreement with the value obtained by S.K.Ghandhi et al. [136]

From these results, it is found that the film characteris-

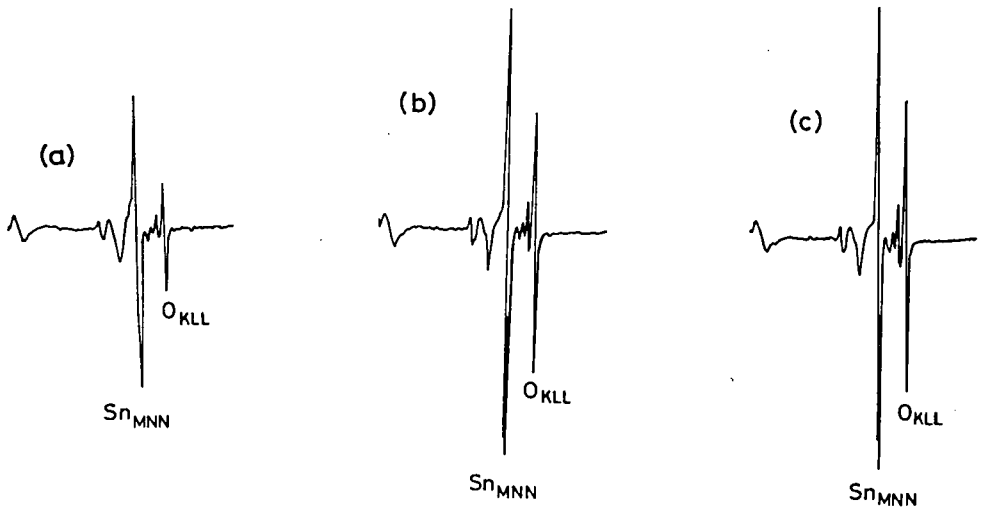

Fig.4.6 Auger spectra for the tin oxide films deposited at different values of I_e: (a) I_e=0, (b) I_e=150 mA and (c) I_e=300 mA

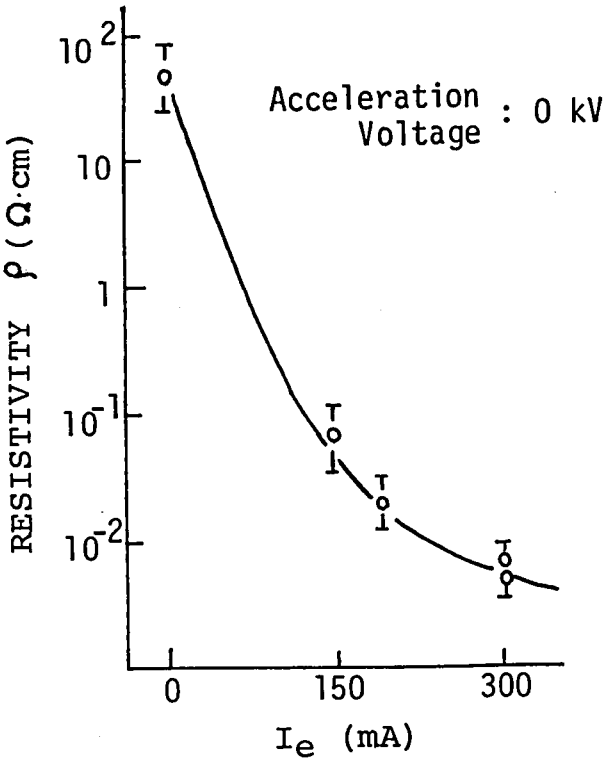

Fig.4.7 Resistivities of tin oxide film deposited at different values of I_e

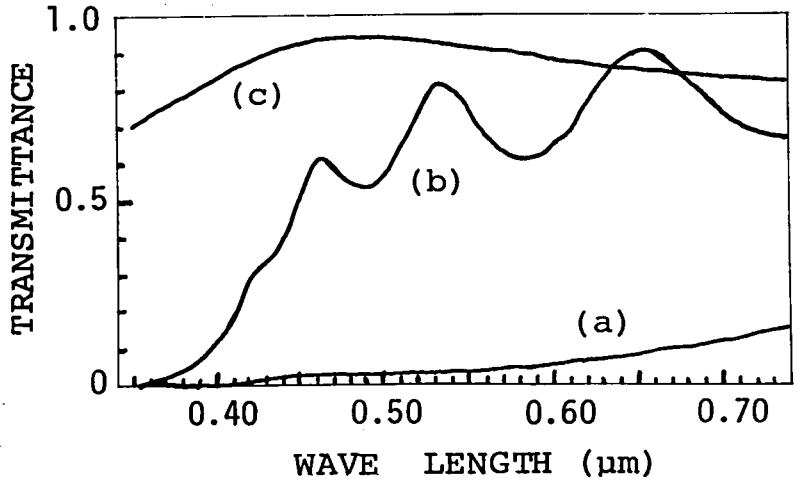

Fig.4.8 Trnasmittance of tin oxide films deposited at different values of I_e, as a function of wavelength: (a) I_e= 0, (b) I_e= 150 mA and (c) I_e= 300 mA

tics such as crystallographic orientation, electrical and optical properties depend upon the ion content during the deposition even at zero acceleration voltage.

§4.2 METAL FILMS [16),17),75)]

Metal films deposited by ICB on an insulating or a metal substrate show good adhesion and a high packing density. The adhesion strength of a copper film deposited on a glass substrate was measured by a pulling method, where the adhesion strength is defined as the force required to peel the deposited film from the substrate. Figure 4.9 shows the relationship between adhesion strength and acceleration voltage. The adhesion strength increases by a factor of 100 as the applied voltage increases from 0 to 10 kV, which is due to the surface cleaning and the increased implantation effects resulting from energetic beam bombardment of the substrate surface [137),138)].

The packing density is the number of atoms per unit volume in a film, which is generally determined by the measurements of film thickness using a stylus, and of the mass per unit area measured by the electrolytic method. If a film is discontinuous or porous because of the deposition conditions employed, the density is expected to be lower than the normal bulk value. Figure 4.10 shows the relative packing density, which is proportional to the number of atoms per unit volume. The packing density increases with increasing acceleration voltage. In the case of gold deposited on a copper of this experiment, the density increases to the value corresponding to the bulk material 19.3 g/cm^3. The high packing density could be mainly due

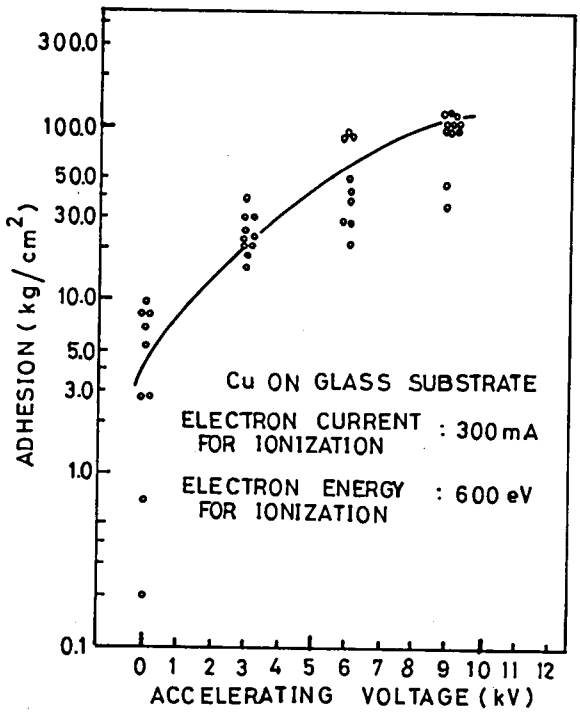

Fig.4.9 Adhesion strength as a function of acceleration voltage

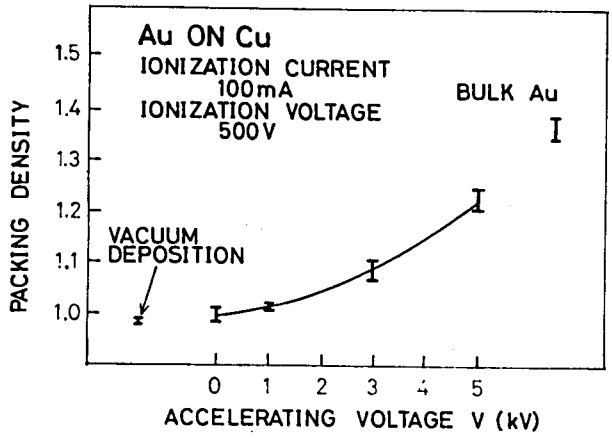

Fig.4.10 Dependence of packing density on acceleration voltage for Au films deposited on a Cu substrate

to the continuous sputtering effect during deposition by the ion bombardment and migration effects of adatoms.

Generally the presence of ionized particles in the vapor influences the condensation process via the critical parameters of the condensation sites. Thus, an increase in the number of nucleation sites in combination with the enhanced migration effect results in the formation of very thin conducting films using the ICB technique. Figure 4.11 shows the relationship between the resistivity and the thickness of gold films deposited on a glass substrate at different acceleration voltages. For thin films of several hundred angstroms, film resisitivity decreases with increasing acceleration voltage. The dependence of resistivity on thickness of films deposited by evaporation is not similar to that observed using the ICB technique and values are higher than those obtained using the ICB technique.

In general, the ratio of film resistivity relative to bulk resistivity is given by [139]

$$\rho_F/\rho_b = 1 + 3\lambda(1-p)/8\bar{t} \qquad (\bar{t} > \lambda) \tag{4.5}$$

and

$$\rho_F/\rho_b = \frac{4}{3}\,\frac{1}{(1+2p)}\,\frac{\lambda}{\bar{t}}\,\frac{1}{\ln(\lambda/\bar{t})} \qquad (\bar{t} << \lambda\ ,\ p<1), \tag{4.6}$$

where $\bar{t}$ is the film thickness, λ is the mean free path of the conduction electrons, and p is the fraction of the electrons elastically scattered from both surfaces of the film. In addition, for the case that impurities and structural defects are included in the film, additional contributions to the above

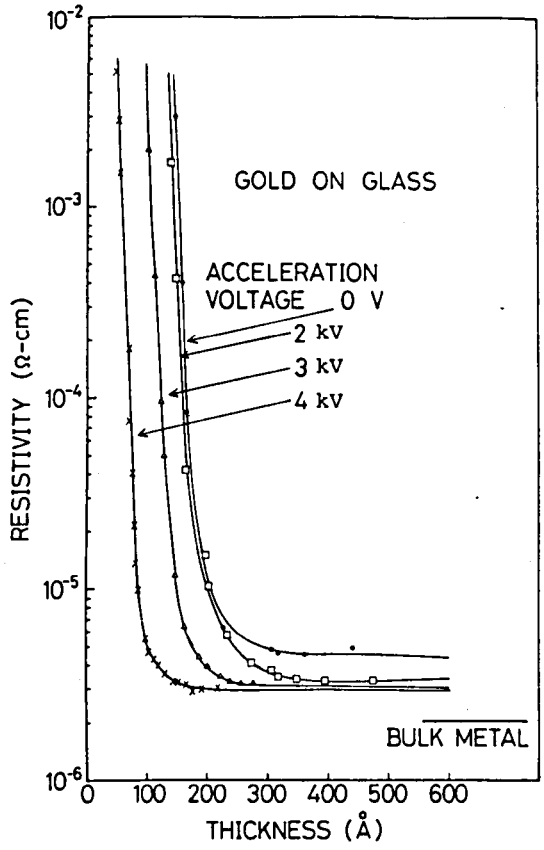

Fig.4.11 Resistivity of Au films on a glass substrate as a function of thickness for different acceleration voltages

mentioned resistivity arises. Resistivity size-effect expressions for films involve three trnasport parameters, p, λ and ρ_b. Although a direct simultaneous determination of these parameters from the measurements of resistivity vs. film thickness alone is not clearly possible, the decrease of resistivity with increasing acceleration voltage for film thickness larger than 400 Å is considered to be due to the increase of p, that is, the increase of surface flatness, and the decrease of impurities and defects included in the film. The resistivity was found to increase with decreasing the film thickness as expressed in Eqs. (4.5) and (4.6), and it was also found that the film deposited at higher acceleration voltage becomes physically continuous at an earlier stage of film formation. Clearly, metal deposition using ICB which has the characteristics of strong adhesion, high packing density and high conductivity ultra thin film, is going to be applied extensively for fabricating flexible circuits on an industrial scale (e.g. copper films on an organic plastic film board).

The ICB deposition of metals can be used to form ohmic contacts without the need for predeposition of a noble metal thus avoiding multilayer deposition. Because ICB permitts the introduction of a heavily doped region and/or of numerous recombination centers in the interface region of the semiconductor, annealing may often be avoided [140),141)]. As an example, in n-type silicon substrate, ohmic contacts have been obtained by depositing silver without any annealing process, as shown in Fig.4.12. For p-type substrates ohmic contacts have been obtained with annealing at 400°C (and using an acceleraion volt-

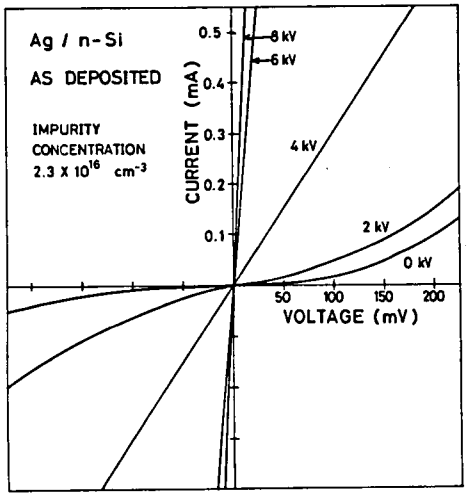

Fig.4.12 V-I characteristics of Ag contacts on a n-Si substrate for different acceleration voltages

age of over 4kV) as shown in Fig 4.13 whereas for highly doped p^+ substrates annealing was not necessary to form an ohmic contact with good adhesion. It seems that the mechanism of the formation of such ohmic contacts is associated with the production of lattice defects which contribute to the formation of numerous recombination centers near the interfacial region, and of a heavily doped region which makes the depletion region so thin that field emission takes place.

The diffusion of Ag deposited onto a Si substrate at different acceleration voltages was measured by the He^+ back-scattering method. Fig.4.14 shows the diffusion characteristics of the deposited film material for various deposition conditions before (Fig.4.14 (a)) and after (Fig.4.14 (b)) annealing at 600 °C. The diffusion depth after annealing the Si substrate is shallower for films deposited at a higher accelerating voltages. The diffusion depth due to annealing of Ag deposited under the high acceleration voltage into the substrate surface layer is suppressed in comparison with that of Ag deposited under the low acceleration voltage. The diffusion depth due to annealing of the film material is always shallower than the calculated value by thermal diffusion theory [142]. Additionally, the suppression of diffusion at higher acceleration voltage is also shown in Fig.4.15 which is the SEM photograph of the silicon substrate surface after annealing the deposited Ag film. In the film deposited at the acceleration voltage of 0 kV, the film was observed to disappear after annealing, which is perhaps due to solid phase diffusion of the Ag into the silicon bulk. For p-type Si, Ag impurity

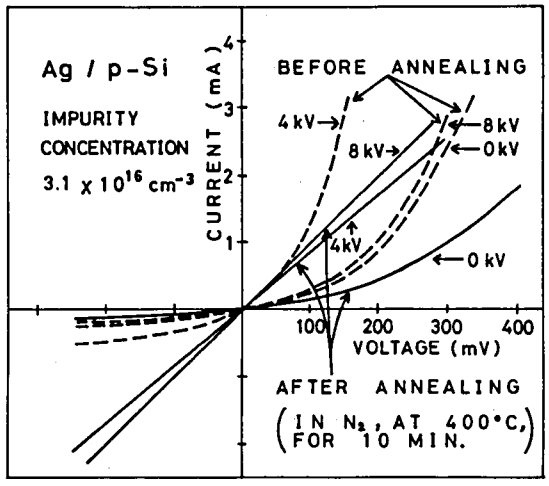

Fig.4.13 V-I characteristics of Ag contacts on a p-Si substrate for different acceleration voltages

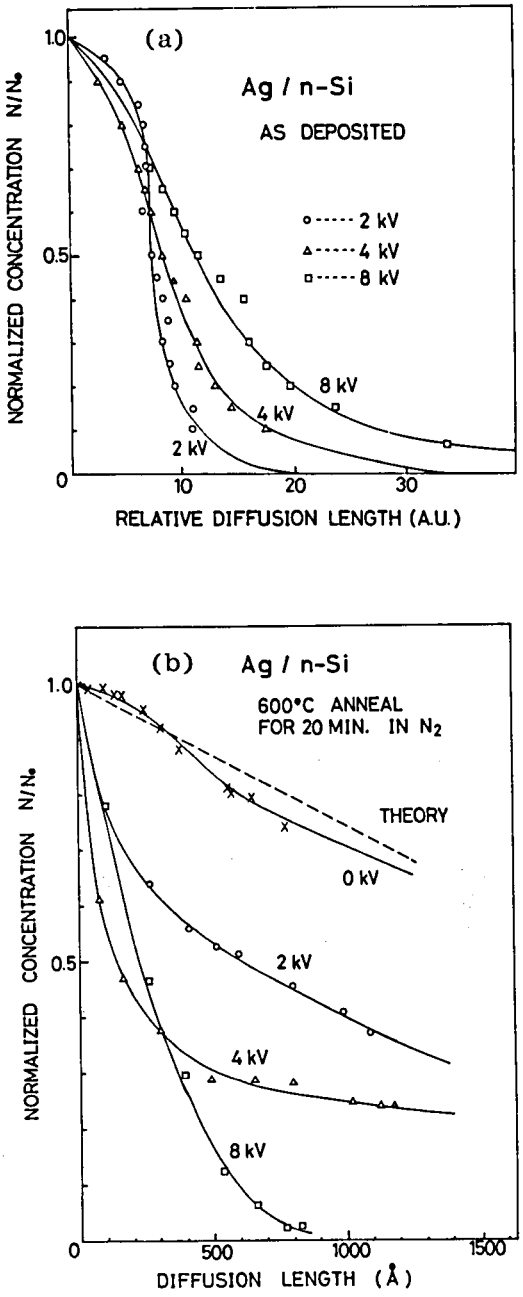

Fig.4.14 Diffusion characteristics of the deposited Ag films into the n-Si substrate surface layer at the different acceleration voltages: (a) before and (b) after annealing in N_2 gas for 20 min at 600°C

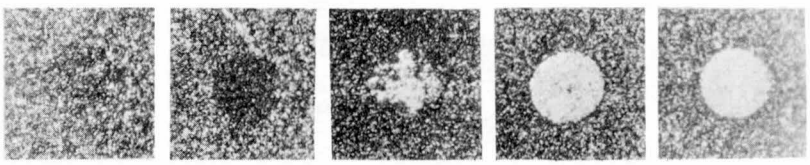

Fig.4.15 SEM images of Ag films annealed at 600°C for 20 min after deposition on the Si substrate

levels which did not appear before the annealing were observed after annealing at 600 °C as shown in Fig.4.16. It is clear from the activation energies of 0.32 eV and 0.21 eV that appear in the figure that electrically active Ag atoms which act as recombination centers are formed. The electrically active Ag is formed by substitution of Ag atoms into the Si vacancies formed by the bombardment of ions [143)-145)].

Therefore, it seems that ohmic contact formation in p-type Si mainly due to the Ag recombination centers by substitutional Ag atoms. On the other hand, for n-type Si, the surface barrier is small enough to be destroyed by the bombardment of the ionized cluster beam, resulting in ohmic contact obtained without any annealing.

To illustrate the usefulness of ohmic contact formation by the ICB technique, the technique was applied to form the contact electrodes of a p-n junction type solar cell. The characteristics of two cells with the same quality substrate for the p-n junction were compared to make clear the effect of the ohmic contact formation by the ionized cluster beam deposition compared with a commercial base as shown in Fig.4.17. The contact electrodes were made by the conventional vacuum deposition on one cell and by ionized cluster beam deposition on the other. To obtain ohmic contact electrode and good adhesion by conventional vacuum deposition, AuSb, Al, and Ag depositions on Si substrate are required. By using the ionized cluster beam deposition, Ag deposition alone is enough to obtain good characteristics for a solar cell and in addition annealing processes after the deposition are not necessary. The I-V

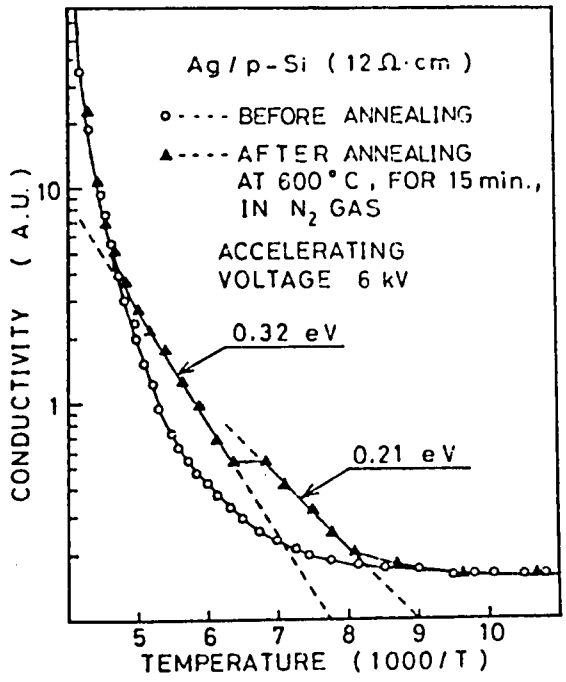

Fig.4.16 Conductivity vs. temperature characteristics

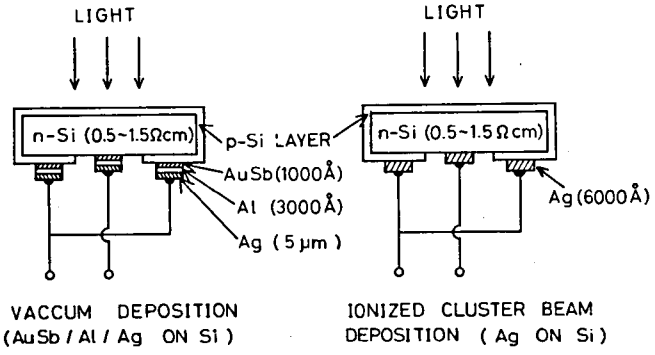

Fig.4.17 Two types of solar cell structures

characteristics of the cell with the contact electrodes made by vacuum deposition are shown in Fig.4.18 together with those of cells with the contact electrodes made by ICB deposition with accelerating voltages in the range 0 - 8 kV. In this experiment, the deposition at the acceleration voltage 6 kV has brought much better characteristic than those at other deposition conditions.

§4.3 SEMICONDUCTOR FILMS

4.3.1 Si Films

Epitaxial Growth [87),146),147)]

Several attempts at low-temperature epitaxial growth to create a shallow but sharp silicon p-n junction have in the past been made [148)]. The methods include the deposition under an ultra high vacuum (in the range of 10^{-12} - 10^{-10} Torr) on a low temperature substrate [149)], the deposition on a room temperature substrate followed by annealing by laser irradiation [150)], etc.

On the other hand, it can be shown that Si epitaxial films can be formed by ionized cluster beam deposition at substrate temperatures lower than 800°C in a vacuum of 10^{-7} - 10^{-6} Torr. Si films were deposited in a chamber which was evacuated by an oil diffusion pump to a base pressure of 1×10^{-7} Torr. Clusters from a source mounted in the vacuum chamber were ionized by electron bombardment with an ionizing current of 100 mA, and were accelerated toward a substrate at the acceleration voltage between 0 - 8 kV. Prior to the deposition, the Si substrate with (111) orientation surface was chemically cleaned with trichloroethlenne, hydrofluoric acid and acetone. The resis-

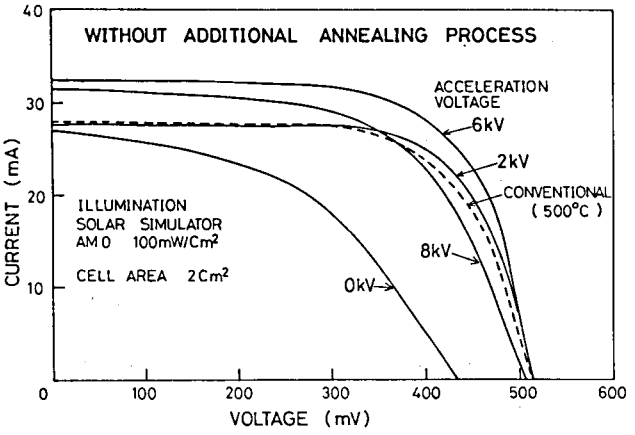

Fig.4.18 V-I characteristics of a solar cell with the contact electrode deposited by the ICB at the cell area of 2 cm^2, the illumination of air mass zero (100 mW/cm^2)

tivities and carrier concentrations of the p-type substrates were approximately 0.2 Ωcm and of the order of 10^{17} cm^{-3}, respectively. High purity n-type Si (phosphorus-doped) was used as a source materials and was loaded into a pyrolytic carbon crucible with a nozzle of 1 mm exit diameter.

The crystalline quality of the film surface was evacuated using the electron diffraction patterns. The single crystalline patterns shown in Fig.4.19 were observed in the films grown at different substrate temperatures T_s of 300°C and 620°C, which are well below reported temperatures for epitaxial growth by other film deposition methods. In the sample deposited at 620°C, Kikuchi lines were clearly visible. Figure 4.20 shows typical backscattering energy spectra using 185 keV H^+ with 8 keV FWHM at a scattering angle of 135° for a Si film deposited at 620°C; the spectra were obtained by channeled <111> and non-channeled incidences [151]. The aperture for scattered beam analysis had a diameter of 0.5 mm, and the ion dose was typically 1 μC. Radiation effects could, therefore, be neglected. The high energy edge at channel 700 corresponds to the protons scattered from Si atoms at the surface. In the channeled spectrum, the Si surface peak of the film was 11.6 x 10^{15} atoms/cm^2, which was probably due to the defects produced by the bombardment of the high energy ions of residual gases, etc.[152),153] The minimum yield, χ_{min} which is expressed by the ratio of the aligned yield to the random yield just below the surface peak, was about 6.7 %. The χ_{min} of the substrate used in this epitaxy was between 4 and 7 % .

Electrical properties of the n-type films 1300 - 1500 Å

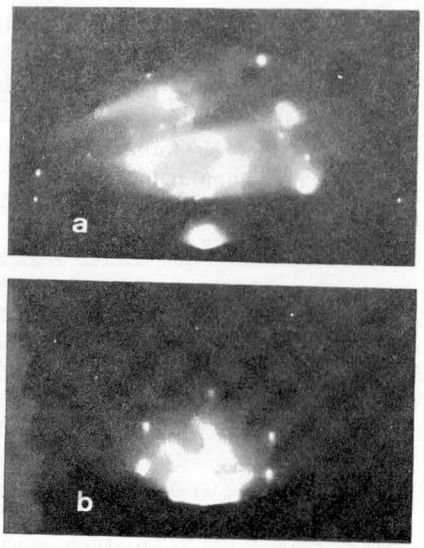

Fig.4.19 Reflectivity diffraction patterns for the films grown at (a) 620°C and (b) 300°C on (111) Si substrates

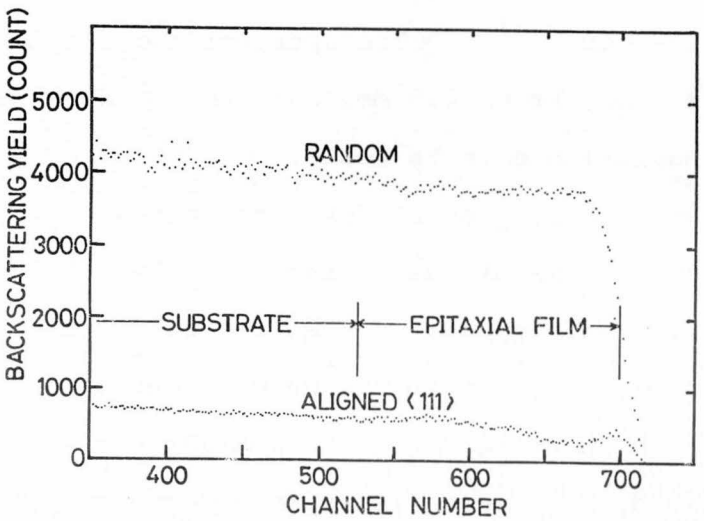

Fig.4.20 Rutherford backscattering analysis of an epitaxial film grown by the ICB deposition at acceleration voltage of 6 kV on a (111) Si single crystal at 620°C

thick deposited on p-type substrates were measured by the van der Pauw method [154]. The dependence of the Hall mobility on accelerating voltage during film growth is shown in Fig.4.21. The data show that the mobility increases with increase in accelerating voltage and with increase in substrate temperature up to a maximum temperature of approximately 700°C.

Figure 4.22 shows the temperature dependence of the carrier concentration in the films deposited at the three substrate temperatures, i.e. 300°C, 620°C and 730°C. The intrinsic region is seen in all the samples measured at high temperatures. At lower temperatures, the donor-exhaustion region is clearly seen; the carrier concentration does not change appreciably with temperature. This suggests that good quality Si films can be obtained [155),156]. The carrier concentration is higher for films deposited at low substrate temperatures than for films deposited at higher temperatures. This is probably due to the difference in the doping concentration, which is caused by the different sticking coefficients of the donor impurities during deposition.

The p-n junction diodes were fabricated, as above, by the deposition of n-type Si films on p-type single Si substrates at different deposition temperatures. Ohmic contacts were made by vacuum deposition of Au-Sb on the n-layer side and Au on the p-layer side. The C-V curves of the diodes are shown in Fig. 4.23. The curves for the samples deposited at 620°C and 300°C show the formation of an abrupt junction [157], while the film deposited at 730°C shows a slight degradation in the junction characteristics. The degradation might be due to the inter-

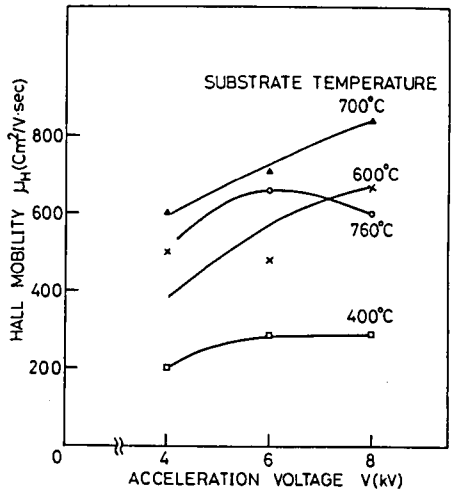

Fig.4.21 Hall mobility vs. acceleration voltage for different substrate temperatures

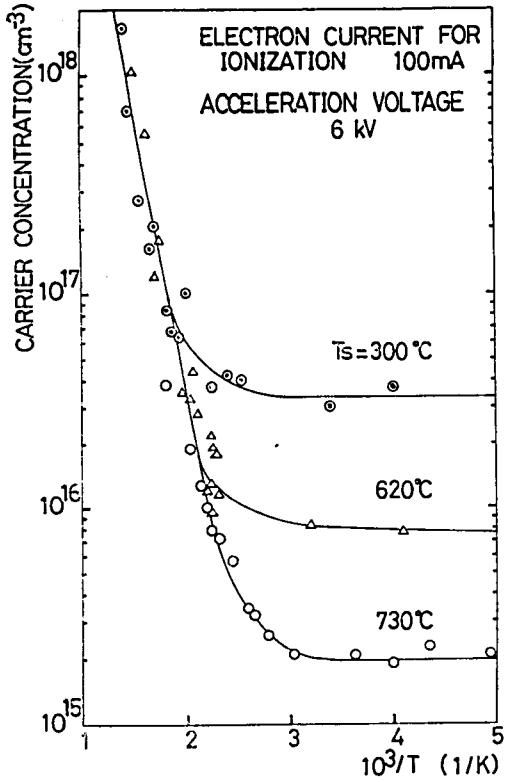

Fig.4.22 Temperature dependence of negative carrier concentrations for films grown at different substrate temperatures

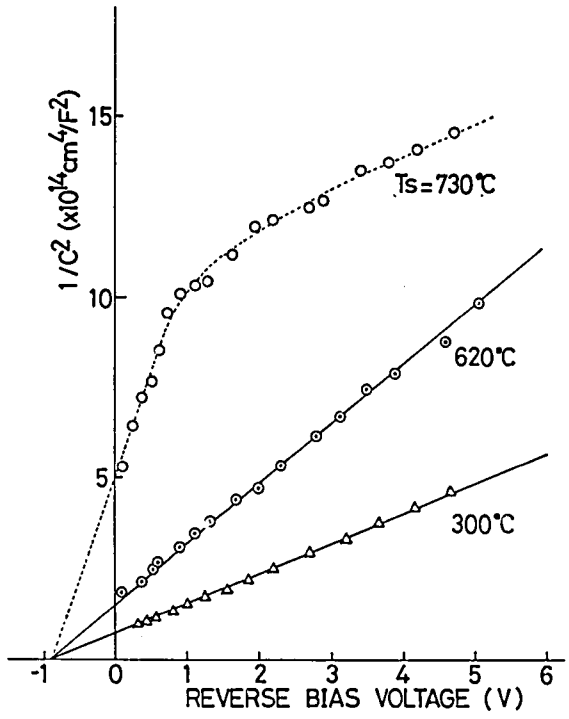

Fig.4.23 C-V characteristics of a p-n junction measured at 1 kHz

diffusion of the impurities during deposition. Under low reverse bias voltages, the slope of the $1/C^2$-V curve is higher than it is under higher reverse bias voltages, which indicates that the film's impurity concentration is lower near the junction than it is in regions farther away from the junction. The carrier concentrations calculated from these curves were about ten times as high as those obtained from the van der Pauw method. The discrepancy might be due to an effect of the film thickness, which might allow an extension of the depletion region across the junction in a region of the grown film, and/or by the presence of donors caused by some residual defects which might exist in the grown film.

These obtained results suggest that it is possible to create a device with a shallow junction depth by ICB. For example, a p-n junction solar cell was fabricated and the photovoltaic characteristics were measured [77),82)]. The junction was made by depositing the n-type Si film onto a p-type Si (6 - 11 Ω cm, (111) orientation) substrate by the ICB technique at different deposition conditions. The contact electrodes are made by conventional vacuum deposition.

The spectral characteristics of such a photovoltaic diode are shown in Fig.4.24, which indicate an increase in the sensitivity as the thickness of a deposit is reduced. The spectral sensitivities of three crystalline states are compared in Fig. 4.25. The broadest range of sensitivity is obtained in a single-crystal layer. Figure 4.26 shows the spectral sensitivity of the short circuit currents of cells with deposited layers about 2000 Å thick using different acceleration voltages.

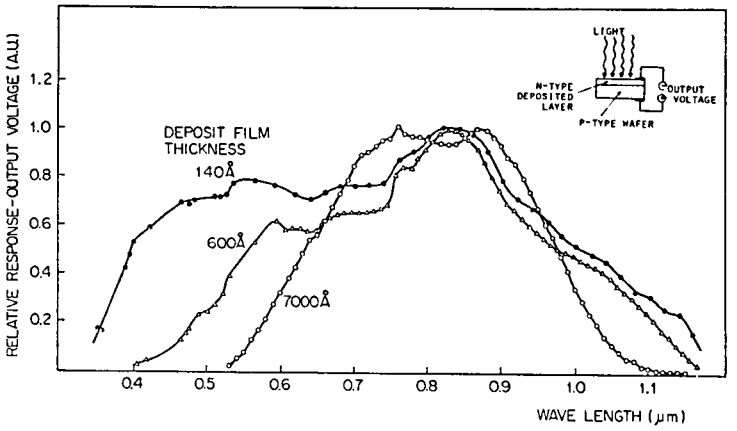

Fig.4.24 Open circui photovoltage vs. wavelength characteristics for different thicknesses of n-Si films on a p-Si substrate

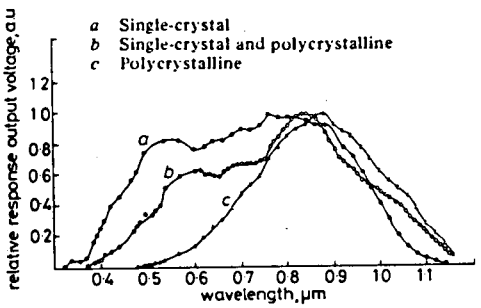

Fig.4.25 Comparison of the spectral sensitivity for the three crystalline states

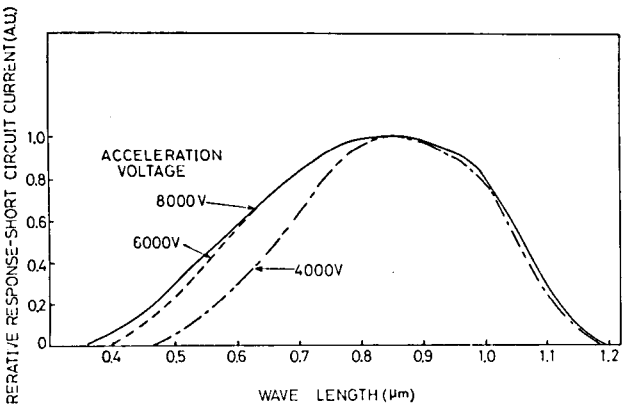

Fig.4.26 Short circuit photocurrent vs. wavelength characteristics

Within the range of the acceleration voltage as shown in these figures, we see that the crystalline quality is improved with increasing an acceleration voltage, as previously shown in the diffraction patterns of Si films of Fig.4.2.

It is understood with this voltage dependence of crystalline quality that the spectral sensitivity becomes broader and more efficient with increasing acceleration voltage. Tha same characteristics are seen in the V-I characteristics of these cells. Optimum fabrication conditions and optimum value of output have not been investigated, but this may be done by adjusting the doping density of impurity, the thickness of an epitaxial layer, the ohmic contact and the electrode shape.

Amorphous Film [158)-172)]

In earlier data of Si deposition by the ICB, it has been shown that crystal structure could be changed from amorphous state to a single crystal by changing of the acceleration voltage for the deposition at a certain substrate temperature [158)]. This experimental data suggested to us the possibility of forming hydrogenated amorphous Si films useful for electron devices. In conventional fabrication methods such as glow discharge or reactive sputtering, the film is deposited from a plasma. Compared with the conventional method, hydrogenated amorphous Si (a-Si:H) films could be prepared by using the ICB technique at a hydrogen pressure as low as 10^{-4} Torr. The a-Si:H films obtained in this experiment were found to be stable after annealing at about 500°C for 30 min [159)]. The properties of these deposited films can be controlled by choosing an adequate

deposition condition, e.g. acceleration voltage is adjusted between 0 - 5 kV, electron current for ionization at 100 mA, substrate temperature at 200 - 235°C, and H_2 pressure between 10^{-5} - 10^{-4} Torr.

Figure 4.27 shows observed dependence upon H_2 pressure in the chamber of $\sqrt{\alpha h\nu}$ versus $h\nu$ measured on the grown a-Si films. Optical band gap (V_{opt}) is the value of $h\nu$ at which $\sqrt{\alpha h\nu}$ extrapolates to zero. As the H_2 pressure increases, the V_{opt} becomes large, so that the hydrogenation of the a-Si films is possible at the low H_2 pressure of 10^{-5} - 10^{-4} Torr. From the measurement of the ion current and the analysis of the residual gas, the hydrogen concentration in the film is estimated to be several atomic per cent or less [159], which is a much smaller percentage than that in films prepared by the glow discharge method. Figure 4.28 shows the dependence of the dark conductivity of the a-Si:H films obtained by ICB at room temperature on the H_2 pressure. As the H_2 pressure increases, the conductivity becomes small. H atoms are considered to passivate the dangling bonds, causing a decrease of the electrical conduction due to the defects. From these results, it is considered that H atoms contained in the a-Si:H films prepared by the ICB technique form Si-H bond more effectively than in the glow discharge method. This could explain the improved thermal stability of films prepared by the ICB technique.

The dependence of $\sqrt{\alpha h\nu}$ vs. $h\nu$ plots on the acceleration voltage is shown in Fig.4.29. The V_{opt} does not change with changing acceleration voltage. The kinetic energy of Si clusters is considered not to have important effect on the H

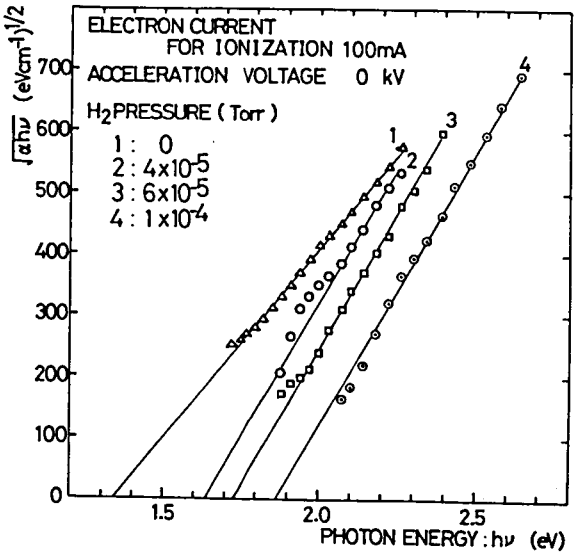

Fig.4.27 Dependence of $\sqrt{\alpha h\nu}$ on the photon energy for the films prepared at the different H_2 pressures

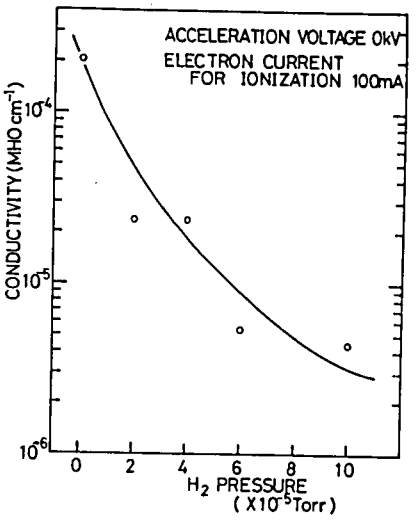

Fig.4.28 H_2 pressure dependence of dark conductivity at the room temperature

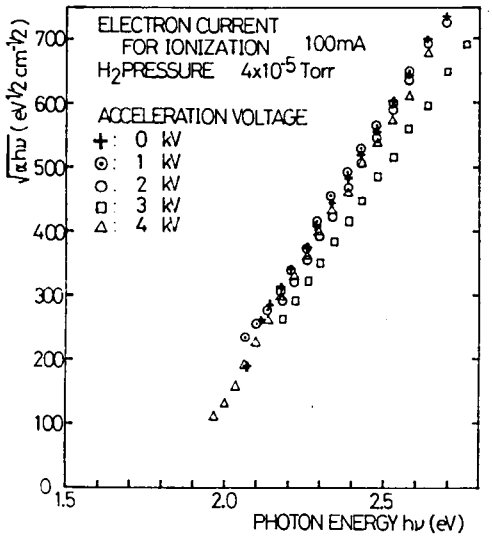

Fig.4.29 Dependence of $\sqrt{\alpha h\nu}$ on the photon energy for the films prepared at the different acceleration voltages

concentration in the film, but does influence the long range order of Si atoms through the migration effect. The dark conductivity at the room temperature tends to decrease with increasing acceleration voltage as shown in Fig.4.30. It is believed from this result that Si-Si bonds are promoted by the acceleration voltage, so that the number of defects causing electrical conduction decreases. Also, as is shown in Fig.4.31, the dependence of the density of the ionized states on the acceleration voltage, was measured from the C-V characteristics of the n-type a-Si:H films deposited on a p-type single crystal Si substrate. As the acceleration voltage increases, the density of the ionized states in the deposited a-Si:H films decreases, which can be explained by the increased number of Si-Si bonds.

Figure 4.32 shows the dependence of $\sqrt{\alpha h\nu}$ vs. $h\nu$ plots on the annealing temperature. The V_{opt} does not change even after annealing at about 500°C for 30 min. The dark conductivity at the room temperature, which is shown in Fig.4.33, does not change after annealing. It is considered that H atoms are contained in the a-Si:H films in such a stable form as Si-H, rather than $Si-H_2$ or $Si-H_3$, which is confirmed by the measurement of infrared absorption [173)-175)], and the packing density is so high that the recrystallization is not promoted by annealing.

As described above, thermally stable a-Si:H films can be obtained by the ICB technique, and the optical and electrical properties can be controlled by the growth conditions such as the H_2 pressure and the acceleration voltage.

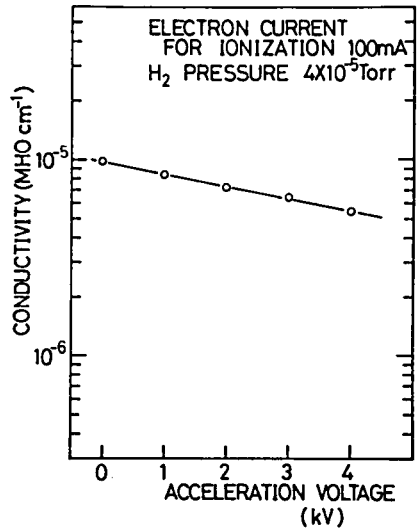

Fig.4.30 Acceleration voltage dependence of dark conductivity at the room temperature

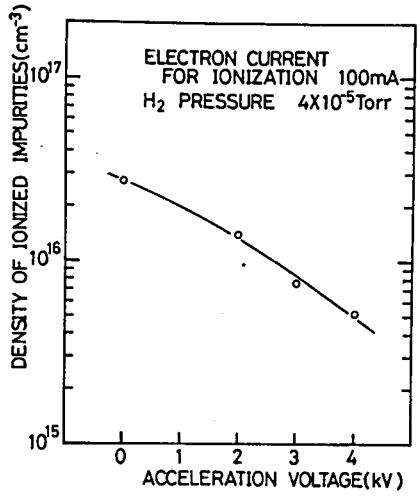

Fig.4.31 Ionized state density of the films prepared at the different acceleration voltages

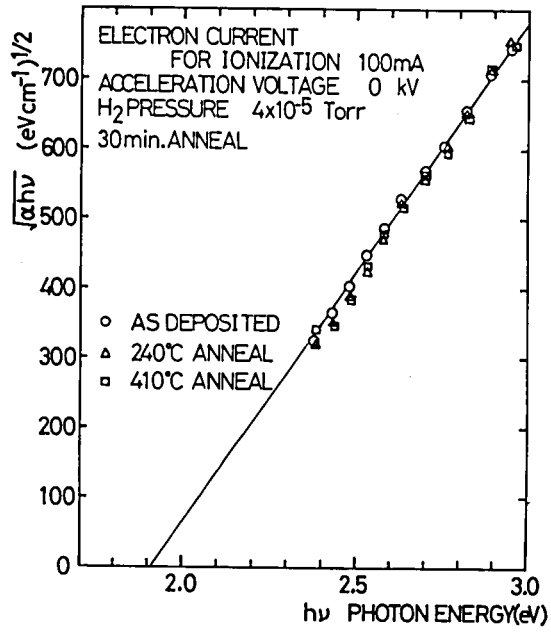

Fig.4.32 Annealing temperature dependence of $\sqrt{\alpha h\nu}$ vs. $h\nu$ plots

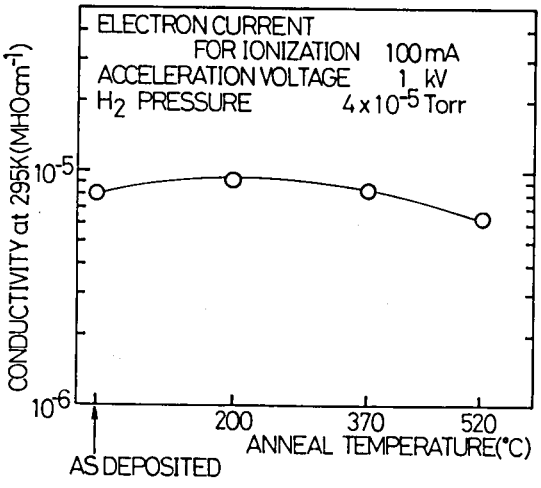

Fig.4.33 Annealing temperature dependence of dark conductivity at the room temperature

4.3.2 Compound Material Films

GaN Film [176)-181)]

Interest in GaN films has increased rapidly, since J.I. Pankove and his co-workers first produced GaN light-emitting diodes (LED's). Up to the present, GaN LED's have been made by the epitaxial growth of GaN on sapphire at 1000°C using the chemical vapor deposition (CVD) technique.

The Ga-cluster beam is formed by the adiabatic expansion of the vapor from a special nozzle into a chamber. After ionization by electron bombardment the ionized and neutral Ga clusters are reached with nitrogen gas onto a ZnO layer deposited on a glass substrate, and then epitaxially grow a GaN film. ZnO film deposited on the glass substrate by R-ICB is considered favorable as a substrate for epitaxial growth of a GaN film, because ZnO films crystallize easily with the c-axis perpendicular to the glass substrate to be desribed later, and the lattice parameter of ZnO is quite close to that of GaN. Figure 4.34 shows the x-ray diffraction patterns of the ZnO and GaN films and of powdered Al_2O_3. The lattice misfit between (002) planes of GaN and of ZnO is seen to be only 0.46 %, which contrasts with the misfit of 16.4 % between (0001) planes of GaN layer and sapphire. Therefore, tha ZnO is excellent as a nucleation layer for the epitaxial growth of a GaN film.

Two scanning electron microscope (SEM) views of the fractured edge of GaN layers grown by R-ICB on the c-axis oriented ZnO films are shown in Fig.4.35 for two different temperatures (a) 400°C and (b) 450°C. The deposition conditions for these GaN layers involved the electron currents for ionization I_e of

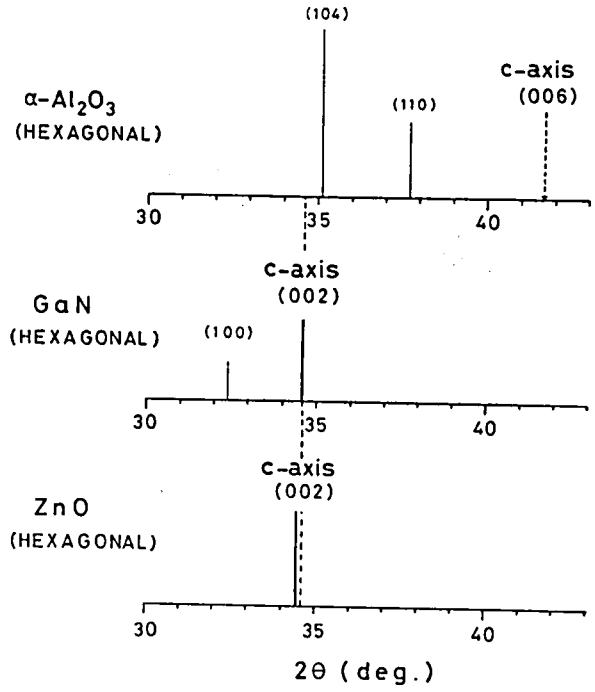

Fig.4.34 x-ray diffraction patterns of ZnO and GaN films together with that of powdered Al_2O_3

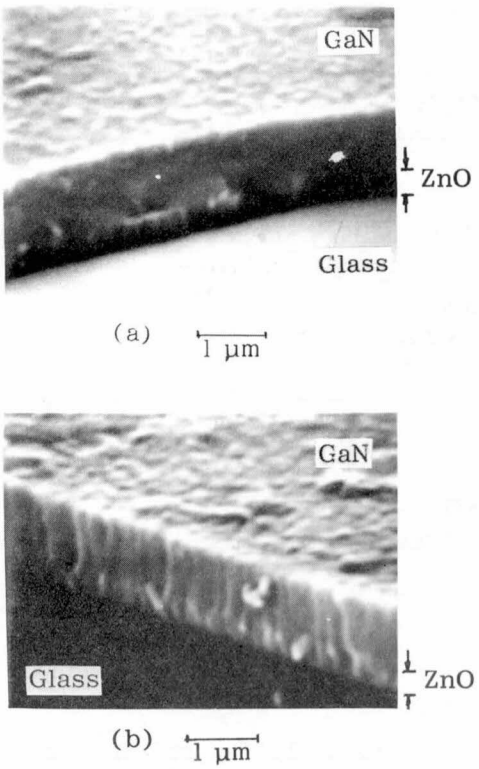

Fig.4.35 SEM views of fractured edges of GaN layers on the c-axis oriented ZnO films for (a) 400°C and (b) 450°C

300 mA, zero acceleration voltage V_a, and nitrogen pressure of 5×10^{-4} Torr. From these experimental results, it is concluded that the R-ICB technique is effective for the epitaxial growth of GaN even at relatively low substrate temperature below 600°C. In this technique crystallization is considered generally to be accelerated by the kinetic energy of clusters and by the ionized state of clusters. The GaN films produced exhibited resistivity of the order of 500 Ω cm, and shows n-type conductivity, probably due to high concentration of the native donor (nitrogen vacancies). The resistivity of the ZnO layer at room temperature was about 1000 Ω cm, and the ZnO layer was found to have no electroluminescent properties.

ZnS:Mn Film [16),17),74),75),184)]

Most of the effects in thin-film DC electroluminescence (EL) development were concentrated on ZnS:Mn, Cu and Cl [182),183)]. DC EL in ZnS:Mn by simultaneous or alternating implantation and vacuum deposition was reported by T.Takagi et al. [58)] in 1973. The cells showed long life under DC operation. BY using the ICB deposition similar results have been obtained.

In the experiments using the ICB technique, ZnS:Mn was deposited at 1 kV with a substrate temperature of 250°C [184)]. After deposition, the film was annealed at 500°C for 1 hr in a vacuum, and then Al was deposited as a contact electrode. Figure 4.36 shows the electron diffraction pattern of the ZnS:Mn film deposited on a rocksalt substrate. The single crystal state is indicated by the pattern shown in this figure.

The current-voltage and the voltage-brightness characteris-

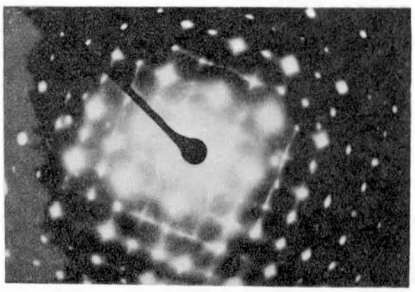

Fig.4.36 HEED pattern of ZnS:Mn film prepared by ICB deposition

tics of the film deposited on a NESA glass by the ICB technique are shown in Figs. 4.37 and 4.38, respectively. The cell shows low impendance characteristics under DC excitation similar to those of a ZnS:Mn cell made by a conventional method, but the ICB cell does not show the rectification characteristics which are exhibited by a DC EL cell fabricated by thermal diffusion processing.

§4.4 OXIDE FILMS

4.4.1 ZnO Films [2),83),84)]

As a typical example of the results of reactive ICB deposition we describe the characteristics of ZnO films. Zn clusters were formed by supersaturation of Zn vapor in an adiabatic expansion through a small nozzle of a crucible, in which Zn was vaporized at 410 - 490 °C to obtain an optimum vapor pressure of 0.1 - 1.0 Torr. Oxygen gas was introduced into the chamber until the gas pressure was 5×10^{-4} Torr. The acceleration voltage (V_a), the electron current for ionization (I_e) and the substrate temperature (T_s) were V_a = 0 - 2 kV, I_e = 0 - 300 mA and T_s = 100 - 250 °C, respectively. In these experiments the deposition parameters, in particular the acceleration voltage V_a, the electron current for ionization I_e and the various kinds of substrates and their temperatures T_s were investigated.

Figure 4.39 shows the x-ray diffraction and RHEED patterns of films deposited on glass substrates at various acceleration voltages with I_e = 300 mA. From these patterns it was found that the films were preferentially oriented along the c-axis

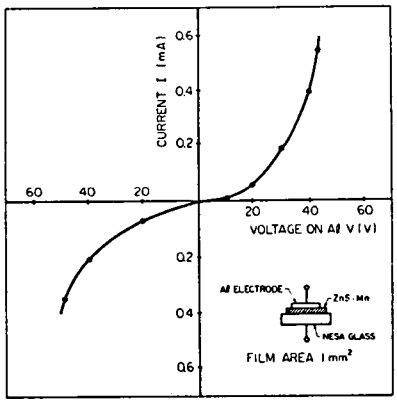

Fig.4.37 V-I characteristics of ZnS:Mn DC EL cell

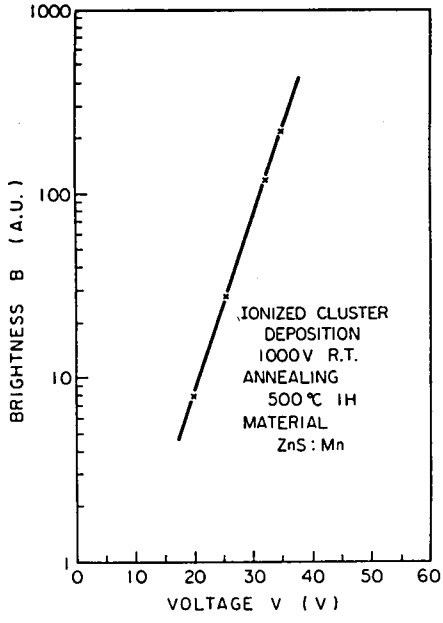

Fig.4.38 Dependence of brightness on the applied voltage under the DC excitation

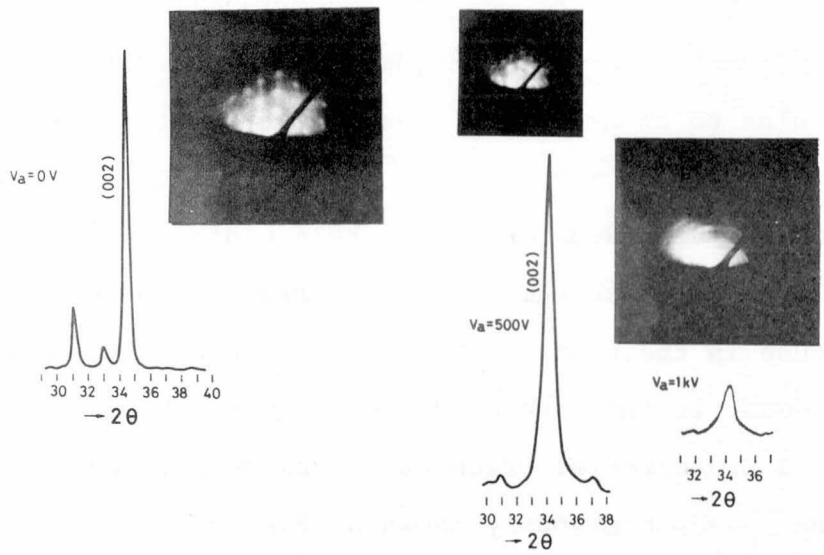

Fig.4.39 x-ray diffraction patterns and RHEED patterns of ZnO films deposited on a glass substrate at different acceleration voltages

when V_a was 500 V or less, but they gradually changed from a preferentially oriented state to a polycrystalline state when they were deposited at higher acceleration voltages[185]. Figure 4.40 shows SEM photographs of the films which indicate that the flatness of the films deposited at higher voltage is better, though the preferential c-axis orientation may be destroyed. These characteristics might be due to migration and sputtering effects of the adatoms during film formation.

A preferential orientation, with the wurtzite c-axis perpendicular to an amorphous substrate surface, increases as the electron current for ionization I_e increases. Figure 4.41 shows the dependencies of the half widths of x-ray rocking curves of ZnO films on the electron current for ionization I_e. The decrease in the half width with increasing I_e indicates an improvement in the crystalline quality of the film. In addition, a preferential orientation can be also enhanced with increasing I_e, as previously shown in Fig. 2.7.

Figure 4.42 shows the RHEED patterns of Li-doped ZnO films deposited on $(1\bar{1}02)$ sapphire substrates at substrate temperatures T_s of 160 and 230 °C for a case of V_a = 1 kV and I_e = 300 mA. The crystallinity is influenced by the substrate temperature even when V_a = 0. Figure 4.43 shows the RHEED patterns obtained for films deposited on different planes of sapphire substrates. Single crystal films can be obtained for both the surface orientations. In particular, the films grown on the $(1\bar{1}02)$ sapphire substrate were found to be preferentially oriented with their c-axis almost parallel to the substrate as shown in Fig. 4.44.

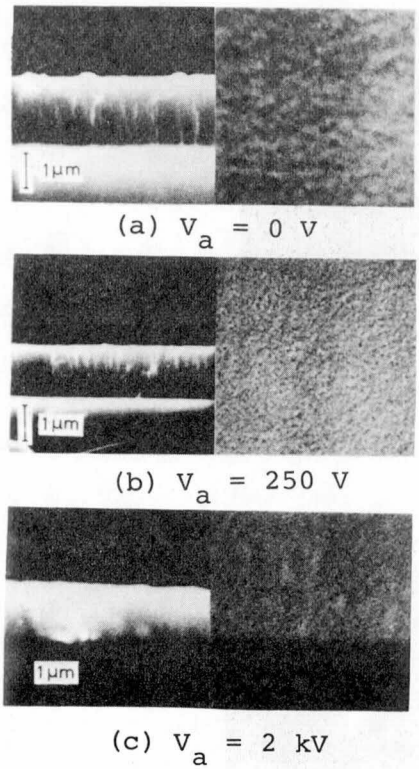

Fig.4.40 SEM photograph of ZnO films deposited on a glass substrate with various acceleration voltages (V_a): (a) V_a= 0 V, (b) V_a=250 V and (c) V_a=2 kV

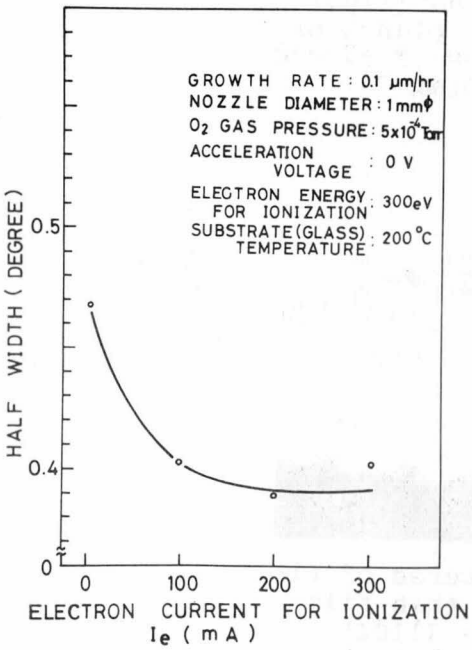

Fig.4.41 Half width of x-ray rocking curves as a function of electron current for ionization

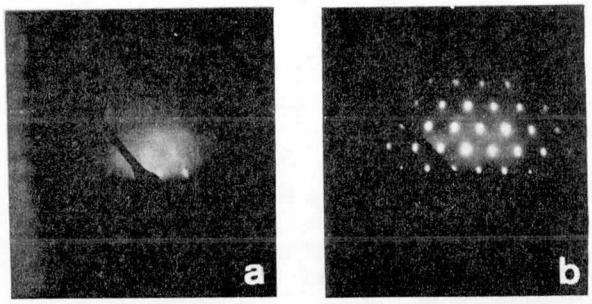

Fig. 4.42 Dependence of RHEED patterns of ZnO films on the substrate temperature: (a) 160°C and (b) 230°C

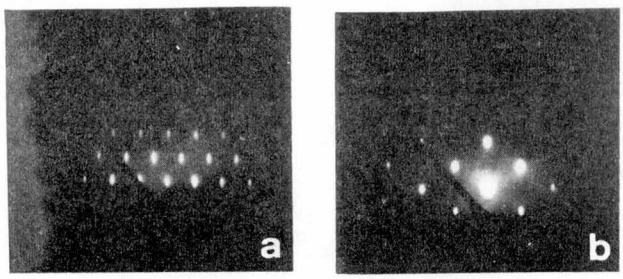

Fig. 4.43 RHEED patterns of ZnO films deposited on (a) the $(1\bar{1}02)$ and (b) the (0001) planes of sapphire substrates: T_s=230°C, V_a= 1kV and I_e= 300mA

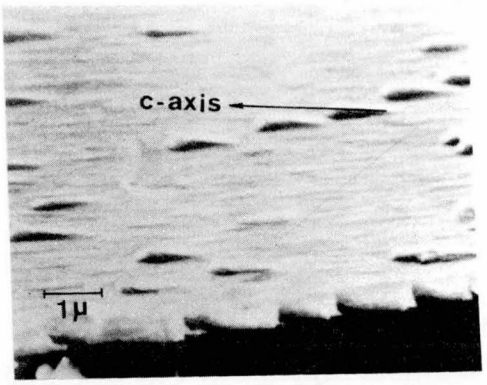

Fig. 4.44 SEM structures of Li-doped ZnO thin film grown on a $(1\bar{1}02)$ sapphire substrate

Figure 4.45 shows the attenuation loss of a He-Ne laser beam by a film as a function of the acceleration voltage during film deposition. The attenuation loss caused by the film is affected by the acceleration voltage as well as by film thickness, crystallinity and surface smoothness. It was found from this figure that an attenuation loss lower than 1 dB/cm with a film thickness of 1 μm could be expected, when the films were prepared at V_a= 0 or above 1 kV.

The surface conductivity of ZnO films deposited by the R-ICB technique can be controlled over the wide range (10^{-3} - 10^{-7} $\mho$ cm^{-1}) by the deposition conditions. The surface conductivity of ZnO films can be reduced by adding doping impurities such as Li or Na using a separate crucible in the R-ICB technique[186),187)]. Figure 4.46 shows temperature dependence of surface conductivity for Li-doped ZnO films deposited onto a glass substrate and onto a sapphire substrate at V_a = 500 V and I_e= 300 mA. The characteristics of undoped ZnO films deposited under the same deposition conditions are also shown. The effect of lithium doping in ZnO films deposited onto sapphire substrates is different from that in films on glass substrates. Lithium-doped ZnO films deposited onto sapphire substrates are characterized by a depletion region corresponding to good crystalline quality, whereas such a depletion region and high surface conductibity are not exhibited by films deposited onto glass substrates. The activation energy E_a of 0.24 eV corresponding to the lithium centre can be clearly distinguished from a donor centre in the undoped film of 0.075 eV due to the excess interstitial zinc donor.

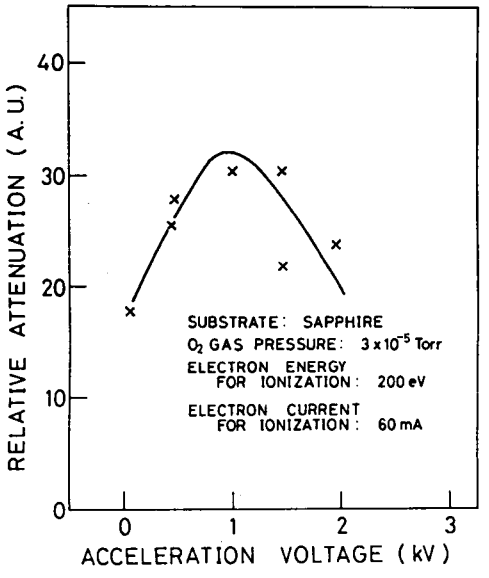

Fig.4.45 Dependence of relative attenuation loss of laser beam in ZnO films on acceleration voltage during the deposition

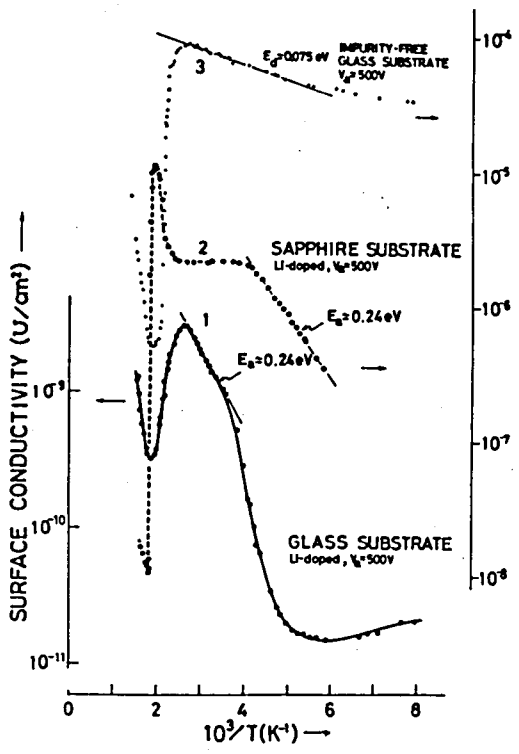

Fig.4.46 Comparison of surface conductivity of: (1) Li-doped ZnO fim deposited on a glass substrate, (2) Li-doped ZnO film deposited on a sapphire substrate and (3) Undoped ZnO film deposited on a glass substrate

A typical CL-spectrum for a Li-doped ZnO epitaxial film deposited at V_a = 1 kV and $T_s \simeq 230$ °C, is in Fig. 4.47 compared with the spectrum of a sapphire substrate without deposit. The sapphire shows two broad luminescence bands in the visible region at room temperature: an exciton band emission at 0.380 μm and a green emission at 0.527 μm. On the other hand, the Li-doped ZnO film shows a sharp red emission at 0.695 μm, with half-width of about 40 Å, and U.V. emission at 0.330 μm caused by the bound exciton band. A possible recombination mechanism causing the red emission is considered to be an electron transition from the metastable state of oxygen vacancy into the paramagnetic Li-center to yield an acceptor center with the substitution of Li atoms for the lattice of Zn atoms [188]. From conductivity measurements of the Li-doped ZnO epitaxial films, an acceptor level due to Li atoms is estimated to be about 0.24 eV above the valence band, whereas the metastable state is localized at the energy level of about 1.4 eV below the conduction band. Therefore, the red emission is due to the transition between the two bands with energy difference corresponding to wavelength 0.695 μm.

4.4.2 BeO Films[86),189]

BeO crystallizes in the wurtzite structure, and is an excellent ionic crystal belonging to space group C_{6V}^4. Lattice constants of this material are a ≃ 2.695 Å and C ≃ 4.390 Å (C/a ≃ 1.65), and the melting point is 2,540 °C. This material is an excellent insulator with resistivity of 10^{13} Ω.cm (at 300 K), and with a large band gap of 11.2 eV[190].

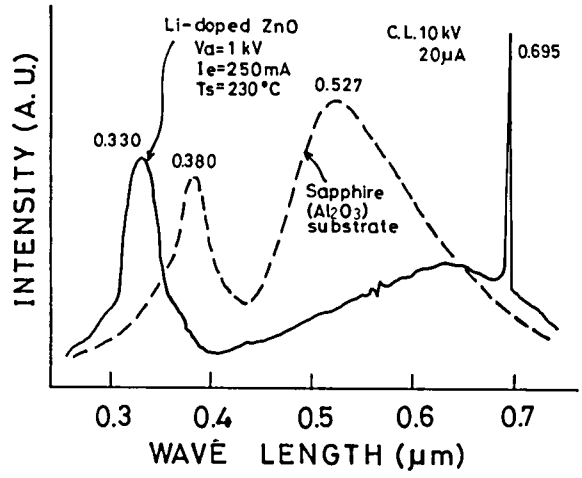

Fig.4.47 Cathodeluminescence spectra of Li-doped ZnO films and sapphire substrate

In addition, the material has a high thermal conductivity of the same order of that of Al, because of great contribution of lattice vibrations. Other interesting properties are the high mechanical hardness (Morse hardness 9) and chemical erosion resistance. It has been difficult to prepare good crystalline BeO films by using conventional fabrication technology, because high operational temperatures exceeding 3,000 °C are required for crystal growth.

Using the R-ICB technique, growth of a BeO film on a glass substrate was achieved using electron current for ionization I_e= 300 mA, acceleration voltage V_a= 0 kV (with only ejection velocities of Be-clusters), substrate temperature T_s= 400 °C and oxygen pressure of 4 X 10^{-4} Torr.

Figure 4.48 shows an x-ray diffraction pattern of a BeO film grown on a glass substrate in comparison with that of a BeO ceramic baked by a conventional thermal method[191]. As seen in this figure, there is a remarkable difference between the results of the BeO ceramic and the BeO film. That is, the ceramic exhibits many peaks such as those corresponding to (101), (002) and (100) planes, whereas the film shows a peak from only the (002) plane indicating the c-axis preferential orientation is clearly enhanced. Figure 4.49 shows a cross section of the BeO film taken with a scanning electron microscope (SEM), from which the column structure can be recognized. Figure 4.50 shows the RHEED pattern of the epitaxial film grown on the (0001) plane of a sapphire substrate under the same conditions as defined above. Because of close agreement in the lattice constant (a ≃ 2.695 Å) of BeO with the distance

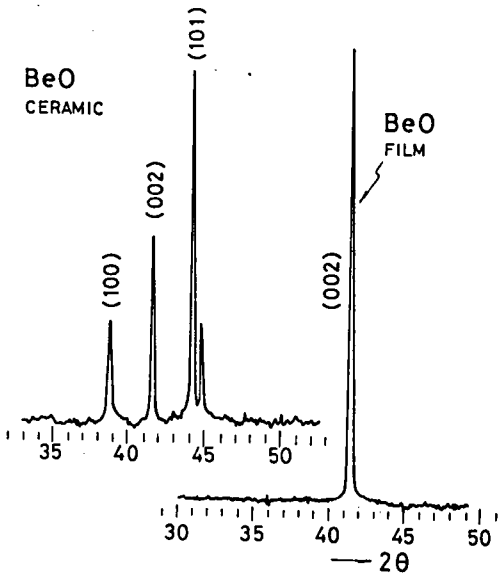

Fig.4.48 x-ray diffraction pattern of a BeO film grown on a glass substrate in comparison with that of a BeO ceramic

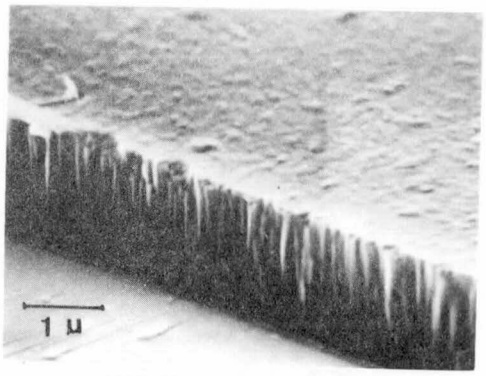

Fig.4.49 SEM structure of BeO thin film grown on a glass substrate

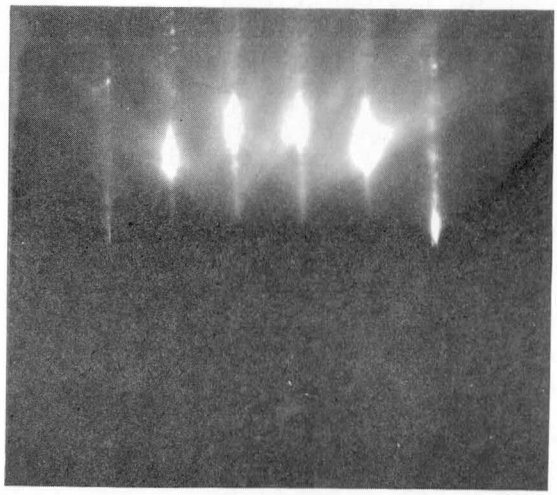

Fig.4.50 RHEED pattern of BeO thin film grown on a (0001) sapphire substrate

(2.742 Å) between the nearest neighbor atoms on the sapphire (0001) plane, the epitaxial growth of good quality BeO films was possible using only ejection velocities of Be clusters.

The presence of vibrational dipoles in a polar material has great influence on the electronic structure and transport properties of the material. These parameters of a polar material can be inferred from investigation of optical properties in the infrared dispersion region. According to the dispersion theory applicable for polar materials, the frequency dependence of the dielectric constant can be written as

$$\varepsilon(\omega) = \varepsilon(\infty) + \frac{\varepsilon(0) - \varepsilon(\infty)}{1 - (\omega/\omega_q^o)^2 - 2\,i\,(\gamma/\omega_q^o)\,(\omega/\omega_q^o)}, \quad (4.7)$$

where $\varepsilon(\infty)$ is the optical dielectric constant, $\varepsilon(0)$ is the static dielectric constant, ω_q^o is the circular infrared dispersion frequency, (i.e., the lattice vibration frequency which gives a transverse wave mode), and γ is the dissipative force.

In order to estimate the dispersion frequency ω_q^o for BeO films prepared by the R-ICB technique, measurements on their infrared reflectivities, R, were made in the wavelength region 2.5 - 25 μm. Figure 4.51 shows the experimental results for BeO films grown on the sapphire (0001) subatrate under the epitaxial condition of I_e= 300 mA, V_a= 0 kV, and T_s= 400 °C[192].

From the result, the dispersion frequency, ω_q^o, was estimated to be 1.39 X 10^{14} sec^{-1}, while the frequency of longitudinal mode, ω_q^1, was roughly estimated to be 1.79 X 10^{14} sec^{-1} from a wavenumber at which the reflectivity decreases rapidly to zero[193].

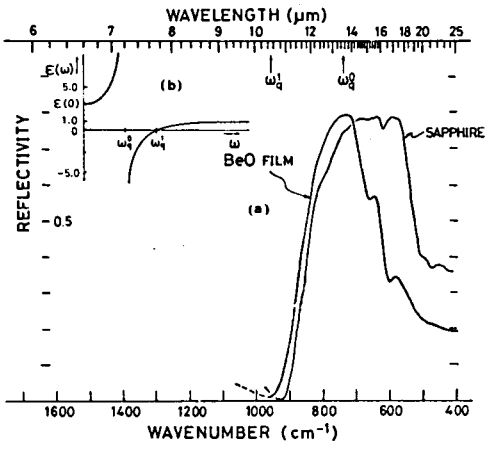

Fig.4.51 Infrared reflectivity of the BeO film grown on a sapphire (0001) substrate at I_e=300 mA, V_a=0 kV and T_s=400 °C

The value of the static dielectric constant $\varepsilon(0)$ was also estimated to be 6.5 ($n \simeq 2.55$) for the BeO film from a value $R = 0.19$ at 400 cm^{-1}, regarding the reflectivity as a constant below the wavenumber. This value was in good agreement with that measured by means of a capacitance bridge. The optical dielectric constant $\varepsilon(\infty)$ was estimated to be 3.92 ($n \simeq 1.98$), which was calculated from the relationship $\varepsilon(\infty) = \varepsilon(0) \cdot (\omega_q^o/\omega_q^1)^2$. This value is in close agreement with that of a single crystal grown from a molybdate solution, i.e., $\varepsilon(\infty) \simeq 2.96$ ($n \simeq 1.72$).

The sound velocity U_s in the optical transverse vibration mode was roughly estimated from the following dispersion relation for polar material[194]:

$$\omega_q^2 = \frac{\Phi(d)}{M} \left[1 \pm \left(1 - \frac{4M}{M_+} \sin^2 \left| qd \right| \right)^{1/2} \right], \quad (4.8)$$

where M is the reduced mass of two constituent elements (m,M), $M_+ = m + M$, $\Phi(d)$ is a dynamical constant related with the distance, d, between two ions, and q is a wave vector in the crystal momentum space, respectively. The high dispersion frequency obtained for BeO films suggests that the optical vibration arises from the constituent Be atoms which have smaller mass than oxygen atoms. Therefore, taking into account $|qd| = \pi/2$ which corresponds to a band edge of the Brillouin zone, the sound velocity U_s at the dispersion frequency ($\omega_q = \omega_q^o$) can be easily obtained by combining a peculiar solution $\omega_q^o = \sqrt{2\ \Phi(d)\ /\ m}$ with $\Phi(d) = (M_+/2) \cdot (U_s/d)^2$, that is,

$$U_s = \omega_q^o \left(\frac{m}{M_+} \right)^{1/2} . \qquad (4.9)$$

Applying m = 9.012, M = 16.0 (m, M are the atomic weights of beryllium and oxygen), and d = 1.65 Å (the Be-O distance in a parallel distance to the c-axis) into Eq.(4.9), the sound velocity could be estimated as U_s = 13.8 x 10^3 m/sec. This value is reasonable as compared with the value, U_s = 12 x 10^3 m/sec [195], which was measured along the c-axis of a flux grown single crystal.

An elastic constant in a direction parallel to the c-axis, $C_{33}^D \simeq 57.9 \times 10^{10}$ N/m^2, could be also obtained from the value of U_s and its known density of BeO, i.e. $\rho \simeq 3.04 \times 10^3$ kg/m^3. This is slightly higher than the value ($C_{33}^D = 49.8 \times 10^{10}$ N/m^2) of sapphire.

The anisotropic thermal conductivities of the c-axis oriented films grown on glass substrates were measured in order to obtain information about the thermal transport mechanism. Figure 4.52 shows a typical example of the results obtained in this study. The values of $\kappa_{ph}^{//}$ and $\kappa_{ph}^{\perp}$, measured with the heat flow parallel and perpendicular to the c-axis of BeO film, are shown as function of temperature. In this result, the value of $\kappa_{ph}^{//}$ is about four times larger than that of $\kappa_{ph}^{\perp}$ in the temperature region up to the Debye temperature θ_D ($\sim$ 1,053 K). The value of $\kappa_{ph}^{//}$ at room temperature was typically 2.6 w/cm·deg, while that of $\kappa_{ph}^{\perp}$ was 0.6 w/cm·deg. The observed high thermal conductivity of BeO should be considered to be due to the contributions of lattice vibration modes, that is, phonon

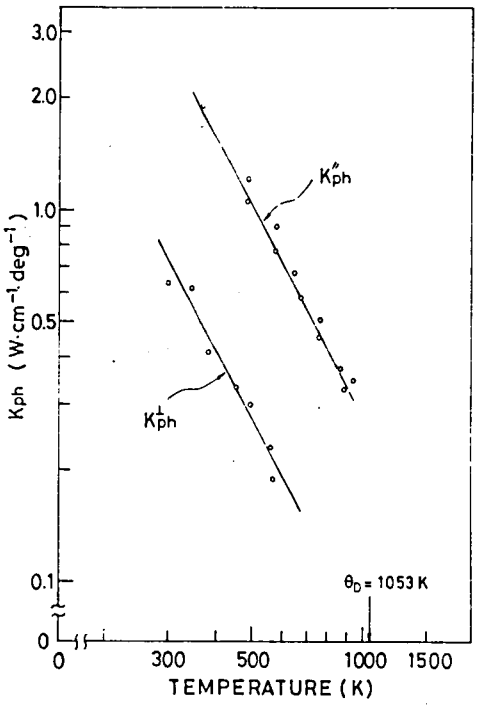

Fig.4.52 Temperature dependence of the anisotropic thermal conductivities κ''_{ph} and $\kappa^{\perp}_{ph}$

modes. According to Debye's theory, the lattice thermal conductivity κ_{ph} in an isotropic medium is given by

$$\kappa_{ph} = \frac{1}{3} \sum \Lambda_{ph} U_s C_{ph} , \qquad (4.10)$$

where Λ_{ph} is the mean free path of the polar phonon, C_{ph} is the phonon specific heat per unit volume. In Eq.(4.10) the mean free path Λ_{ph} can be expressed in terms of the net density of lattice thermal phonons and the capture cross section, so that Λ_{ph} as well as C_{ph} can be considered to be independent of the crystallographic anisotropy of materials. The anisotropic lattice thermal conductivity as shown in Fig.4.52 can be roughly accounted for by considering the anisotropy of the sound velocity U_s.

The sound velocity parallel to the c-axis, $U_s^{//}$, was about 13.8×10^3 m/sec as mentioned above, while the velocity perpendicular to the c-axis $U_s^{\perp}$, was estimated to be 3.2×10^3 m/sec from a mean value of a resonant frequency obtained from the experiment on surface waves and a pitch of interdigital fingers formed on the BeO film surface. The ratio of $U_s^{//}$ to $U_s^{\perp}$ is 4.3, which in turn is in good agreement with that of $\kappa_{ph}^{//}$ to $\kappa_{ph}^{\perp}$. As shown in this figure, both $\kappa_{ph}^{//}$ and $\kappa_{ph}^{\perp}$ were found to be proportional to T^{-2} in this temperature region. This temperature dependence observed in BeO films can be explained by a simplified model for the thermal conductivity of the lattice applicable for a chemically pure ionic crystal [196].

The results are tabulated in Table 4.1, compared with those of Al_2O_3 (sapphire) and SiO_2 (quartz). The high lattice

Table 4.1 Values of κ_{ph}'s of typical polar oxides (BeO, Al_2O_3 and SiO_2), together with those of Θ_D and C_{33}^D

Materials	κ_{ph} (w/cm·deg)	Θ_D (K)	C_{33}^D ($\cdot 10^{10}$ N/m^2)
BeO	2.6	1,053	57.9
Al_2O_3 (sapphire)	0.25	919	47.8
SiO_2 (quartz)	0.014	470	11.04

thermal conductivity of BeO shown in this Table can be attributed to the high Debye temperature Θ_D and the large elastic constant C_{33}^D, which are closely related with the dispersion frequency ω_q.

An attempt to grow a BeO film on a Si-(111) wafer was made. Figure 4.53 shows an SEM photograph of the fractured edge of an Al/BeO/Si structure, in which BeO film was deposited on Si-(111) wafer using I_e = 300 mA, V_a = 0 kV and T_s = 400°C, with an Al film then evaporated using a conventional method. As seen in the photograph, the c-axis of BeO film is aligned in perpendicular to the Si surface. The thermal conduction from the Si wafer, therefore, depends on $\kappa_{ph}^{//}$ of BeO film, which was estimated to be 2.6 w/cm·deg. From these results, the BeO films are expected to be useful to solve serious thermal transfer problems in semiconductor devices such as power transistor, large scale integrated (LSI) circuits and semiconductor lasers.

§4.5 SUMMARY

Film formation mechanisms based upon the effects of ions and ion energies associated with the ICB technique were investigated. The kinetic energy of accelerated particles is converted to sputtering energy, implantation energy, thermal energy and migration energy. In particular, the migration energy is enhanced with increasing the acceleration voltage. Also, the presence of ionized particles in the source materials, even without acceleration of the ionized particles, was found to influence quality of the films. In addition, characteristics of metal, semiconductor and oxide films prepared by the ICB

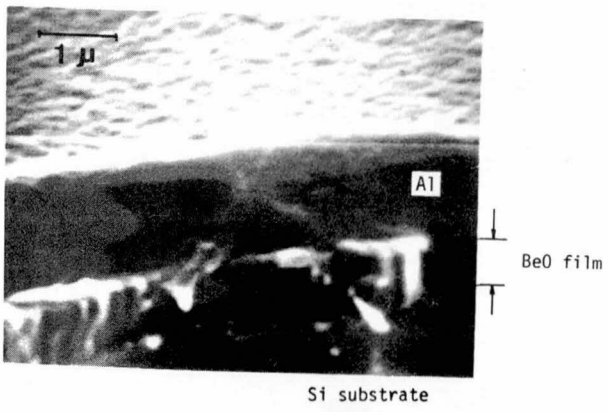

Fig.4.53 SEM photograph of the fractured edge of an Al/BeO/Si structure

and R-ICB techniques were investigated and prospective applications to electron devices were identified.

V CONCLUDING REMARKS

Developmental results using the ICB and R-ICB deposition techniques have been discussed from the standpoint of ion-based mechanisms. The ionization of clusters paly an important role in the film formation process, i.e. the presence of ions has a great influence on the critical parameters (such as coalescence and nucleation) in the condensation process and on the chemical activity, even without an acceleration voltage.

When an acceleration voltage is applied, epitaxial film growth can be achieved at much lower substrate temperature and the crystallographic and physical characteristics of the film, particularly the adhesion strength, the packing density and the surface flatness, can be improved. The energy required for crystal growth depends on the type of the source material and the substrate material or both.

In chapter II, main roles of ions in the film formation have been studied. The effective incident energy required for film formation is in the order of a few eV to several hundred eV. The presence of ions has strong influence on the film formation process even without any acceleration or even when a few per cent of ions are contained in the total mass flux. In this chapter, various kinds of ion-based techniques have also been investigated, where atomic, molecular or cluster ions have been used with or without neutral particles. Film formation by conventional ion plating in plasma has been performed with the vaporized-metal ions accelerated to the substrate across the cathode dark space. In this case a large

fraction of the kinetic energy of the ions can be transferred to neutral particles through collisions. For example, if the Ar gas pressure is 10^{-2} Torr and applied voltage is 3 kV, only 5 - 10 % of the total particles which arrive at the substrate are ionized, and incident energy of these ionized particles is about 300 eV. Neutral particles, which are twenty times more numerous than the ions, arrive at the substrate with an energy of approximately 135 eV. This suggests that the kinetic energy is also about 100 - 300 eV even in the plasma method, and neutral particles also play an important role in film formation.

For ion beam deposition using modified ion implantation apparatus with deceleration field, high energetic ions extracted into a high vacuum region are utilized for film formation after deceleration to several tens to several hundred eV. In the Ionized Cluster Beam technique, clusters which consist of about 500 - 2000 individual loosely coupled atoms are used. These clusters are partially ionized (practically, ionized clusters comprise 10 - 50 % of the total and each ionized cluster has only one charge), and are accelerated to the substrate by the applied voltage of up to a few kV. However, it should be noted that, even for the acceleration potential of a few kV, the energy of each atom is of the order of a few eV.

In chapter III, mechanisms of cluster formation and experimental results related to cluster size and distribution have been described. The cluster is considered to be formed by condensation through an adiabatic expansion. The size has been estimated from the kinetic equation $E = \frac{1}{2} NmU^2$, where E

is the kinetic energy of the cluster beam, U is the flow velocity, m is the mass of an atom and N is the cluster size. The energy and the velocity of the cluster have been measured for Ag by the electrostatic 127° energy analyzer and by the rotating disk system. The energy and velocity of the clusters are observed to be higher than those of the atoms, and from these results the cluster size has been estimated to be 500 - 1000 atoms. The transmission electron microscopy has been used to confirm these results for Ag clusters, in which the size has also been estimated to be about 2000, when it is assumed that the lattice distance is 4.07 Å and that the Ag clusters deposited on a grid has f.c.c structure.

In chapter IV, film formation mechanisms with the ICB technique based on the effects of ions contained in the cluster beam and their kinetic energies have been studied. The kinetic energy of accelerated particles is converted to sputtering energy, thermal energy, implantation energy and migration energy. In particular, the migration energy is enhanced with increasing the acceleration voltage. Also, the presence of ionized particles in the source materials, even without acceleration of the ionized particles, greatly influences the film properties such as crystalline, electrical and optical properties. In this chapter, the characteristics of films prepared by the ICB technique have also been shown. To summarize them is as follows:

Metal films on insulating or metal substrates show good adhesion, high packing densities and good conductivity. These characteristics are improved by increasing the acceleration voltage. For the case of Ag films deposited on a Si substrate,

ohmic contact can be obtained using acceleration voltages of over 4 kV. For the n-type Si substrate, ohmic contacts can be obtained without any annealing process. Whereas for the p-type Si substrate, annealing at 400°C is necessary to obtain good ohmic contact, for the highly doped P^+ substrate the additional annealing can be eliminated. Ohmic contact formation to p-type Si is mainly due to the Ag recombination centers formed by substitutional Ag atoms. On the other hand, for the n-type Si, the surface barrier is small enough to be destroyed by the bombardment of the ionized cluster beam. Therefore, ohmic contact can be obtained without any annealing.

For the semiconductor films, Si epitaxial films on Si (111) substrates by the ICB deposition can be obtained at low substrate temperatures of 300°C - 730°C in a vacuum range of 10^{-7} - 10^{-6} Torr. The results obtained from measurements by medium energy ion channeling and backscattering, from Hall effect and from C-V characteristics show that epitaxial films of about the same quality as the substrate can be grown. The Hall mobilities of the films grown at the substrate temperature of 730°C and 300°C were 800 $cm^2/V \cdot sec$ and 200 $cm^2/V \cdot sec$, respectively, and increased with increasing acceleration voltage and substrate temperature up to 700°C. The p-n junction diodes formed by deposition of n-type Si on p-type substrates at low substrate temperatures had good and sharp junctions. Preparation and characterization of the electrical and optical properties of thermally stable hydrogenated amorphous silicon (a-Si:H) films by the ICB technique have also been described. As the H_2 pressure during the deposition increased even in low hydrogen gas pressures of 10^{-5} - 10^{-4} Torr,

the optical band gap of the deposited films changed from 1.3 to 1.8 eV. The optical band gap did not change after annealing at about 500°C for 30 min. The dark conductivity at room temperature of the film did not change after annealing. It was confirmed by infrared absorption measurements that H atoms are contained in the a-Si:H films in a stable form as Si-H, rather than $Si-H_2$ or $Si-H_3$. In the ICB technique, forming of Si-Si bonds is considered to be promoted by the kinetic energy and electric charge, thereby decreasing the number of dangling bonds and decreasing the number of H atoms needed to passivate them. As compound semiconductor films, preparations of GaN and ZnS:Mn films could be successfully performed. ZnS:Mn films have shown the low impedance characteristics of the light-emitting diode by DC excitation.

For oxide films by the R-ICB technique, crystallographic and electrical properties of ZnO films have been described. The major results obtained are as follows: (1) the film formation process is closely related to acceleration voltage V_a and to ionized cluster content in the cluster beam which is determined by the electron current for ionization I_e; (2) thin films deposited onto glass substrates are preferentially oriented with the c-axis normal to the substrate at V_a = 0 - 500 V and I_e = 300 mA; (3) epitaxial growth of ZnO films is achieved at V_a = 1 kV and I_e = 300 mA by using different sapphire substrates; (4) the effect of lithium doping in ZnO films deposited onto glass substrates is completely different from that in the undoped films, e.g. low surface conductivity of 10^{-7} - 10^{-11} $\upsilon\,cm^{-1}$ can be seen for the Li-doped ZnO films; (5) the sharp

cathodoluminescence at 0.695 μm observed for the Li-doped ZnO films is considered to be due to the electron trnasition from the metastable state of oxygen vacancy into the paramagnetic Li-center.

Preparation of BeO thin films have also been successfully achieved by the R-ICB technique. Transparent BeO films with c-axis preferential orientation which is peculiar to a hexagonal structure have been obtained on glass substrates, and single crystal epitaxial films have been formed on sapphire substrates at low substrate temperatures below 400°C. Optical and thermal properties of films have been investigated in detail. A strong reststrahlen reflection peak was observed in the vicinity of 13.5 μm wavelength, and from this the frequencies of the transverse and longitudinal vibration modes were determined. Anisotropic lattice thermal conductivities parallel and perpendicular to the c-axis of the films were measured, and the values of $\kappa_{ph}^{//} \simeq 2.6$ w/cm·deg and $\kappa_{ph}^{\perp} \simeq 0.6$ w/cm·deg at 300 K were obtained. It was also shown that the thermal conductivities of BeO films are proportional to T^{-2} below Debye temperature $\Theta_D \simeq$ 1,053 K for this material.

From the results obtained in this thesis, the Ionized Cluster Beam (ICB) technique was found to have a great ability to be used in analyzing film formation and in preparing thin film devices with functionable, controllable and reproducible properties. The role of ions in film formation is predominant and the characteristics of films can be improved by the process of ionization. This fact, therefore, suggests that even conventional preparation methods for thin films, e.g. molecular

beam epitaxy, in which only neutral particles are used, could have remarkably improved features, if ions were to also be utilized. In addition, although discussion in this thesis regarding the great influence of ions on film formation has been mainly qualitative, this work will stimulate investigation toward more detailed theory regarding condensation and growth process of thin films. A number of complicated interdependencies among the important factors affecting the film formation presently prevent progress of theoretical understandings of the processes.

It is believed that high surface tension forces prevented generation of vaporized-metal clusters. This in itself is an interesting phenomenon which will provide stimulation to scientists and engineers engaged in the fields of nuclear physics, statistical physics, epitaxial growth and deposition, etc, because cluster states of materials are not known in detail, but cluster beams have several advantages for film formation. It can be concluded from the many experimantal results that a cluster consists of about 500 - 2000 loosely coupled atoms. The electronic state of cluster, the coupling energy between the constituent atoms of a cluster, etc. could not be measured, because it was not possible to obtain fine control over the clusre size. If it would be possible to control the cluster size, much information which could be obtained experimentally would be useful to analyze the cluster formation kinetics.

The Ionized Cluster Beam (ICB) technique has many features which are promising for film formation. From the standpoint that this technique should be applied to preparation of thin

film devices which utilize those features of Ionized Cluster Beam deposition and epitaxy which can not be achieved by any other preparation methods, several kinds of applications have been considered. It is probable that further applications of the ICB technique to thin film devices will be identified.

REFERENCES

1) T.Takagi, K.Matsubara, H.Takaoka and I.Yamada: Proc. of Intern. Conf. on Ion Plating and Allied Techniques (IPAT'79), London, 1979, (CEP Consultants Ltd., Edinburgh, 1979) P.174.

2) T.Takagi, K.Matsubara, H.Takaoka and I.Yamada: Thin Solid Films 63 (1979) 41.

3) Chr.Weissmantel: Proc. of 7th Intern. Vac. Congr. and 3rd Intern. Conf. on Solid Surf., Vienna, 1977, (F.Berger and Sohne,Vienna, 1977) P.1533.

4) Chr.Weissmantel, K.Bewilogua, H.J.Erler and G.Reisse: Proc. of Intern. Conf. on Ion Plating and Allied Techniques (IPAT '79), London, 1979, (CEP Consultants Ltd., Edinburgh, 1979) P.272.

5) V.O.Babaev, J.V.Bykov and M.B.Guseva: Thin Solid Films 38 (1976) 1.

6) E.H.Hirsch and I.K.Varga: Thin Solid Films 52 (1978) 445.

7) Y.Namba and T.Mori: J.Vac.Sci.Technol. 13 (1976) 693.

8) Y.Namba and T.Mori: Thin Solid Films 39 (1976) 119.

9) M.Marinov and D.Dobrev: Thin Solid Films 42 (1977) 265.

10) M.Marinov: Thin Solid Films 46 (1977) 267.

11) D.Dobrev and M.Marinov: C.R.Acad. Bulg. Sci. 26(2) (1973) 231.

12) J.Frans, P.R.Stuart and R.B.Withers: Thin Solid Films 60 (1979) 231.

13) D.G.Teer and B.L.Delcea: Proc. of Intern. Conf. on Ion Plating and Allied Techniques (IPAT'77), Edinburgh, 1977, (CEP Consultants Ltd., Edinburgh, 1977) P.58.

14) T.Takagi, I.Yamada, M.Kunori and S.Kobiyama: Proc. of 2nd Intern. Conf. on Ion Sources, Vienna, 1972, (SGAE, Vienna, 1972) P.790.

15) T.Takagi,I.Yamada and A.Sasaki: Thin Solid Films 39 (1976) 207.

16) T.Takagi, I.Yamada and A.Sasaki: Proc. of Intern. Conf. on Low Energy Ion Beams, Salford, 1977, Inst. Phys. Conf. Ser. No.38 (1978) Chap.3, P.142.

17) T.Takagi, I.Yamada and A.Sasaki: Thin Solid Films 45 (1977) 569.

18) D.J.McGinty: J. Chem. Phys. 58 (1973) 4733.

19) J.K.Lee, J.A.Barber and F.F.Abraham: J. Chem. Phys. 58 (1973) 3166.

20) W.D.Kristensen,E.J.Jensen and R.M.J.Cotterill: J.Chem.Phys. 60 (1974) 4161.

21) S.Schiller, V.Heisig and K.Goedicke: Proc. of 7th Intern. Vac. Congr. and 3rd Intern. Conf. on Solid Surf., Vienna, 1977, (F.Berger and Sohne, Vienna, 1977) P.1545.

22) P.Sigmund: Phys. Rev. 184 (1969) 383.

23) K.Miyake, K.Yagi and T.Tokuyama: Proc. of Intern. Conf. on Low Energy Ion Beams, Salford, 1977, Inst. Phys. Conf. Ser. No.38 (1978) Chap.2, P.78.

24) K.Yagi, K.Miyake and T.Tokuyama: Proc. of Intern. Conf. on Low Energy Ion Beams, Salford, 1977, Inst. Phys. Conf. Ser. No.38 (1978) Chap.3, P.136.

25) A.Fontell and E.Arminen: Can. J. Phys. 47 (1969) 2405.

26) K.L.Chopra: J. Appl. Phys. Letters 7 (1965) 140.

27) K.L.Chopra and M.R.Randlett: J. Appl. Phys. 39 (1968) 1874.

28) D.B.Dove: J. Appl. Phys. 35 (1964) 2785.

29) L.Holland: "Vacuum Deposition of Thin Films" (John Wiley & Sons, Inc., New York, 1956)

30) R.F.Bunshah and A.C.Raghuram: J. Vac. Sci. Technol. 9 (1972) 1385.

31) A.C.Raghuram and R.F.Bunshah: J. Vac. Sci. Technol. 9 (1972) 1389.

32) R.F.Bunshah: Proc. of 7th Intern. Vac. Congr. and 3rd Intern. Conf. on Solid Surf., Vienna, 1977, (F.Berger and Sohne, Vienna, 1977) P.1553.

33) R.F.Bunshah: Proc. of Intern. Conf. on Ion Plating and Allied Techniques (IPAT'77), Edinburgh, 1977,(CEP Consultants Ltd., Edinburgh, 1977) P.207.

34) D.S.Campbell: "Active and Passive Thin Film Devices" (Ed. T.J.Counts) (Acad. Press, London, 1978) Chap.2.

35) K.L.Chopra: "Thin Film Phenomena" (McGraw Hill, New York, 1969) Chap.2.

36) J.L.Vossen and J.J.Cuoms: "Thin Film Processes" (Eds.J.L. Vossen and W.Kern) (Acad. Press, New York, 1978) Chap.II-1

37) C.W.Pitt: Proc. of Intern. Conf. on Ion Plating and Allied Techniques (IPAT'77), Edinburgh, 1977, (CEP Consultants Ltd., Edinburgh, 1977) P.149.

38) G.S.Anderson, Wm.N.Mayer and G,K,Wehner: J. Appl. Phys. 33 (1962) 2991.

39) D.A.Fraser: "Thin Film Processes" (Eds. J.L.Vossen and W.Kern) (Acad. Press, New York, 1978) Chap.II-3.

40) G.D.Hughes: Proc. of Intern. Conf. on Ion Plating and Allied Techniques (IPAT'77), Edinburgh, 1977 (CEP Consultants Ltd., Edinburgh, 1977) P.169.

41) D.Gerstenberg and C.J.Calbick: J. Appl. phys. 35 (1964) 402.

42) E.Krikorian and R.J.Sneed: J. Appl. Phys. 37 (1966) 3674.

43) R.N.Castellens: Thin Solid Films 46 (1977) 213.

44) L.I.Maissel: "Handbook of Thin Film Technology" (Eds. L.I. Maissel and R.Glang) (McGraw Hill, New York, 1970) Chap.4.

45) J.M.E.Harper: "Thin Film Processes" (Eds. J.L.Vossen and W.Kern) (Acad. Press, New York, 1978) Chap.II-5.

46) M.W.Thomson: Phys. Mag. 18 (1968) 361.

47) P.A.Walley: Proc. of Intern. Conf. on Ion Plating and Allied Techniques (IPAT'77), Edinburgh, 1977, (CEP Consultants Ltd., Edinburgh, 1977) P.1.

48) T.Spalvins: J. Vac. Sci. Technol., 17 (1980) 315.

49) D.M.Mattox: Electrochem. Tech. 2 (1964) 295.

50) D.M.Mattox: Proc. of 6th Intern. Vac. Congr. (1974) P.443.

51) W.D.Davis and T.A.Vanderslice: Phys. Rev. 131 (1963) 219.

52) D.G.Teer: Proc. of Intern. Conf. on ion Plating and Applied Techniques (IPAT'77), Edinburgh, 1977, (CEP Consultants Ltd., Edinburgh, 1977) P.13.

53) W.E.Flynt: Proc. of 3rd Symp. on Electron Beam Technol., (1961) P.368.

54) B.A.Probyn: Brit. J. Appl. Phys. (J. Phys. D.) Ser.2, 1 (1968) 457.

55) E.G.Spencer, P.H.Schmidt, D.C.Joy and F.J.Sansalone: J. Appl. Phys. Letters 29 (1976) 118.

56) Y.Murayama: J. Vac. Sci. Technol. 12 (1975) 876.

57) Y.Murayama and E.Yamamoto: Proc. Of Symp. on Ion Sources and Appl. Technol., Tokyo, 1977, (The Inst. Electr. Eng. of Japan, 1977) P.113.

58) T.Takagi, I.Yamada, A.Sasaki and T.Ishibashi: IEEE Trans. Electron Devices, ED-20 (1973) 1110.

59) J.Dudonis and L.Panevicius: Thin Solid Films 36 (1976) 117.

60) S.Aisenberg and R.Chabot: J. Appl. Phys. 42 (1971) 2953.

61) J.S.Colligon, W.A.Grant, J.S.Williams and R.P.W.Lawson: Inst. Phys. Conf. Ser. No.28 (1976) Chap.9, P.357.

62) J.Amano, P.Bryce and R.P.W.Lawson: J. Vac. Sci. Technol. 13 (1976) 591.

63) J.Amano and R.P.W.Lawson: J. Vac. Sci. Technol. 14 (1977) 831.

64) J.Amano and R.P.W.Lawson: J. Vac. Sci. Technol. 14 (1977) 836.

65) J.Amano and R.P.W.Lawson: J. Vac. Sci. Technol. 15 (1978) 113.

66) G.E.Thomas and E.E.de Kluizenaar: Proc. of 3rd Intern. Congr. on Surf. Phys. and Chem., Grenoble, 1977, (Societe Francaise du Vide, Paris, 1977) P.136.

67) A.E.T.Kuiper, G.E.Thomas and W.J.Shouter: J.Cryst. Growth 37 (1978) 332.

68) T.Tsukizoe, T.Nakai and N.Ohmae: J. Appl. Phys. 48 (1977) 4770.

69) K.Miyake, K.Yagi and T.Tokuyama: Proc. of Symp. on Ion Sources and Appl. Technol., Tokyo, 1977, (The Inst. Electr. Eng. of Japan, 1977) P.103.

70) K.Yagi, S.Tamura and T.Tokuyama: Jap. J. Appl. Phys. 16 (1977) 245.

71) J.Geerk and O.Meyer: Surf. Sci. 32 (1972) 222.

72) W.B.Shepherd: Rec. of 11th Symp. on Electron, Ion and Laser Beam Tech., Boulder, 1971, (IEEE Catalog No.71, C23-ED) P.323.

73) T.Takagi, I.Yamada and A.Sasaki: J. Vac. Sci. Technol. 12 (1975) 1128.

74) T.Takagi, I.Yamada and A.Sasaki: Technical Digest of Intern. Electron Devices meeting, Washington D.C., 1976, P.605.

75) T.Takagi, I.Yamada and A.Sasaki: Proc. of Intern. Conf. on Ion Plating and Allied Techniques (IPAT'77), Edinburgh, 1977, (CEP Consultants Ltd., Edinburgh, 1977) P.50.

76) T.Takagi, I.Yamada, A.Sasaki, S.Itoh, M.Ozawa, W.Kodama, K.Tominaga and T.Hattori: Proc. of 7th Intern. Vac. Congr. and 3rd Intern. Conf. on Solid Surf., Vienna, 1977, (F.Berger and Sohne, Vienna, 1977) P.1603.

77) T.Takagi, I.Yamada and A.Sasaki: Proc. of 7th Intern. Vac. Congr. and 3rd Intern. Conf. on Solid Surf., Vienna, 1977, (F.Berger and Sohne, Vienna, 1977) P.1915.

78) T.Takagi, I.Yamada and A.Sasaki: Proc. of 6th Intern. Conf. on Molecular Beams, Noordwijkerhout, 1977, P.53.

79) T.Takagi, I.Yamada and A.Sasaki: Proc. of Intern. Conf. on Low Energy Ion Beams, Salford, 1977, Inst. Phys. Cond. Ser. No.38 (1977) Chap.5, P.229.

80) T.Takagi, I.Yamada, K.Matsubara and H.Takaoka: J. Cryst. Growth 45 (1978) 318.

81) I.Yamada, K.Matsubara, M.Kodama, M.Ozawa and T.Takagi: J. Cryst. Growth 45 (1978) 326.

82) T.Takagi, I.Yamada and A.Sasaki: IEE Trans. Solid State and Electron Devices 2 (Special Issue) (1978) S.40.

83) T.Takagi, I.Yamada and K.Matsubara: Thin Solid Films 58 (1979) 9.

84) K.Matsubara, I.Yamada, N.Nagao, K.Tominaga and T.Takagi: Surf. Sci. 86 (1979) 290.

85) T.Takagi, K.Matsubara, N.Kondo, K.Fujii and H.Takaoka: Jap. J. Appl. Phys. 19 (1980) Supple. 19-1, 107.

86) T.Takagi, K.Matsubara and H.Takaoka: J. Appl. Phys. 51 (1980) 5419.

87) I.Yamada, F.W.Saris, T.Takagi, K.Matsubara, H.Takaoka and S.Ishiyama: Jap. J. Appl. Phys. 19 (1980) L.181.

88) J.B.Theeten, R.Madar, A.Mircea-Roussel, A.Rocher and G. Lawrence: J. Cryst. Growth 37 (1979) 317.

89) K.Morimoto, H.Watanabe and S.Itoh: J. Cryst. Growth 45 (1978) 334.

90) A.E.T.Kuiper, G.E.Thomas and W.J.Shouter: J. Cryst. Growth 45 (1978) 332.

91) S.B.Sample, R.Bullini and D.A.Decher: Proc. of 11th Symp.

on Electron, Ion and Laser Technol., 1971, (IEEE Catalog No.71C23-ED) P.359.

92) R.Clampitt, L.Gowland and K.L.Aitken: Proc. of Intern. Conf. on Ion Plating and Allied Techniques (IPAT'77), Edinburgh, 1977, (CEP Consultants Ltd., Edinburgh, 1977) P.70.

93) R.Clampitt and D.K.Jefferies:Proc. of Intern. Conf. on Low Energy Ion Beams, Salford, 1977, Inst. Phys. Conf. Ser. No.38 (1978) Chap.1, P.12.

94) R.Clampitt: Thin Solid Films 58 (1979) 129.

95) R.F.C.Fanow, A.G.Cullins, A.J.Grant, G.R.Jones and R. Clampitt: Thin Solid Films 58 (1979) 189.

96) R.E.Leckenly, E.J.Robbins and P.A.Trevalion: Proc. Roy. Soc. (London) A280 (1964) 409.

97) P.P.Wegner and J.Y.Parlange: Naturewissenshaften 57 (1970) 525.

98) C.A.Moses and G.D.Stein: J.Fluids Engineering 100 (1978) 311.

99) O.F.Hagener: Proc. of 6th Intern. Symp. on Rarefied Gas Dynamics (Acad. Press Inc., New York) 2 (1969) 1465.

100) J.I.Yellott: Engineering 137 (1934) 303.

101) J.I.Yellott: Engineering 143 (1937) 647.

102) R.C.Tolman: J. Chem. Phys. 17 (1949) 333.

103) F.P.Buff and J.K.Kirkwood: J. Chem. Phys. 18 (1950) 991.

104) V.K.LaMev and G.M.Pound: J.Chem. Phys. 17 (1949) 1337.

105) R.Becker and W.Döring: Ann. Phys. 5 (1936) 719.

106) T.Takaoka, I.Yamada, H.Usui, S.katayama and T.Takagi: Proc. of 4th Symp. on Ion Sources and Ion Appl. Technol., Tokyo, 1980, (The Inst. Electr. Eng. of Japan, 1980) P.65.

107) B.J.Wu, P.P.Wegner and G.D.Stein: J. Chem. Phys. 68 (1978) 308.

108) O.F.Hagena: "Molecular Beams and Low Gas Density Gas-dynamics" (Ed. P.P.Wegner) (Marcel Dekker, Inc., New York, 1974) Chap.2.

109) H.J.Freund and S.H.Bauer: J. Phys. Chem. 81 (1977) 994.

110) D.J.Frurip and S.H.Bauer: J. Phys. Chem. 81 (1977) 1001

and 1007.

111) S.H.Bauer and D.J.Frurip: J. Phys. Chem. 81 (1977) 1015.

112) M.Epstein and D.E.Posner: Int. J. Heat Mass Transfer, 13 (Permagon Press, 1970, U.K.) 1393.

113) A.Yokozeki and G.D.Stein: J. Appl. Phys. 49 (1978) 2224.

114) O.F.Hagena and W.Obert: J. Chem. Phys. 56 (1972) 1793.

115) R.Klingelhöfer and H.O.Moser: J. Chem. Phys. 43 (1972) 4575.

116) F.T.Greene and T.A.Milne: J. Chem. Phys. 59 (1963) 3150.

117) T.A.Milne and F.T.Greene: J. Chem. Phys. 47 (1967) 4096.

118) T.A.Milne, A.E.Vandegrift and F.T.Greene: J. Chem. Phys. 52 (1970) 1552.

119) J.A.Armstrong,Jr.: "An Investigation of the Physical Properties of Small Molecular Clusters Formed via Homogeneous Nucleation in Nozzle Beams" (The Doctoral Thesis in Northwestern University, 1973)

120) P.P.Wegner and G.D.Stein: Proc. of 12rh Symp. (International) on Combustion (The Combustion Inst, Union Trust Bldg., 1969) 1183.

121) T.Takagi, I.Yamada, K.Matsubara and H.Takaoka: Proc. of 2nd Intern. Meeting on Small Parti. and Inorganic Clusters, Lausanne, 1980, P.43 and P.94.

122) F.Bottiglioni, J.Coutant and M.Fois: Phys. Rev. A 6 (1972) 1830.

123) I.F.Zartman: Phys. Rev. 37 (1931) 383.

124) J.B.Anderson and J.B.Fenn: Phys. of Fluids 8 (1965) 780.

125) J.R.Arthru and T.R.Brown: J. Vac. Sci. Instr. 39 (1968) 200.

126) M.H.Schwartz and R.P.Andres: J. Aerosol Sci. 7 (1976) 281.

127) O.F.Hagena and A.K.Varma: Rev. Sci. Instr. 39 (1968) 47.

128) C.G.Granqvist and R.A.Buhrman: J. Appl. Phys. 47 (1976) 2200.

129) O.F.Hagena: Phys. of Fluids 17 (1974) 894.

130) I.Yamada, H.Inokawa, H.Usui and T.Takagi: Proc. of 4th Symp. on Ion Sources and Ion Appl. Technol., Tokyo, 1980, (The Inst. Electr. Eng. of Japan, 1980) P.69.

131) M.Kamiyama and S.Sugata: "Thin Film Handbook" (Ohmu Sha Syoten, Tokyo, 1964) 1-8-4

132) K.L.Chopra: "Thin Film Phenomena" (McGraw Hill, New York, 1969) Chap.4.

133) C.A.Neugebauer: "Handbook of Thin Film Technology" (Eds. L.I.Maissel and R.Glang) (McGraw Hill, New York, 1970) Chap.8.

134) H.Takaoka, K.Matsubara and T.Takagi: Proc. of 4th Symp. on Ion Sources and Ion Appl. Technol., Tokyo, 1980, (The Inst. Electr. Eng. of Japan) P.143.

135) K.Suzuki, M.Mizuhashi and H.Sakata: Shinku(Vacuum) 21 (1978) 158.

136) S.K.Ghandhi, R.Siviy and J.M.Borrego: Appl. Phys. Lett. 34 (1979) 833.

137) D.M.Mattox: Sandia Corporation Monograph

138) T.Narusawa, S.Komiya and A.Hiraki: Appl. Phys. Lett. 22 (1973) 389.

139) S.B.Soffer: J. Appl. Phys. 36 (1965) 3947.

140) E.H.Phodenick: "Metal-Semiconductor Contacts" (Clarendon Press, Oxford, 1978)

141) E.H.Nicollian and A.K.Sinha: "Thin Films-Interdiffusion and Reactions" (Eds. J.M.Poate, K.N.Tu and J.W.Mayer) (John Wiley & Sons, New York, 1978) Chap.13.

142) J.W.Mayer, L.Eriksson and J.A.Davis: "Ion Implantation in Semiconductors" (Acad. Press, New York and London, 1970)

143) G.L.Pearson and J.Bardeen: Phys. Rev. 75 (1949) 865.

144) J.D.Struthers: J. Appl. Phys. 28 (1957) 516.

145) W.E.Dash: J. Appl. Phys. 31 (1960) 2275.

146) I.Yamada, M.Ozawa, K.Matsubara and T.Takagi: Proc. of 2nd Symp. on Ion Sources and Appl. Technol., Tokyo, 1978, (The Inst. Electr. Eng. of Japan, 1978) P.85.

147) H.Takaoka, S.Ishiyama, K.Matsubara, I.Yamada and T.Takagi: Proc. of 3rd Symp. on Ion Sources and Appl. Technol., Tokyo, 1979, (The Inst. Electr. Eng. of Japan, 1979) P.125.

148) J.W.Matthews: "Epitaxial Growth" (Acad. Press, New York, 1975)

149) T.Sakamoto, T.Takahashi, E.Suzuki, A.Shoji, H.Kawanami, Y.Komiya and Y.Tarui: Surf. Sci. 86 (1979) 102.

150) D.Hoonhout, G.B.Kerkdijk and F.W.Saris: Phys. Lett. 66A (1978) 145.

151) G.Carter and W.A.Grant: "Ion Implantation of Semiconductors" (Edward Arnold Ltd., 1976)

152) I.Yamada, D.Marton and F.W.Saris: Appl. Phys. Lett. 37 (1980) 563.

153) R.M.Tromp, R.Garrett, I.Yamada, H.E.Roosendaal and F.W.Saris: Rad. Effects Lett. 43 (1979) 217.

154) L.J.Van der Pauw: Phil. Res. Rep. 13 (1958) 1.

155) J.S.Blakemore: "Solid State Physics" (W.B.Saunders Co., Philadelphia, 1974)

156) S.M.Sze: "Physics of Semiconductor Devices" (John Wiley & Sons, New York, 1969) Chap.2.

157) J.N.Shive: "The Properties, Physics and Design of Semiconductor Devices" (D.Van Nostrand Co., Inc., Princeton, 1959)

158) I.Yamada, I.Nagai, S.Ishiyama and T.Takagi: Proc. of 4th Symp. on Ion Sources and Ion Appl. Technol., Tokyo, 1980, (The Inst. Electr. Eng. of Japan, 1980) P.115.

159) I.Yamada, I.Nagai, S.Ishiyama and T.Takagi: Proc. of 4th Symp. on Ion Sources and Ion Appl. Technol., Tokyo, 1980, (The Inst. Electr. Eng. of Japan, 1980) P.117.

160) L.L.Kazmerski: "Polycrystalline and Amorphous Thin Films and Devices" (Acad. Press, New York, 1980)

161) M.H.Brodsky: "Amorphous Semiconductors" (Springer-Verlag Berlin Heidelberg, New York, 1979)

162) N.F.Mott and E.A.Davis: "Electronic Processes in Non-Crystalline Materials" (Clarendon Press, Oxford, 1979)

163) V.Augelli, R.Murri, S.Galassinin and A.Tepore: Thin Solid Films 69 (1980) 315.

164) D.E.Carlson, C.R.Wronski, J.I.Pankove, P.J.Zanzucche and D.L.Staebler: RCA Rev. 38 (1977) 211.

165) M.H.Brodsky, R.S.Title, K.Weiser and G.D.Pettit: Phys. Rev. B 1 (1970) 2632.

166) M.H.Brodsky: THin Solid Films 50 (1978) 57.

167) D.E.Carlson: IEEE Trans. on Electron Devices ED-24 (1977) 449.

168) W.E.Spencer, P.G.Le Comber, S.Kinmond and M.H.Brodsky: Appl. Phys. Lett. 28 (1976) 105.

169) B.O.Seraphin: Solar Energy Materials 1 (1979)11.

170) J.I.Pankove, M.A.Lampert and M.L.Tarny: Appl. Phys. Lett. 32 (1978) 439.

171) C.C.Tsai and H.Fritzsche: Solar Energy Materials 1 (1979) 29.

172) Y.Nakagome, H.Matsumura and S.Furudawa: Jap. J. Appl. Phys. 19 (1980) L.87.

173) M.H.Brodsky, M.Cardona and J.J.Cuomo: Phys. Rev. B 16 (1977) 3556.

174) G.Lucovsky: J. Vac. Sci. Technol. 16 (1979) 1225.

175) K.C.Pandey: IBM J. Res. Develop. 22 (1978) 250.

176) K.Matsubara, T.Horibe, H.Takaoka and T.Takagi: Proc. of 4th Symp. on Ion Sources and Ion Appl. Technol., Tokyo, 1980, (The Inst. Electr. Eng. of Japan, 1980) P.137.

177) J.I.Pankove and E.R.Levin: J. Appl. Phys. 46 (1975) 1647.

178) J.I.Pankove: IEEE Trans. on Electron Devices ED22 (1975) 721.

179) M.Boulou, M.Furtado and G.Jacob: Phils. Tech. Rev. 37 (1977) 237.

180) G.Jacob and D.Bois: Appl. Phys. Lett. 30 (1977) 412.

181) J.I.Pankove and J.A.Hutchby: J. Appl. Phys. 47 (1976) 5387.

182) A.Vecht and N.J.Werring: J. Appl. Phys. 3 (1970) 105.

183) T.Inari and T.Takeda: Jap. J. Appl. Phys. 3 (1964) 802.

184) T.Takagi, I.Yamada and A.Sasaki: Reprint of 4th Intern. Conf. on Ion Implantation in Semiconductors and Other Materials, Osaka, 1974, (Plenum Publishing co., New York, 1974) P.275.

185) S.Maniv and A.Zangvil: J. Appl. Phys. 49 (1978) 2787.

186) G.Weise, E.M.Fechner, G.Owainn and D.Kraut: Thin Solid Films 32 (1976) 87.

187) A.R.Hutson: Phys. Rev. 108 (1957) 222.

188) O.F.Schirmer: J. Phys. Chem. Solids (Pergomon Press, 1968) 29 (1968) 1407.

189) K.Matsubara, H.Takaoka and T.Takagi: Proc. of 4th Symp. on Ion Sources and Ion Appl. Technol., Tokyo, 1980, (The Inst. Electr. Eng. of Japan) P.147.

190) E.Loh: Solid State Commun. 2 (1964) 269.

191) H.E.Swanson and E.Tatge: Natl. Bur. Stand. (U.S.) Circ. 539 (1)

192) J.R.Durig, R.C.Lord, W.J.Gardner and L.H.Johnston: J. Opt. Soc. Am. 52 (1962) 1078.

193) G.Picus, E.Burstein, B.W.Henvis and M.Hass: J. Phys. Chem. Solids 8 (1959) 282.

194) C.Kittel: "Introduction to Solid State Physics" (John Wiley & Sons, Inc., New York, 1976) Chap.4 and 5.

195) S.B.Austerman,D.A.Berlincourt and H.A.Krueger: J. Appl. Phys. 34 (1963) 339.

196) J. Callaway: Phys. Rev. 113 (1959) 1046.

ADDENDUM

1) T.Takagi, I.Yamada, K.Matsubara and H.Takaoka:
"Ionized-Cluster Beam Epitaxy", Journal of Crystal Growth, Vol.45, 1978, PP.318-325.

2) I.Yamada, H.Takaoka, K.Matsubara and T.Takagi:
"Thin Film Type Solar Cells Fabricated by Ionized-Cluster Beam Technique", 1978 Joint Convention (KANSAI Section) of the Institutes of Electrical Engineers, Paper No.S2-8, P.S19, October 28th-29th 1978.

3) H.Takaoka, I.Yamada, K.Matsubara and T.Takagi:
"Surface-Migration Effects of Adatoms in Ionized-Cluster Beam Epitaxy", 1978 Joint Convention (KANSAI Section) of the Institutes of Electrical Engineers, Paper No.G5-37, P.G209, October 28th-29th 1978.

4) H.Takaoka, I.Yamada, K.Matsubara and T.Takagi:
"Thin-Film-Formation Mechanism of Ionized-Cluster Beam Epitaxy", The Fall Meeting of JSAP, Paper No.3a-F-11, P.125, November 3rd-5th 1978.

5) T.Takagi, K.Matsubara, H.Takaoka and K.Tominaga:
"Epitaxial Growth of ZnO Thin Films by Reactive Ionized-Cluster Beam Technology", Journal of the Japanese Association of Crystal Growth, Vol.5, No.3, November 1978, P.12.

6) H.Takaoka, S.Ishiyama, I.Yamada, K.Matsubara and T.Takagi:
"Characteristics of Si Thin Films Prepared by Ionized-Cluster Beam Technology", Journal of the Japanese Association of Crystal Growth, Vol.5, No.3, November 1978, P.57.

7) T.Takagi, K.Matsubara, H.Takaoka and I.Yamada:
"Some Investigations of the Roles Played by Ions in Ion-Based Film Formation", Proceedings of the 3rd Symposium on Ion Sources and Application Technology, Tokyo, PP.119-124, February 19th-22nd 1979.

8) K.Matsubara, H.Takaoka, M.Kato, I.Yamada and T.Takagi:
"Properties of Impurity-Doped ZnO Films Prepared by

Reactive Ionized-Cluster Beam Technology", Proceedings of the 3rd Symposium on Ion Sources and Application Technology, Tokyo, PP.133-134, February 19th-22nd 1979.

9) K.Matsubara, N.Kondo, K.Fujii, H.Takaoka and T.Takagi: "Domain Growing Mechanism and Curie Point Writing of MnBi Films Prepared by Multitype Ionized-Cluster Beam Technology", Proceedings of the 3rd Symposium on Ion Sources and Application Technology, Tokyo, PP.131-132, February 19th-22nd 1979.

10) H.Takaoka, S.Ishiyama, K.Matsubara, I.Yamada and T.Takagi: "A Study of Film Formation Mechanism in Ionized-Cluster Beam Epitaxy", Proceedings of the 3rd Symposium on Ion Sources and Application Technology, Tokyo, PP.125-126, February 19th-22nd 1979.

11) K.Matsubara, H.Takaoka, M.Kato and T.Takagi: "CL-Properties of Li-Doped ZnO-Single Crystal Films Prepared by Ionized-Cluster Beam Technology", The Spring Meeting of JSAP, Paper No.28a-C-3, P.225, March 27th-30th 1979.

12) H.Takaoka, S.Ishiyama, K.Matsubara, I.Yamada and T.Takagi: "Thin-Film-Formation Mechanism of Ionized-Cluster Beam Epitaxy (II)", The Spring Meeting of JSAP, Paper No.28a-C-2, P.224, March 27th-30th 1979.

13) T.Takagi, K.Matsubara, H.Takaoka and I.Yamada: "Ion Beam Epitaxial Technique and Applications", Proceedings of the International Conference on Ion Plating and Allied Techniques - IPAT 79 - (University College London, London, the United Kingdom, July 3rd-5th 1979) (CEP Consultants Ltd.) PP.174-185.

14) T.Takagi, K.Matsubara, H.Takaoka and I.Yamada: "New Developments in Ionized-Cluster Beam and Reactive Ionized-Cluster Beam Deposition Techniques", Thin Solid Films, Vol.63, October 1979, PP.41-51.

15) T.Takagi, K.Matsubara, N.Kondo, K.Fujii and H.Takaoka: "Magnetooptical Properties of MnBi Films Prepared by

Ionized Cluster Beam Deposition Technique", Japanese Journal of Applied Physics, Vol.19, Supplement 19-1, April 1980, PP.507-511.

16) T.Takagi,K.Matsubara and H.Takaoka:
"CL-Properties of Li-Doped ZnO Epitaxial Films Prepared by Ionized-Cluster Beam Technique", Paper of Technical Group on Electron Devices, IECEJ, Paper No.ED79-44, PP.1-8.

17) T.Takagi, K.Matsubara, I.Yamada and H.Takaoka:
"Li-ZnO and BeO Films Prepared for Optical Wave Guides by Reactive Ionized-Cluster Beam Technique", Papers of the 3rd All-Round Symposium of the Professional Group of "Optical Electronics" Supported with the Grant-in-Aid for Scientific Research of the Ministry of Education, Paper No.S-18, PP.57-60, July 25th-26th 1979.

18) I.Yamada, F.W.Saris, T.Takagi, K.Matsubara, H.Takaoka and S.Ishiyama:
"Crystalline and Electrical Characteristics of Silicon Films Deposited by Ionized-Cluster Beams", Japanese Journal of Applied Physics, Vol.19, No.4, 1980, PP.L181-L184.

19) T.Takagi, K.Matsubara and H.Takaoka:
"Optical and Thermal Properties of BeO Thin Films Prepared by Reactive Ionized-Cluster Beam Technique", Journal of Applied Physics, Vol.51, No.10, October 1980, PP.5419-5424.

20) K.Matsubara, H.Takaoka and T.Takagi:
"Preparation of BeO Thin Films by Reactive Ionized-Cluster Beam Technique", The Spring Meeting of JSAP, Paper No.1p-B-6, P.276, April 1st-4th 1980.

21) K.Matsubara, H.Takaoka and T.Takagi:
"Optical and Thermal Properties of BeO Films Prepared by R-ICB Technique", The Spring Meeting of JSAP, Paper No.1p-B-7, P.276, April 1st-4th 1980.

22) I.Yamada, H.Takaoka, S.Ishiyama, K.Matsubara and T.Takagi:
"Crystallinity and Abrupt Junction of Si Epitaxial Films Prepared by Ionized-Cluster Beams", The Spring Meeting of JSAP, Paper No.1p-B-9, P.277, April 1st-4th 1980.

23) H.Takaoka, I.Yamada, H.Usui, S.Katayama and T.Takagi:
"Analysis of Vapourized-Metal Cluster Ion Beam", Proceedings of the 4th Symposium on Ion Sources and Ion Application Technology, Tokyo, PP.65-68, June 24th-26th 1980.

24) K.Matsubara, H.Horibe, H.Takaoka and T.Takagi:
"Electrical Properties of GaN Light-Emitting Diodes Made by R-ICB Technique", Proceedings of the 4th Symposium on Ion Sources and Ion Application Technology, Tokyo, PP.137-140, June 24th-26th 1980.

25) H.Takaoka, K.Matsubara and T.Takagi:
"Crystallographic Properties of Tin Oxide Thin Films Prepared by R-ICB Technique", Proceedings of the 4th Symposium on Ion Sources and Ion Application Technology, Tokyo, PP.143-146, June 24th-26th 1980.

26) K.Matsubara, H.Takaoka and T.Takagi:
"Thermal Transport Properties of Crystallized BeO Thin Films by R-ICB Technique", Proceedings of the 4th Symposium on Ion Sources and Ion Application Technology, Tokyo, PP.147-150, June 24th -26th 1980.

27) H.Takaoka, H.Usui, S.Katayama and T.Takagi:
"Energy Analysis of Vapourized-Metal Cluster Ion Beam", The Fall Meeting of JSAP, Paper No.17p-F-12, P.334, October 17th-19th 1980.

28) H.Horibe, K.Matsubara, H.Takaoka and T.Takagi:
"Growth of GaN Films by R-ICB Technique and Their Electrical Properties", The Fall Meeting of JSAP, Paper No.17a-W-3, P.226, October 17th-19th 1980.

29) K.Matsubara, H.Takaoka, N.Kondo and T.Takagi:
"A Study on the Growth Mechanism of Preferentially Oriented Thin Films", The Fall Meeting of JSAP, Paper No.18a-W-9, P.242, June 17th-19th 1980.

30) T.Takagi, I.Yamada, K.Matsubara and H.Takaoka:
"Formation Mechanisms of Vapourized-Metal Cluster Ions", Proceedings of the 2nd International Meeting on the Small

Particles and Inorganic Clusters, Ecole Polytechnique Federale, Lausanne, Switzerland, PP.43-44, September 8th-12th 1980.

31) T.Takagi, K.Matsubara, I.Yamada and H.Takaoka: "Film Formation Technique by Ionized Cluster Beam", Proceedings of the 2nd International Meeting on the Small Particles and Inorganic Clusters, Ecole Polytechnique Federale, Lausanne, Switzerland, PP.94-95, September 8th-12th 1980.